

INVESTIGATION OF HAPTIC MANIPULATORS WITH LINEAR EQUATIONS  
OF MOTION

A THESIS SUBMITTED TO  
THE GRADUATE SCHOOL OF NATURAL AND APPLIED SCIENCES  
OF  
MIDDLE EAST TECHNICAL UNIVERSITY

BY

ARAS KIZILBEY

IN PARTIAL FULFILLMENT OF THE REQUIREMENTS  
FOR  
THE DEGREE OF MASTER OF SCIENCE  
IN  
MECHANICAL ENGINEERING

AUGUST 2019



Approval of the thesis:

**INVESTIGATION OF HAPTIC MANIPULATORS WITH LINEAR  
EQUATIONS OF MOTION**

submitted by **ARAS KIZILBEY** in partial fulfillment of the requirements for the degree of **Master of Science in Mechanical Engineering Department, Middle East Technical University** by,

Prof. Dr. Halil Kalıpçılar  
Dean, Graduate School of **Natural and Applied Sciences**

\_\_\_\_\_

Prof. Dr. M. A. Sahir Arıkan  
Head of Department, **Mechanical Engineering**

\_\_\_\_\_

Prof. Dr. Reşit Soylu  
Supervisor, **Mechanical Engineering, METU**

\_\_\_\_\_

**Examining Committee Members:**

Assoc. Prof. Dr. Ergin Tönük  
Mechanical Engineering, METU

\_\_\_\_\_

Prof. Dr. Reşit Soylu  
Mechanical Engineering, METU

\_\_\_\_\_

Assist. Prof. Dr. Ahmet Buğra Koku  
Mechanical Engineering, METU

\_\_\_\_\_

Assist. Prof. Dr. Ulaş Yaman  
Mechanical Engineering, METU

\_\_\_\_\_

Assist. Prof. Dr. Kutluk Bilge Arıkan  
Mechanical Engineering, TEDU

\_\_\_\_\_

Date: 27.08.2019

**I hereby declare that all information in this document has been obtained and presented in accordance with academic rules and ethical conduct. I also declare that, as required by these rules and conduct, I have fully cited and referenced all material and results that are not original to this work.**

Name, Surname: Aras Kızılbey

Signature:

## **ABSTRACT**

### **INVESTIGATION OF HAPTIC MANIPULATORS WITH LINEAR EQUATIONS OF MOTION**

Kızılbey, Aras  
Master of Science, Mechanical Engineering  
Supervisor: Prof. Dr. Reşit Soylu

August 2019, 131 pages

In this thesis, linearization of the equations of motion of haptic interfaces and the effects of such linearization on haptic applications are examined.

Three and six DOF configurations of the Phantom Premium™ 1.5 have been selected as the haptic manipulators to be investigated. By utilizing the generic computer code that has been developed for hybrid manipulators composed of revolute and prismatic joints, the equations of motion for the aforementioned two haptic manipulator types are derived in symbolic form.

Using the concept of Linearity Number (LN), linearization of the equations of motion of the three and six DOF haptic interfaces have been attempted. It has been already shown that there exist completely linear three DOF serial spatial manipulators. Since Phantom Premium 1.5 contains a parallelogram mechanism, however, it is a hybrid manipulator. To the author's knowledge, the existence of linear six DOF spatial manipulators, on the other hand, is uncertain. In this study, complete linearization of the three DOF haptic interface is achieved. To the author's knowledge, such a result does not exist in the literature. Furthermore, non-existence of fully linear equations of motion for the selected six DOF configuration is shown.

The effects of linearization on the performance of three DOF haptic interfaces are investigated by considering two performance criteria of a haptic interaction which are Stable Impedance Range and Transparency Bandwidth. Mathematical models and specific simulation environments are formed for Stable Impedance Range and Transparency Bandwidth simulations. The numerical values of these two performance criteria are calculated via simulations. The relationship between the aforementioned performance criteria and the degree of linearity of the haptic manipulator is also investigated.

Keywords: Equations of Motion, Linearization, Linearity Number, Haptic Interface

## ÖZ

### DOĞRUSAL HAREKET DENKLEMLERİNE SAHİP HAPTİK MANİPÜLATÖRLERİN İNCELENMESİ

Kızılbey, Aras  
Yüksek Lisans, Makina Mühendisliği  
Tez Danışmanı: Prof. Dr. Reşit Soylu

Ağustos 2019, 131 sayfa

Bu tezde, haptik manipülatörlerin hareket denklemlerinin lineer hale getirilmesi ve bu lineerleştirmenin haptik uygulamalar üzerindeki etkisi incelenmiştir.

Haptik manipülatör olarak; üç ve altı serbestlik derecesine sahip iki ayrı konfigürasyonu bulunan Phantom Premium™ 1.5 seçilmiştir. Bu konfigürasyonlara ait hareket denklemleri, döner ve kayar mafsallardan oluşan hibrit manipülatörlerin hareket denklemlerini türetmesi amacıyla geliştirilen standart bir bilgisayar kodu ile sembolik formda elde edilmiştir.

Lineerlik Endeksi (LE) kavramı kullanılarak, üç ve altı serbestlik dereceli haptik arayüzlerin hareket denklemleri lineerleştirilmeye çalışılmıştır. Önceki araştırmalarda, üç serbestlik derecesine sahip seri uzaysal manipülatörlerin lineer denklemlere sahip olabilecekleri gösterilmiştir; fakat Phantom Premium 1.5 üzerinde paralelogram mekanizmasının bulunduğu hibrit bir manipülatördür. Bunun yanı sıra; yazarın yaptığı araştırmalar çerçevesinde altı serbestlik derecesine sahip uzaysal manipülatörleri lineerleştirmenin mümkün olup olmadığının tam olarak bilinmediği görülmüştür. Bu çalışmayla birlikte, üç serbestlik dereceli uzaysal hibrit haptik arayüzün hareket denklemleri ilk kez (yazarın bilgisi dahilinde) lineer hale

getirilmiştir. Ek olarak seçilen altı serbestlik dereceli manipülatörü ise tamamen lineerleştirmenin mümkün olmadığı ortaya konmuştur.

Lineerizasyonun haptik arayüzlerin performansına etkisini görmek adına üç serbestlik derecesine sahip konfigürasyon ile Kararlı Empedans Aralığı ve Şeffaflık Bant Genişliği performans kriterleri için simülasyonlar icra edilmiştir. Her iki performans kriteri için ayrı ayrı matematiksel modeller ve simülasyon ortamları tasarlanmış ve performans kriterlerinin numerik değerleri elde edilmiştir. Simülasyonlar sonucunda ilgili performans kriterleri ve lineerlik endeksi arasındaki ilişki detaylı bir şekilde incelenmiştir.

Anahtar Kelimeler: Hareket Denklemleri, Lineerizasyon, Lineerlik Endeksi, Haptik Manipülatör

To my dear mom, Elmas

## ACKNOWLEDGEMENTS

I would like to express my gratitude to my thesis supervisor Prof. Dr. Reşit Soylu for his guidance, support, and encouragements throughout this research. Benefiting from his deep knowledge and valuable experiences is a privilege for me.

I would like to thank Atae Jafari-Tabrizi and Onurcan Kaya for their great friendship and help. I am also thankful to personnel of METU Library where I spent my days and nights. I would like to express my deep thanks to Hatice Hatipoğlu, an enthusiastic physics engineer who always supports and believes in me. Without her, it is not possible to complete this study.

Above all, I want to present my infinite gratitude to my mother, Elmas for her endless love and patience from the very my first moment of my life.

## TABLE OF CONTENTS

ABSTRACT .....	v
ÖZ .....	vii
ACKNOWLEDGEMENTS .....	x
TABLE OF CONTENTS .....	xi
LIST OF TABLES .....	xiv
LIST OF FIGURES .....	xv
LIST OF ABBREVIATIONS .....	xviii
LIST OF SYMBOLS .....	xix
CHAPTERS	
1. INTRODUCTION .....	1
2. DERIVATION OF DYNAMIC EQUATIONS OF HAPTIC INTERFACES .....	7
2.1. Kinematic Notation.....	7
2.2. Kinematic and Dynamic Properties of Haptic Interfaces .....	13
2.2.1. Three Degrees of Freedom Haptic Interface .....	13
2.2.2. Six Degrees of Freedom Haptic Interface .....	15
2.3. Kinematic Analysis.....	18
2.3.1. Orientation of the Links .....	18
2.3.2. Angular Velocity of the Links .....	19
2.3.3. Position of the Link Origins .....	21
2.3.4. Position of the Link Mass Centers .....	24
2.3.5. Velocity of the Link Origins .....	25
2.3.6. Velocity of the Link Mass Centers .....	26

2.4. Dynamic Analysis .....	27
3. OPTIMIZATION OF HAPTIC INTERFACES.....	33
3.1. Definition and Calculation of the Linearity Number .....	33
3.2. Optimization of the Three Degrees of Freedom Configuration .....	35
3.2.1. Analytical Method.....	36
3.2.2. Numerical Method .....	45
3.3. Optimization of the Six Degrees of Freedom Configuration .....	49
4. PERFORMANCE SIMULATIONS OF HAPTIC INTERFACES.....	51
4.1. Stable Impedance Range Simulations .....	51
4.1.1. Simulation Model.....	53
4.1.1.1. Model of the Haptic Interface .....	53
4.1.1.2. Model of the Compensator.....	54
4.1.1.3. Model of the Virtual Environment .....	57
4.1.1.4. Composition of the Simulation Model.....	57
4.1.2. Stable Impedance Range Calculation Methodology .....	61
4.1.3. Simulation Conditions .....	63
4.1.4. Simulation Results and Assessments .....	67
4.1.4.1. Results of Simulation Type 1 .....	68
4.1.4.2. Results of Simulation Type 2 .....	70
4.1.4.3. Assessments of Stable Impedance Range Simulations.....	73
4.2. Transparency Bandwidth Simulations .....	74
4.2.1. Simulation Model.....	75
4.2.1.1. Model of the Haptic Interface .....	76
4.2.1.2. Model of the Compensator.....	77

4.2.1.3. Model of the Virtual Environment .....	77
4.2.1.4. Composition of the Simulation Model.....	79
4.2.2. Transparency Bandwidth Calculation Methodology .....	81
4.2.3. Simulation Conditions .....	84
4.2.4. Simulation Results and Assessments .....	87
4.2.4.1. Results of Simulation Type 1 .....	88
4.2.4.2. Results of Simulation Type 2 .....	89
4.2.4.3. Assessments of Transparency Bandwidth Simulations .....	92
5. CONCLUSION AND FUTURE WORK .....	95
REFERENCES .....	99
APPENDICES	
A. Results of Dynamic Analysis .....	105
B. LN of Haptic Interfaces.....	113
C. Optimization of Three Degrees of Freedom Configuration .....	119
D. Optimization of Six Degrees of Freedom Configuration .....	131

## LIST OF TABLES

### TABLES

Table 2.1. Link Lengths of the Three DOF Haptic Device.....	14
Table 2.2. DH Parameters of the Three DOF Haptic Device.....	15
Table 2.3. Definition for the Inertial Properties .....	15
Table 2.4. Link Lengths of the Six DOF Haptic Device.....	16
Table 2.5. DH Parameters of the Six DOF Haptic Device.....	18
Table 3.1. Design Parameters of the Three DOF Haptic Device .....	36
Table 3.2. Free Design Parameters of the Three DOF Haptic Device.....	39
Table 3.3. Manipulator with Different Degrees of Linearity .....	48
Table 3.4. Design Parameters of the Six DOF Haptic Device .....	49
Table 4.1. Inherent Damping of the Manipulator .....	64
Table 4.2. Initial Condition of the Virtual Wall .....	65
Table 4.3. Conditions of the Simulation Types .....	65
Table 4.4. Results of the Stable Impedance Range Simulations for the First DOF – Simulation Type 1.....	69
Table 4.5. Conditions of the Simulation Types .....	85
Table 4.6. Results of the Transparency Bandwidth Simulations for the First DOF – Simulation Type 1.....	89

## LIST OF FIGURES

### FIGURES

Figure 1.1. Haptic System Interaction Scheme [13] .....	3
Figure 2.1. Adapted Kinematic Convention.....	8
Figure 2.2. The Unit Basis Vectors of Reference Frame I.....	9
Figure 2.3. Rotations about Unit Basis Vectors .....	11
Figure 2.4. Link Orientations and Numberings of the Three DOF Haptic Device ...	13
Figure 2.5. Reference Frames and DH Parameters of the Three DOF Haptic Device a) Side View-1 b) Side View-2 c) Top View .....	14
Figure 2.6. Link Orientations and Numberings of the Six DOF Haptic Device .....	16
Figure 2.7. Reference Frames and DH Parameters of the Six DOF Haptic Device a) Side View-1 b) Top View c) Side View-2 d) End Effector .....	17
Figure 2.8. Angular Velocity of Link $i$ .....	20
Figure 2.9. Origin Position of Link $i$ .....	22
Figure 2.10. Origins of Parallel Links .....	23
Figure 2.11. Mass Center Position of Link $i$ .....	24
Figure 3.1. Mass Center Position Vector of Link 2 a) Side View b) Front View ....	41
Figure 3.2. Rotation Axis of the Parallelogram Mechanism a) Side View b) Front View .....	42
Figure 3.3. Mass Center Positions of the Example Solution.....	45
Figure 4.1. Haptic Interface Model for the Stable Impedance Range Simulations ...	54
Figure 4.2. Layout of the Compensator Block for the Stable Impedance Range Simulations .....	55
Figure 4.3. Compensator Block for the Stable Impedance Range Simulations .....	56
Figure 4.4. Virtual Environment Block for the Stable Impedance Range Simulations .....	57
Figure 4.5. Open-Loop Impedance Control Scheme of a Haptic Interface [32] .....	58

Figure 4.6. Complete Layout of the Simulation Model for the Stable Impedance Range Simulations .....	59
Figure 4.7. Safety Switch Block .....	63
Figure 4.8. Damping at Joint 1 .....	64
Figure 4.9. Maximum Stable Impedance vs LN Graph for the First DOF – Simulation Type 1.....	69
Figure 4.10. Maximum Stable Impedance vs LN Graph – Simulation Type 1 and Type 2 .....	71
Figure 4.11. Stable Impedance Range Differences Between Simulation Type 1 and Type 2 .....	72
Figure 4.12. Haptic Interface Model for the Transparency Bandwidth Simulations.	76
Figure 4.13. Application of the Desired Path and Measurement of the User Forces	77
Figure 4.14. Ideal Virtual Environment Model for the Transparency Bandwidth Simulations.....	78
Figure 4.15. Implemented Virtual Environment Model for the Transparency Bandwidth Simulations .....	78
Figure 4.16. Complete Layout of the Simulation Model for the Transparency Bandwidth Simulations .....	79
Figure 4.17. Example Chirp Signal .....	82
Figure 4.18. Frequency Response of the Transparency Transfer Function .....	84
Figure 4.19. Transparency Bandwidth vs LN Graph for the First DOF – Simulation Type 1 .....	88
Figure 4.20. Transparency Bandwidth vs LN Graph – Simulation Type 1 and Type 2 .....	90
Figure 4.21. Transparency Bandwidth Differences Between Simulation Type 1 and Type 2 .....	91
Figure 0.1. First Actuator Torque .....	105
Figure 0.2. Second Actuator Torque.....	107
Figure 0.3. Third Actuator Torque .....	108
Figure 0.4. Validity Check of the Derived Equations.....	109

Figure 0.5. Comparison with Available Equations.....	111
Figure 0.6. LN of Three DOF Configuration .....	113
Figure 0.7. LN of Six DOF Configuration .....	115
Figure 0.8. Example Manipulator Designs for LN = 0 .....	119
Figure 0.9. Example Manipulator Designs for LN = 0.001 .....	121
Figure 0.10. Example Manipulator Designs for LN = 0.01 .....	123
Figure 0.11. Example Manipulator Designs for LN = 0.1 .....	125
Figure 0.12. Example Manipulator Designs for LN = 1 .....	127
Figure 0.13. Example Manipulator Designs for LN = 2 .....	129
Figure 0.14. LN Optimization of Six DOF .....	131

## LIST OF ABBREVIATIONS

### ABBREVIATIONS

<b>DAC</b>	Digital-to-Analog Converter
<b>DH</b>	Denavit-Hartenberg
<b>DOF</b>	Degrees of Freedom
<b>LE</b>	<i>Lineerlik Endeksi</i>
<b>LN</b>	Linearity Number
<b>MCP</b>	Mass Center Position
<b>METU</b>	Middle East Technical University
<b>TEDU</b>	<i>Türk Eğitim Derneği</i> University
<b>ZOH</b>	Zero-Order Hold

## LIST OF SYMBOLS

### SYMBOLS

$\alpha_i$	Twist angle of joint $i+1$ with respect to joint $i$
$a_i$	Effective length of link $i$
$\hat{C}^{(i,i+1)}$	Link-to-link transformation matrix that transforms the reference frame attached to link $i$ to the reference frame attached to link $i+1$
$\bar{C}(\theta)$	$N \times ((N^2 + N)/2)$ matrix of Coriolis and Centrifugal Forces
$\bar{C}_{cvt}(\theta, \dot{\theta})$	$N \times N$ matrix of Coriolis and Centrifugal Forces
$D_0$	Vector differentiation in the Base Frame
$dB$	Decibel
$F_e$	Desired force at the haptic display's end-effector
$F_h$	The force that is applied by the user to the end-effector of the haptic display
$G_T$	Transparency transfer function
$\bar{G}(\theta)$	$N \times 1$ column matrix of gravity terms
$g$	Gravitational acceleration
$\bar{H}(\theta)$	$N \times N$ mass matrix
$J_i$	Joint $i$
$J$	Jacobian Matrix of the haptic display that defines the relationship between the joint velocity and the end-effector velocity

$\mathbf{c}\hat{\mathbf{I}}_i^{(1)}$	Inertia tensor of link $i$ defined in Reference Frame I and calculated at the center of gravity of link $i$
$\mathbf{k}_i$	Kinetic energy of link $i$
$\mathbf{K}$	Sum of the kinetic energies of the individual links
$\mathbf{L}_i$	Link $i$
$\mathcal{L}$	Lagrangian
$\ell_i$	Length of link $i$
$\mathbf{m}_i$	Mass of link $i$
$\mathbf{N}$	Manipulator's DOF
$\mathbf{O}_i$	Origin of link $i$
$\vec{\mathbf{P}}_i$	Position vector of $\mathbf{O}_i$ measured from the origin of Base Frame
$\bar{\mathbf{P}}_i$	Matrix representation of vector $\vec{\mathbf{P}}_i$ resolved in the Base Frame
$\mathbf{c}\vec{\mathbf{P}}_i$	Position vector of the mass center of link $i$ measured from the origin of Base Frame
$\mathbf{c}\bar{\mathbf{P}}_i$	Matrix representation of vector $\mathbf{c}\vec{\mathbf{P}}_i$ resolved in the Base Frame
$\sigma$	Standard deviation
$\mathbf{q}_e$	Desired joint position
$\mathbf{q}_h$	Actual joint position of the haptic interface
$\mathbf{q}_h^*$	Sensed joint position of the haptic interface
$\dot{\mathbf{q}}_h$	Actual joint velocity of the haptic interface
$\dot{\mathbf{q}}_h^*$	Sensed joint velocity of the haptic interface

$\ddot{\mathbf{q}}_h$	Actual joint acceleration of the haptic interface
$\ddot{\mathbf{q}}_h^*$	Sensed joint acceleration of the haptic interface
$\theta_i$	Rotation angle of link i with respect to link i-1
$\dot{\theta}_i$	Joint velocity of joint i
$\bar{\mathbf{r}}_i$	Mass center position column matrix of link i, defined in Reference Frame I, and defined from the origin of Reference Frame I-1
$\widehat{\mathbf{R}}_1(\theta_k)$	Rotation matrix that expresses rotation about $\bar{\mathbf{u}}_1^{(i)}$ with a magnitude of $\theta_k$
$s_i$	Offset between link i-1 and link i
$\bar{\boldsymbol{\tau}}$	N x 1 actuator torque column matrix
$\boldsymbol{\tau}_c$	Joint torque resulting from the desired force at the haptic display's end-effector
$\boldsymbol{\tau}_D$	Joint torque calculated by the ideal virtual environment
$\boldsymbol{\tau}_e$	Desired joint torque implemented to the haptic device by the virtual environment
$\boldsymbol{\tau}_f$	Feedforward torque introduced by the compensator
$\boldsymbol{\tau}_h$	Joint torque resulting from the force applied by the user to the end-effector of the haptic display
$\boldsymbol{\tau}_{imp}$	Joint torque calculated by the implemented virtual environment
$\boldsymbol{\tau}_M$	Torque transmitted to the user
$\bar{\mathbf{u}}_1^{(i)}$	X component of the unit basis vector of Reference Frame I
$\bar{\mathbf{u}}_2^{(i)}$	Y component of the unit basis vector of Reference Frame I

$\bar{u}_3^{(i)}$	Z component of the unit basis vector of Reference Frame I
$\bar{u}_1$	Matrix representation of unit basis vector $\vec{u}_1^{(i)}$ resolved in Reference Frame I
$\bar{u}_1^{(i/j)}$	Matrix representation of unit basis vector $\vec{u}_1^{(i)}$ resolved in Reference Frame J
$u_i$	Potential energy of link i
$U$	Sum of the potential energies of the individual links
$\vec{v}$	Vector independent of any reference frame
$\bar{v}^{(i)}$	Matrix representation of vector $\vec{v}$ resolved in Reference Frame I
$\tilde{v}^{(i)}$	Cross-product matrix of $\bar{v}^{(i)}$
$\vec{V}_i$	Velocity vector of $O_i$ measured from the origin of Base Frame
$\bar{V}_i$	Matrix representation of vector $\vec{V}_i$ resolved in the Base Frame
${}^c\vec{V}_i$	Velocity vector of the mass center of link i measured from the origin of Base Frame
${}^c\bar{V}_i$	Matrix representation of vector ${}^c\vec{V}_i$ resolved in the Base Frame
$v_e$	Desired velocity of the end-effector defined in the task space
$v_h$	Resulting velocity of the end-effector defined in the task space
$\vec{\omega}_{i/i-1}$	Rotation vector of link i with respect to link i-1
$\bar{\omega}_{i/i-1}^{(i)}$	Rotation matrix of vector $\vec{\omega}_{i/i-1}$ resolved in Reference Frame I
$\bar{\omega}_i$	Rotation matrix of vector $\vec{\omega}_{i/0}$ resolved in the Base Frame
${}^jZ_r$	Impedance of the haptic display

$\hat{Z}_r$	Modeled impedance of the haptic display
$Z_e$	Impedance of the (implemented) virtual environment
$Z_D$	Impedance of the ideal virtual environment
$Z_M$	Transmitted Impedance



## CHAPTER 1

### INTRODUCTION

Robotic manipulators have inherently complex dynamics due to the interactions between the joints, varying payloads and varying forces including Coriolis, centripetal and gravitational. This non-linear dynamics leads to errors in high-speed position response and significant performance degradation even at low-speed operations. Hence, simplification of manipulator dynamics has great importance.

Many methods are proposed to obtain simpler equations of motion over the years. Relocation of the actuator, a method suggested by Youcef-Taumi in [1], is one of the approaches; however, accumulated error in clearances and non-rigid behavior of transmissions, due to remote actuation, cause loss in precision during the operation of a manipulator. Arakelian [2] tries to decouple manipulator dynamics by adding either auxiliary links or gears. The first method excessively increases the manipulator mass, the latter one, on the other hand, leads to shocks which have negative effects such as noise and perturbation. Besides mechanical methods, there are some control systems [3]–[7] that provide high-quality control of a non-linear manipulator. However, these methods are complicated, costly and still need to be improved for applications that require high speed and precision.

In addition to the aforementioned approaches, equations of motion can also be linearized by redesigning the manipulator. In order to determine the design parameters, different approaches can be adopted. Asada [8] uses the concept of inertia ellipsoid which is only practical for two and three DOF manipulators. Yang and Tzeng [9] attempt to linearize the manipulator dynamics by eliminating the coefficient of non-linear terms in the kinetic and potential energy equations of the manipulator. Similarly, Park and Cho [10] work on the energy equations and specify

conditions for simplifying non-linear dynamics. Youcef-Taumi and Asada [11] have developed conditions for a decoupled and/or invariant inertia matrix. Soylu [12] proposes the concept of Linearity Number (LN) that can be used for designing the kinematic and inertial parameters of a manipulator in order to obtain fully linear, or as linear as possible, equations of motion.

LN is a scalar index that shows the degree of linearity of a serial manipulator. It can be used both for design and comparison purposes. Restrictions on the kinematic and/or inertial parameters of the manipulator, which make it either completely or partially linear, can be determined by LN. On the other hand, LN of previously designed manipulators can also be calculated in order to compare the linearities of different manipulators. When a manipulator is completely linear, LN will be zero; and it increases as the nonlinearity increases.

LN has several advantages compared to the other techniques. First of all, it can be computed in closed form. Rather than defining the conditions for full linearity, the optimization procedure can also be applied to non-linearizable manipulators and manipulators with additional design restrictions. Linearization can be realized in a restricted region, rather than the whole joint space, which provides better information about the linearity of a certain task. A four DOF robot stated as non-linearizable in [9] has been linearized by using LN [12].

It is known that linearized manipulators have positive effects on controller design, but there is limited research about additional positive and negative effects of linearization. Throughout this study, the effects of linearization on one of the popular subjects of recent years, haptic displays, have been investigated.

A haptic display is a mechanical device that transfers kinesthetic information (information about body pose and movement), or tactile stimuli on the surface of the body to the user. A wide variety of devices that can be used as haptic display exist. A haptic device can be either in the form of a serial manipulator or a parallel manipulator. Phantom (Sensable), Omega (Force Dimension), HapticMaster (Moog

FCS), ARMin (ETH Zurich) and CyberGrasp (CyberGloveSystems) are some examples of haptic devices.

A haptic interface that measures position and generates contact force (and/or their time derivatives or spatial distribution) is defined as an impedance display. Conversely, admittance displays measure force and transmit movement to the user. These interfaces can be used both with the real environment for teleoperation (remote operation) and the virtual environment. The virtual environment is a computer-generated model of a physical world that can behave as impedance or admittance. The interaction of haptic interface with the human and real/virtual environment is summarized in Figure 1.1.

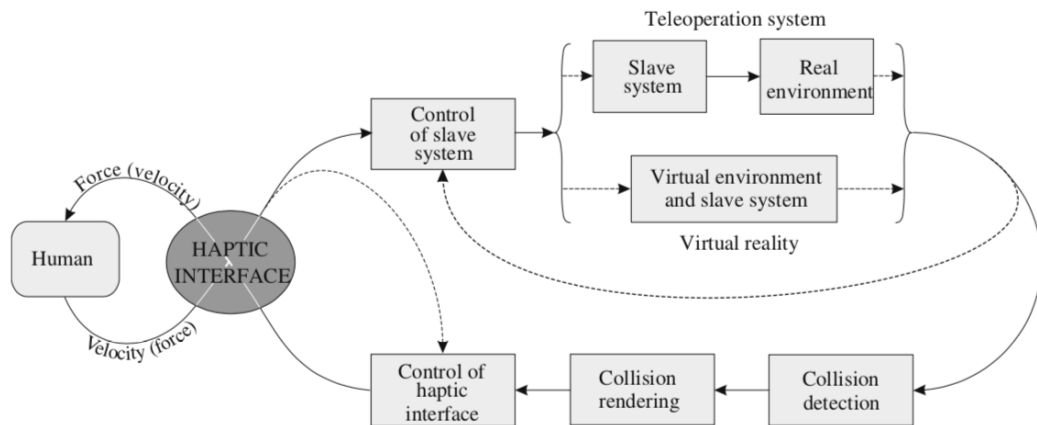


Figure 1.1. Haptic System Interaction Scheme [13]

In order to evaluate the performance of a haptic interface, several metrics are defined in [14], [15]. Among those listed benchmark criteria, range of stable impedances and force bandwidth that can be conveyed transparently become prominent since many researchers mostly seek to increase the performance of them in their studies [16]–[23].

Two main objectives of this thesis are listed below.

The first goal is to design the inertial parameters of chosen haptic interfaces in order to have completely linear equations of motion. As a haptic device, Phantom Premium™ 1.5 (formerly Sensable Phantom Premium 1.5) is examined due to its reputation in the research area. This haptic device has two different variants which possess three and six DOF.

In previous studies, linearization of a spatial serial manipulator having three DOF has been realized; however, Phantom Premium 1.5 contains a special parallelogram which renders it to be a hybrid structure. In addition to that, to the author's knowledge, complete linearization of a spatial six DOF manipulator has not been achieved yet and the possibility of full linearization is not known.

The second objective of this study is to seek a correlation between linearity and performance of a haptic interface. For this purpose, manipulators possessing different linearity levels have been designed by using the concept of LN. Therefore, these manipulators can be compared and a relationship, between linearization and selected performance criteria (such as stable impedance range and transparency bandwidth), can be investigated.

The outline of the thesis is given below.

In the second chapter, derivation procedure for the equations of motion of Phantom Premium 1.5 is presented for the three and six DOF versions. At the beginning of the chapter, the kinematic notation that is used is introduced. Then, the kinematic and dynamic properties such as link lengths, orientations, masses, mass center positions, moments and products of inertia definitions are explained for both variants. In the next section, after the kinematic and dynamic analyses, the equations of motions are derived in closed form. Dynamic analysis is performed by using the Lagrangian Method. In the last section, the equations of motion of the three DOF Phantom device that have been obtained are compared against the previously derived equations of motion in literature.

In the third chapter, the optimization process that is used in order to linearize the equations of motion is presented. In the first part, the concept of LN and its calculation procedure are explained. In the second section, LN of three DOF haptic interfaces is minimized by implementing both analytical and numerical methods. While complete linearization of the three DOF manipulator containing a parallelogram is realized via the analytical method, the numerical method is applied to derive manipulators at different linearity levels (which are to be used in the performance simulations). In the last section of the chapter, LN of a six DOF haptic interface is minimized and the possibility of complete linearization is investigated.

In the fourth chapter, there exists two sections that are dedicated to two different types of performance simulations of a three DOF haptic interface. In the first section of the chapter, a mathematical model of the three DOF haptic interface, compensator and virtual environment; and their Simulink<sup>®</sup> implementation for the stable impedance range simulations are introduced. Then, the calculation methodology of the stable impedance range of a haptic device is given. The assumptions and simulation conditions are also described in this section. In the last part of the first section, the results obtained from the simulations are presented and a correlation is sought between the stable impedance range and LN. In the second section, the transparency bandwidth simulations are discussed. A similar outline for the stable impedance simulations is also followed for the transparency bandwidth calculations. At the beginning of the section, the simulation model is described. Then, the calculation methodology of the transparency bandwidth of a haptic device is given. The adopted assumptions and conditions of the transparency bandwidth simulation are explained as well. At the end of the section, the simulation results and the related assessments are presented.

In the final chapter, conclusions regarding the linearization procedure of three and six DOF haptic interfaces and the performance tests of the manipulators at different linearity levels are presented. Furthermore, recommendations for future work are provided.



## CHAPTER 2

### DERIVATION OF DYNAMIC EQUATIONS OF HAPTIC INTERFACES

In this chapter, the methodology that is used during the derivation of the equations of motions of the haptic devices with three and six DOF configurations is presented. In the first section of the chapter, the kinematic notation used in the derivation is introduced. The kinematic and dynamic properties of the chosen manipulator configurations are explained in Section 2.2. In Section 2.3, kinematic analysis is performed (in order to obtain each link's orientation, angular velocity, origin and mass center position and velocity). In the last part of the chapter, Section 2.4, the equations of motion are obtained by using Lagrange's equations. The validity of the obtained equations of motion is also checked in this section.

#### 2.1. Kinematic Notation

In order to define the robotic manipulator geometry, body-fixed reference frames are attached to each link. Although it is possible to locate these frames arbitrarily, a convention has to be followed for consistency and efficient calculation. Denavit and Hartenberg introduced a convention in order to standardize the selection of these coordinate frames in 1955. Thereafter, many adaptations of this convention have been suggested. Throughout this study, a common version, due to Richard P. Paul, is used. The adapted convention is shown on three successive axes of the serial chain robotic manipulator depicted in Figure 2.1.

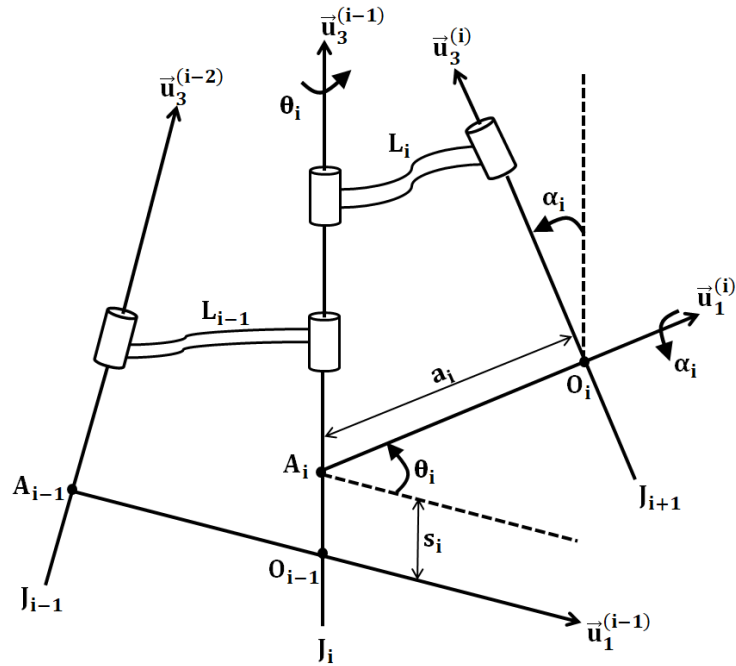


Figure 2.1. Adapted Kinematic Convention

The kinematic convention can be summarized as below.

- Link is a rigid body member of the mechanical system.
- Single-axis joint is a one DOF kinematic element that provides relative motion between links.
- $L_i$  represents link  $i$ .
- $J_i$  represents joint  $i$ .
- $O_i$  represents the origin of link  $i$ .
- Stationary base is link 0.
- The first moving link is link 1.
- Joint between link  $i$  and link  $i-1$  is joint  $i$ .
- $\bar{u}_3^{(i)}$  is the unit basis vector coincident with the axis of joint  $i+1$ .

- $\vec{u}_1^{(i)}$  is the unit basis vector along the common normal between the axis of joints numbered with  $i$  and  $i+1$ .
- $\theta_i$  is the angle between  $\vec{u}_1^{(i-1)}$  and  $\vec{u}_1^{(i)}$  measured about  $\vec{u}_3^{(i-1)}$ . It is called the rotation angle of link  $i$  with respect to link  $i-1$ .
- $a_i$  is the distance from  $\vec{u}_3^{(i-1)}$  to  $\vec{u}_3^{(i)}$  measured along  $\vec{u}_1^{(i)}$ . It is called the effective length of link  $i$ .
- $\alpha_i$  is the angle between  $\vec{u}_3^{(i-1)}$  and  $\vec{u}_3^{(i)}$  measured about  $\vec{u}_1^{(i)}$ . It is called the twist angle of joint  $i+1$  with respect to joint  $i$ .
- $s_i$  is the distance from  $\vec{u}_1^{(i-1)}$  to  $\vec{u}_1^{(i)}$  measured along  $\vec{u}_3^{(i-1)}$ . It is called the offset between link  $i-1$  and link  $i$ .

Besides the DH convention, notations used in order to define vectors, rotation matrices, link-to-link transformation matrices and cross-product matrices are presented below.

Firstly, a vector independent of any reference frame is denoted by  $\vec{v}$ . If one needs to express the vector  $\vec{v}$  in a reference frame, unit basis vector notation specified in equation (2.1) must be used (see Figure 2.2).

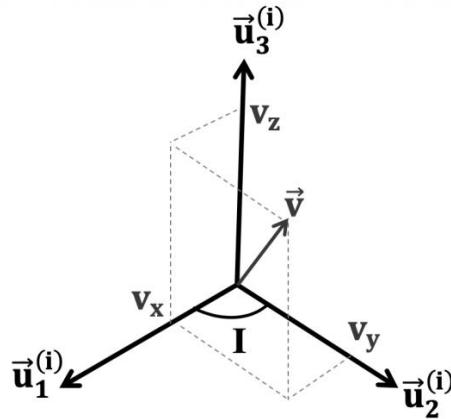


Figure 2.2. The Unit Basis Vectors of Reference Frame I

$$\vec{v} = v_x \vec{u}_1^{(i)} + v_y \vec{u}_2^{(i)} + v_z \vec{u}_3^{(i)} \quad (2.1)$$

where

$v_x$  : The x magnitude of  $\vec{v}$  resolved in Reference Frame I

$v_y$  : The y magnitude of  $\vec{v}$  resolved in Reference Frame I

$v_z$  : The z magnitude of  $\vec{v}$  resolved in Reference Frame I

$\vec{u}_1^{(i)}$  : The x component of the unit basis vector of Reference Frame I

$\vec{u}_2^{(i)}$  : The y component of the unit basis vector of Reference Frame I

$\vec{u}_3^{(i)}$  : The z component of the unit basis vector of Reference Frame I

Secondly, the matrix representation of a vector is needed to be specified. While vector  $\vec{v}$ , resolved in Reference Frame I, is simply denoted by  $\bar{v}^{(i)}$ , for the unit basis vectors (namely  $\vec{u}_1^{(i)}$ ,  $\vec{u}_2^{(i)}$  and  $\vec{u}_3^{(i)}$ ), two different matrix notations are used with respect to the resolved reference frame.

If the unit basis vector of Reference Frame I is resolved in the same reference frame, its matrix representation is denoted by  $\bar{u}_{...}^{(i/i)} = \bar{u}_{...}$ . Therefore, equation (2.1) is obtained in matrix form as below.

$$\bar{v}^{(i)} = v_x \bar{u}_1 + v_y \bar{u}_2 + v_z \bar{u}_3 = \begin{bmatrix} v_x \\ v_y \\ v_z \end{bmatrix} \quad (2.2)$$

If the unit basis vector of Reference Frame I is resolved in another reference frame (i.e., Reference Frame J), its matrix representation is denoted by  $\bar{u}_{...}^{(i/j)}$ . Therefore, equation (2.1) is obtained in the matrix form as below.

$$\vec{v}^{(j)} = v_x \vec{u}_1^{(i/j)} + v_y \vec{u}_2^{(i/j)} + v_z \vec{u}_3^{(i/j)} \quad (2.3)$$

Thirdly, a rotation matrix, which represents rotations about the coordinate axes of a reference frame, is introduced [24]. For instance, Reference Frame I and rotations about its unit basis vectors are shown in Figure 2.3.

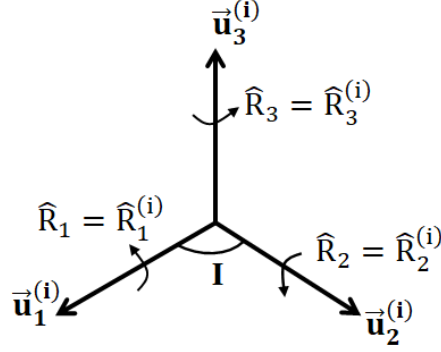


Figure 2.3. Rotations about Unit Basis Vectors

Rotation about  $\vec{u}_1^{(i)}$ , by an angle  $\theta_1$ , can be expressed by the rotation matrix

$$\hat{R}_1(\theta_1) = e^{\vec{u}_1 \theta_1} = \begin{bmatrix} 1 & 0 & 0 \\ 0 & \cos\theta_1 & -\sin\theta_1 \\ 0 & \sin\theta_1 & \cos\theta_1 \end{bmatrix} \quad (2.4)$$

Rotation about  $\vec{u}_2^{(i)}$ , by an angle  $\theta_2$ , can be expressed by the rotation matrix

$$\hat{R}_2(\theta_2) = e^{\vec{u}_2 \theta_2} = \begin{bmatrix} \cos\theta_2 & 0 & \sin\theta_2 \\ 0 & 1 & 0 \\ -\sin\theta_2 & 0 & \cos\theta_2 \end{bmatrix} \quad (2.5)$$

Rotation about  $\vec{u}_3^{(i)}$ , by an angle  $\theta_3$ , can be expressed by the rotation matrix

$$\hat{R}_3(\theta_3) = e^{\vec{u}_3 \theta_3} = \begin{bmatrix} \cos\theta_3 & -\sin\theta_3 & 0 \\ \sin\theta_3 & \cos\theta_3 & 0 \\ 0 & 0 & 1 \end{bmatrix} \quad (2.6)$$

Furthermore, in serial manipulators, one must complete two successive rotations in order to transform Reference Frame I to Reference Frame I+1. To achieve this task, the first rotation must be along the  $\vec{u}_3^{(i-1)}$  axis with a magnitude of  $\theta_i$  and the second rotation must be along the  $\vec{u}_1^{(i)}$  axis with a magnitude of  $\alpha_i$  (see Figure 2.1). Hence, link-to-link transformation matrix,  $\hat{C}^{(i,i+1)}$ , which transforms the reference frame attached to link i to the reference frame attached to link i+1, is obtained by combining two rotation matrices as given in equation (2.7) [24].

$$\hat{C}^{(i,i+1)} = \hat{R}_3(\theta_i)\hat{R}_1(\alpha_i) = e^{\vec{u}_3\theta_i}e^{\vec{u}_1\alpha_i} \quad (2.7)$$

Lastly, the cross-product matrix is explained as follows.

The cross-product of two vectors is given in equation (2.8).

$$\vec{z} = \vec{v} \times \vec{q} \quad (2.8)$$

The matrix representation of equation (2.8), resolved in the Reference Frame I, yields

$$\vec{z}^{(i)} = \tilde{v}^{(i)}\vec{q}^{(i)} \quad (2.9)$$

where  $\tilde{v}^{(i)}$  is, the cross-product matrix of  $\vec{v}^{(i)}$ , given by equation (2.10).

$$\tilde{v}^{(i)} = \begin{bmatrix} 0 & -v_z & v_y \\ v_z & 0 & -v_x \\ -v_y & v_x & 0 \end{bmatrix} \quad (2.10)$$

Note that the matrix form of a vector resolved in Reference Frame I (i.e.,  $\vec{v}^{(i)}$ ) is given by equation (2.2).

## 2.2. Kinematic and Dynamic Properties of Haptic Interfaces

The haptic devices to be investigated are selected to be the three and six DOF configurations of Phantom Premium 1.5. The six DOF configuration is constructed by adding the three DOF model's end-effector a gimbal that provides additional position sensing and force-feedback at pitch, roll and yaw axes. Therefore, the first three DOFs of the three and six DOF haptic manipulators are identical. Their detailed kinematic and dynamic properties are explained in the following sections.

### 2.2.1. Three Degrees of Freedom Haptic Interface

The manipulator is composed of one fixed base, five moving links and five revolute joints. In order to ease the actuation, a parallelogram mechanism is constructed by adding link 2a and link 3a. Link orientations and numberings for the three DOF configuration is presented in Figure 2.4 [25].

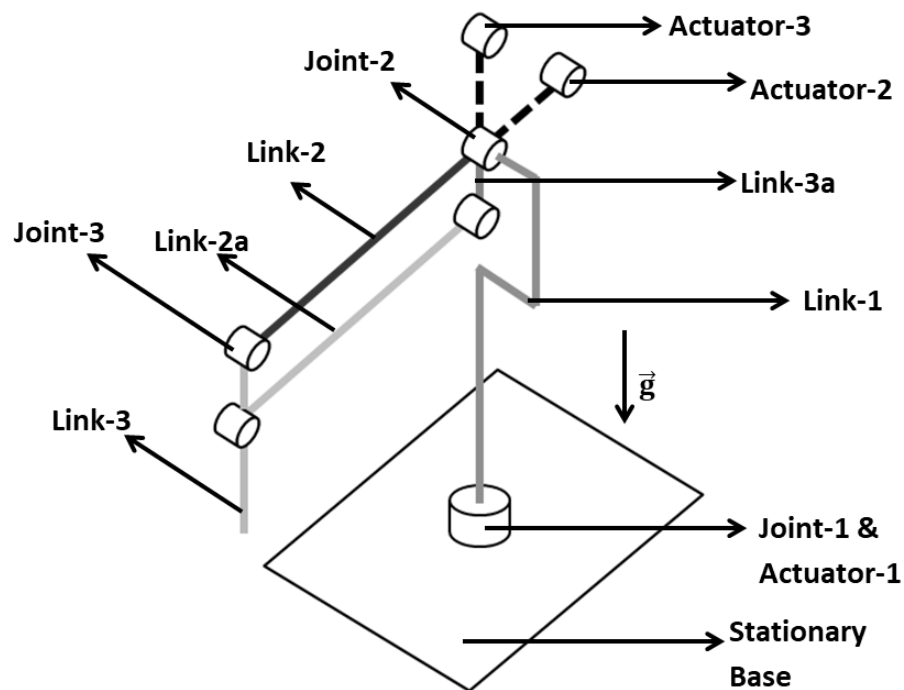


Figure 2.4. Link Orientations and Numberings of the Three DOF Haptic Device

Link lengths corresponding to each link are given in Table 2.1.

Table 2.1. Link Lengths of the Three DOF Haptic Device

Link Number	Parameter	Length [mm]
1	$\ell_1$	300
2	$\ell_2$	215
3	$\ell_3$	170
2a	$\ell_{2a}$	215
3a	$\ell_{3a}$	32.5

The reference frame assignments and the associated four DH parameters are illustrated in Figure 2.5.

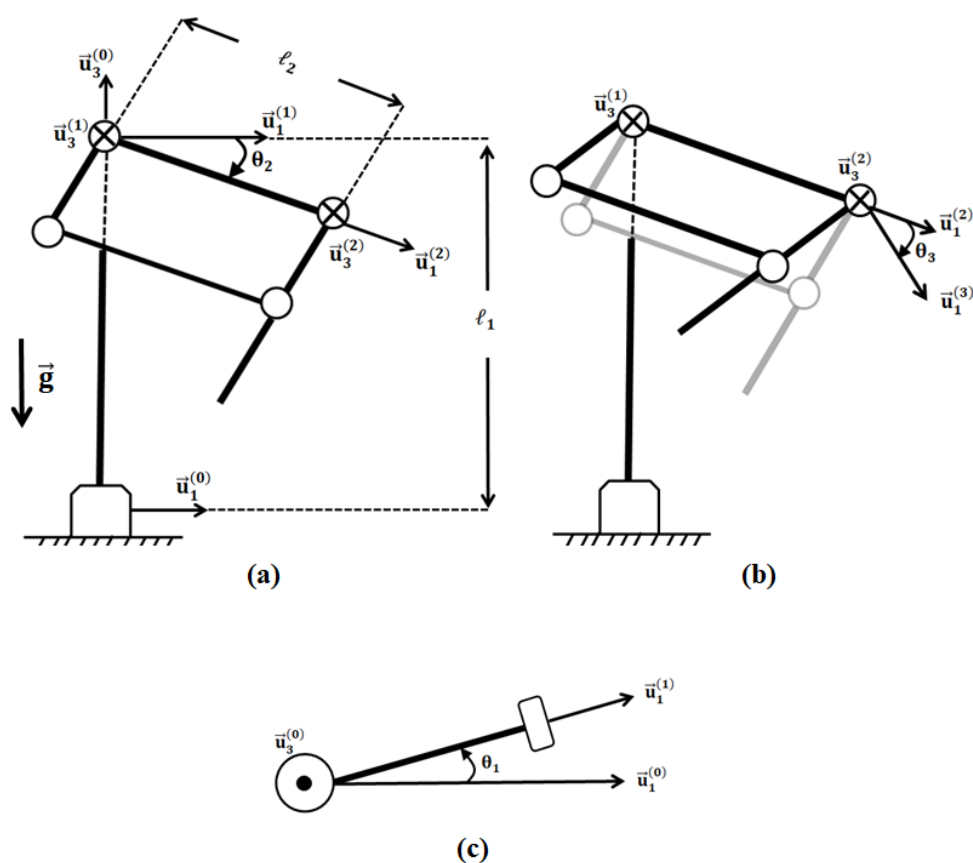


Figure 2.5. Reference Frames and DH Parameters of the Three DOF Haptic Device  
 a) Side View-1 b) Side View-2 c) Top View

The four DH parameters for each link are given in Table 2.2. Note that  $\theta_i$  is the only joint variable since the manipulator does not contain any prismatic joints.

Table 2.2. *DH Parameters of the Three DOF Haptic Device*

$i$	$a_i$	$\alpha_i$	$s_i$	$\theta_i$
1	0	$-\pi/2$	$\ell_1$	$\theta_1$
2	$\ell_2$	0	0	$\theta_2$
3	0	$-\pi/2$	0	$\theta_3$

Besides the kinematic parameters, there are inertial parameters such as masses, mass center positions, moments and products of inertias that affect the dynamics of the manipulator. Although their values are to be determined via optimization, their definitions will be presented at this point. As an example, detailed explanation is given for link  $i$  in Table 2.3.

Table 2.3. *Definition for the Inertial Properties*

Link Property	Explanation
$m_i$	Mass of link $i$
$\bar{\mathbf{r}}_i = \begin{bmatrix} r_{xi} \\ r_{yi} \\ r_{zi} \end{bmatrix}$	X, Y and Z components of the mass center position vector of link $i$ (Defined from the origin of Reference Frame I-1.)
$\hat{\mathbf{I}}_i^{(i)} = \begin{bmatrix} XX_i & -XY_i & -XZ_i \\ -XY_i & YY_i & -YZ_i \\ -XZ_i & -XY_i & ZZ_i \end{bmatrix}$	Inertia tensor of link $i$ (Defined in Reference Frame I and calculated at the center of gravity of link $i$ .)

### 2.2.2. Six Degrees of Freedom Haptic Interface

For the six DOF configuration, only the properties of the additional links are explained since the kinematic and dynamic properties of the first three links are the

same. Orientations and numberings of the last three links are given in Figure 2.6 [26].

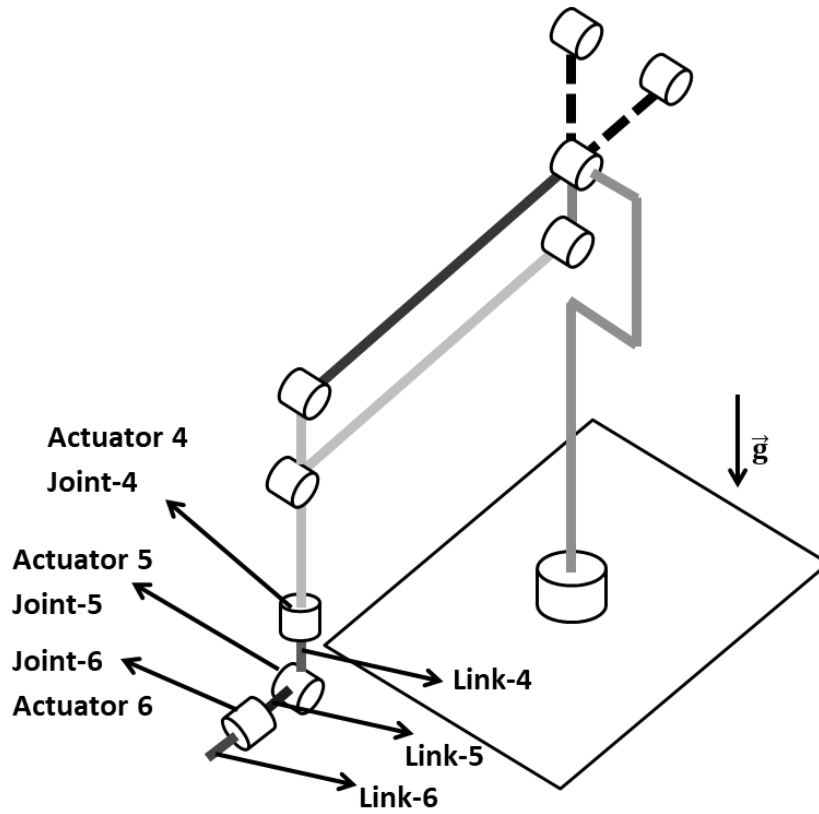


Figure 2.6. Link Orientations and Numberings of the Six DOF Haptic Device

Additional link lengths are provided in Table 2.4.

Table 2.4. Link Lengths of the Six DOF Haptic Device

Link Number	Parameter	Length [mm]
4	$\ell_4$	0
5	$\ell_5$	0
6	$\ell_6$	30

Reference frame assignments and the four DH parameters for the last three links are shown in Figure 2.7.

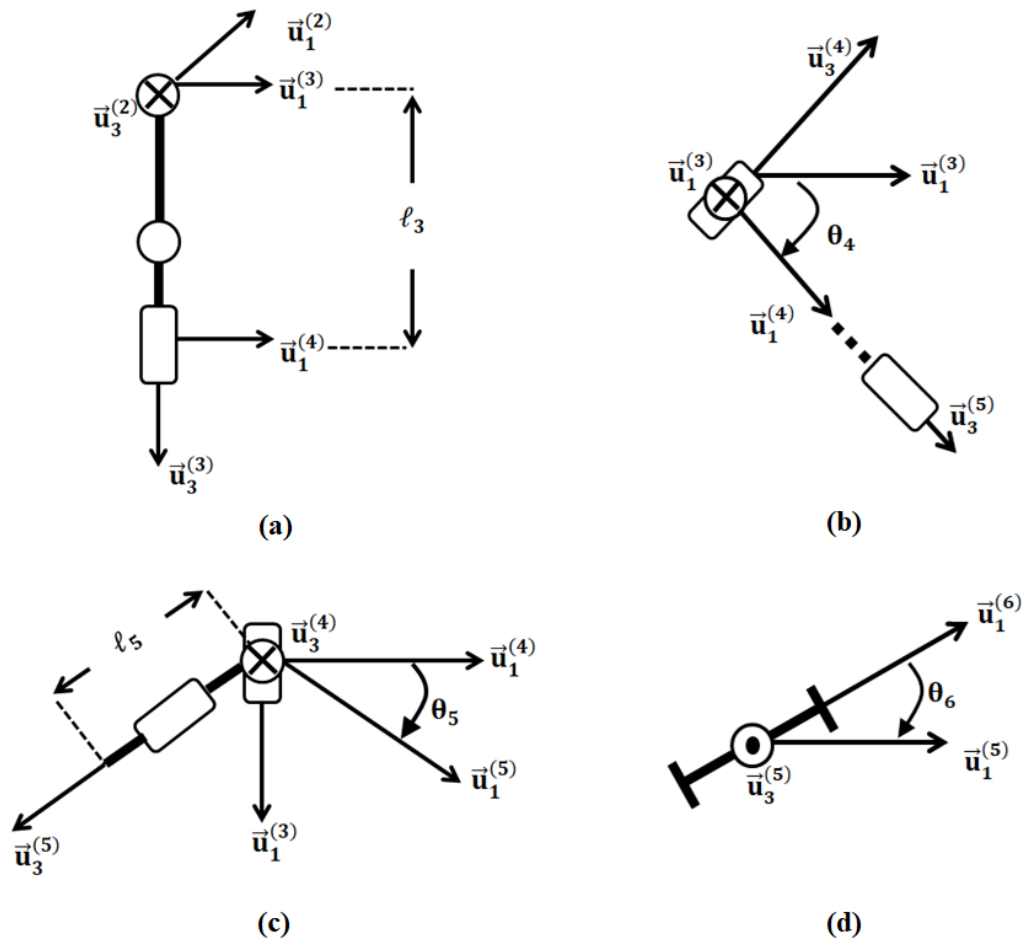


Figure 2.7. Reference Frames and DH Parameters of the Six DOF Haptic Device  
a) Side View-1 b) Top View c) Side View-2 d) End Effector

Note that at the top view given in Figure 2.7 (b),  $\vec{u}_1^{(4)}$  and  $\vec{u}_3^{(5)}$  seem as if they are on the same plane although they are separated with the rotation of joint 5. Besides, the neutral position of joint 5 is obtained by rotating it  $-\pi/2$  radians in the direction of  $\vec{u}_3^{(4)}$ .

Four DH parameters for each of the added links are given in Table 2.5. Similar to the first configuration, the added three joints are all revolute joints, which makes each  $s_i$  a constant (rather than variable) parameter.

Table 2.5. *DH Parameters of the Six DOF Haptic Device*

$i$	$a_i$	$\alpha_i$	$s_i$	$\theta_i$
4	0	$\pi/2$	$l_3$	$\theta_4$
5	0	$-\pi/2$	0	$\theta_5 - \pi/2$
6	0	0	$l_5$	$\theta_6$

For the manipulator's dynamic properties, one may refer to Table 2.3 in Section 2.2.1.

### 2.3. Kinematic Analysis

In order to obtain the Lagrange's equations, the kinematic properties mentioned below need to be calculated [27], [28].

- Link orientations
- Link angular velocities
- Position of link origins and mass centers
- Velocity of link origins and mass centers

#### 2.3.1. Orientation of the Links

The transformation matrix that rotates a vector defined in a link frame to the Base Frame can be calculated, for each link, as below.

Stationary Base

$$\hat{C}^{(0,0)} = \hat{I} = \begin{bmatrix} 1 & 0 & 0 \\ 0 & 1 & 0 \\ 0 & 0 & 1 \end{bmatrix} \quad (2.11)$$

Link 1

$$\hat{C}^{(0,1)} = e^{\tilde{u}_3 \theta_1} e^{\tilde{u}_1 \alpha_1} \quad (2.12)$$

Link 2

$$\hat{C}^{(0,2)} = \hat{C}^{(0,1)}\hat{C}^{(1,2)} \quad (2.13)$$

Link 3

$$\hat{C}^{(0,3)} = \hat{C}^{(0,2)}\hat{C}^{(2,3)} \quad (2.14)$$

Link 2a

It has the same orientation with link 2.

Link 3a

It has the same orientation with link 3.

Link 4

$$\hat{C}^{(0,4)} = \hat{C}^{(0,3)}\hat{C}^{(3,4)} \quad (2.15)$$

Link 5

$$\hat{C}^{(0,5)} = \hat{C}^{(0,4)}\hat{C}^{(4,5)} \quad (2.16)$$

Link 6

$$\hat{C}^{(0,6)} = \hat{C}^{(0,5)}\hat{C}^{(5,6)} \quad (2.17)$$

### 2.3.2. Angular Velocity of the Links

From Figure 2.8, it can be observed that link  $i$  rotates, with respect to link  $i-1$ , along the  $\vec{u}_3^{(i-1)}$  axis with a magnitude of  $\dot{\theta}_i$ .

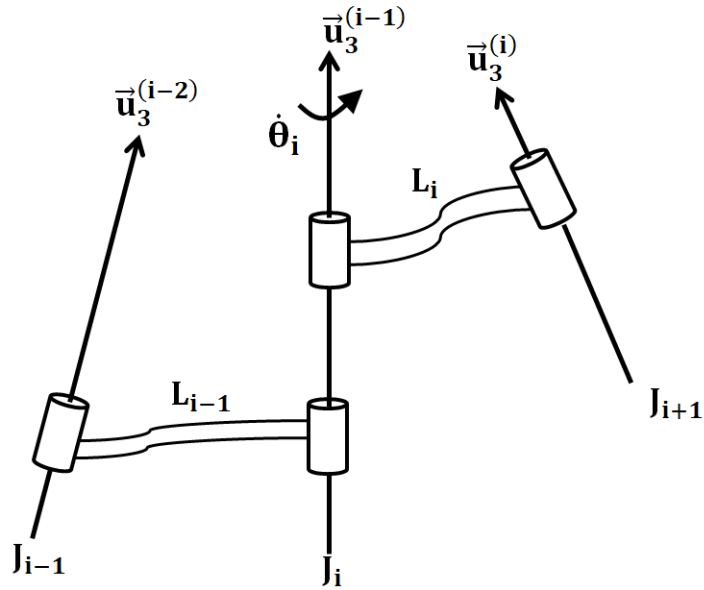


Figure 2.8. Angular Velocity of Link i

So, the rotation rate of link i, with respect to link i-1, can be formulated as

$$\vec{\omega}_{i/i-1} = \dot{\theta}_i \vec{u}_3^{(i-1)} \quad (2.18)$$

Recall that angular velocities can be combined as shown below.

$$\vec{\omega}_{i/0} = \vec{\omega}_{i/i-1} + \vec{\omega}_{i-1/0} \quad (2.19)$$

By inserting equation (2.18) into equation (2.19)

$$\vec{\omega}_{i/0} = \vec{\omega}_{i-1/0} + \dot{\theta}_i \vec{u}_3^{(i-1)} \quad (2.20)$$

Matrix form of equation (2.20) in the Base Frame can be written as

$$\vec{\omega}_{i/0}^{(0)} = \vec{\omega}_{i-1/0}^{(0)} + \dot{\theta}_i \vec{u}_3^{(i-1/0)} \quad (2.21)$$

Then, by transforming  $\bar{u}_3^{(i-1/0)}$  into  $\bar{u}_3$ , one obtains

$$\bar{\omega}_{i/0}^{(0)} = \bar{\omega}_{i-1/0}^{(0)} + \dot{\theta}_i \hat{C}^{(0,i-1)} \bar{u}_3 \quad (2.22)$$

For a more simplified representation, let, now,  $\bar{\omega}_{i/0}^{(0)} = \bar{\omega}_i$ . Hence, equation (2.22) becomes

$$\bar{\omega}_i = \bar{\omega}_{i-1} + \dot{\theta}_i \hat{C}^{(0,i-1)} \bar{u}_3 \quad (2.23)$$

As a result, equation (2.23) can be used for defining the angular velocity of the links where  $i$  is the link number and  $\bar{\omega}_0 = \bar{0}$ . On the other hand, recall that parallel links 2a and 3a have the same angular velocities with link 2 and link 3 respectively.

### 2.3.3. Position of the Link Origins

In Figure 2.9, the vector from the origin of the Base Frame to the origin of link  $i$  is shown. In terms of joint and link parameters, this vector is defined by

$$\vec{P}_i = \vec{P}_{i-1} + s_i \vec{u}_3^{(i-1)} + a_i \vec{u}_1^{(i)} \quad (2.24)$$

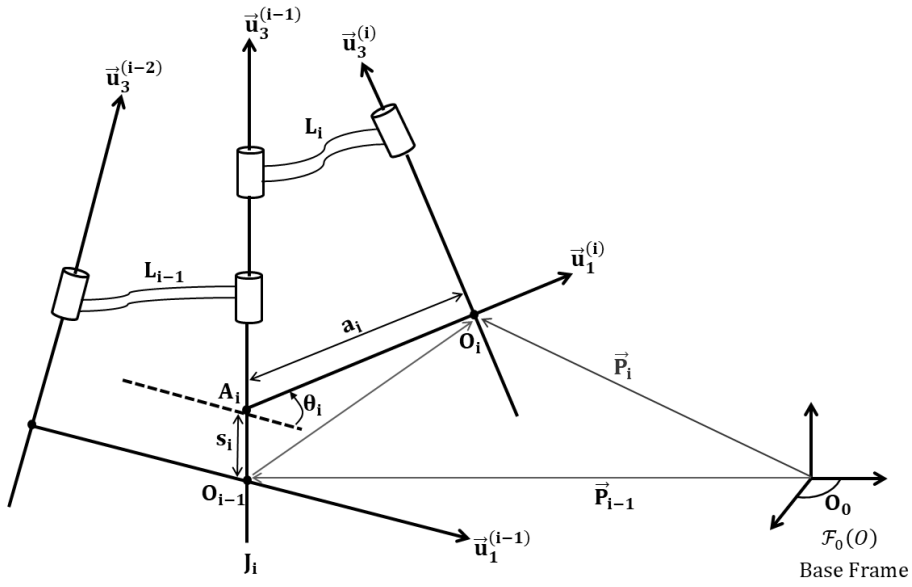


Figure 2.9. Origin Position of Link i

Equation (2.24) can be rewritten in the Base Frame as

$$\bar{P}_i = \bar{P}_{i-1} + s_i \bar{u}_3^{(i-1/0)} + a_i \bar{u}_1^{(i/0)} \quad (2.25)$$

Then, by transforming  $\bar{u}_1^{(i/0)}$  and  $\bar{u}_3^{(i-1/0)}$  into  $\bar{u}_1$  and  $\bar{u}_3$  respectively, one obtains

$$\bar{P}_i = \bar{P}_{i-1} + s_i \hat{C}^{(0,i-1)} \bar{u}_3 + a_i \hat{C}^{(0,i)} \bar{u}_1 \quad (2.26)$$

Finally, the position of the link origin can be calculated, in the Base Frame, from equation (2.26) for all links except for the parallel ones. Note that  $\bar{P}_0 = \bar{0}$  and i refers to the link number.



### 2.3.4. Position of the Link Mass Centers

Location of the mass centers is obtained by adding the  $\vec{r}_i$  vector, defined in Table 2.3, to the previous link's origin.

$${}^c\vec{P}_i = \vec{P}_{i-1} + \vec{r}_i \quad (2.29)$$

Equation (2.29) can be rewritten in the Base Frame by resolving vector  $\vec{r}_i$  in the  $i^{\text{th}}$  Frame as

$${}^c\vec{P}_i = \vec{P}_{i-1} + \hat{C}^{(0,i)}\vec{r}_i \quad (2.30)$$

Except for the parallel links, the mass centers positions are obtained from equation (2.30) where  $i$  refers to the link number. A detailed sketch is shown in Figure 2.11.

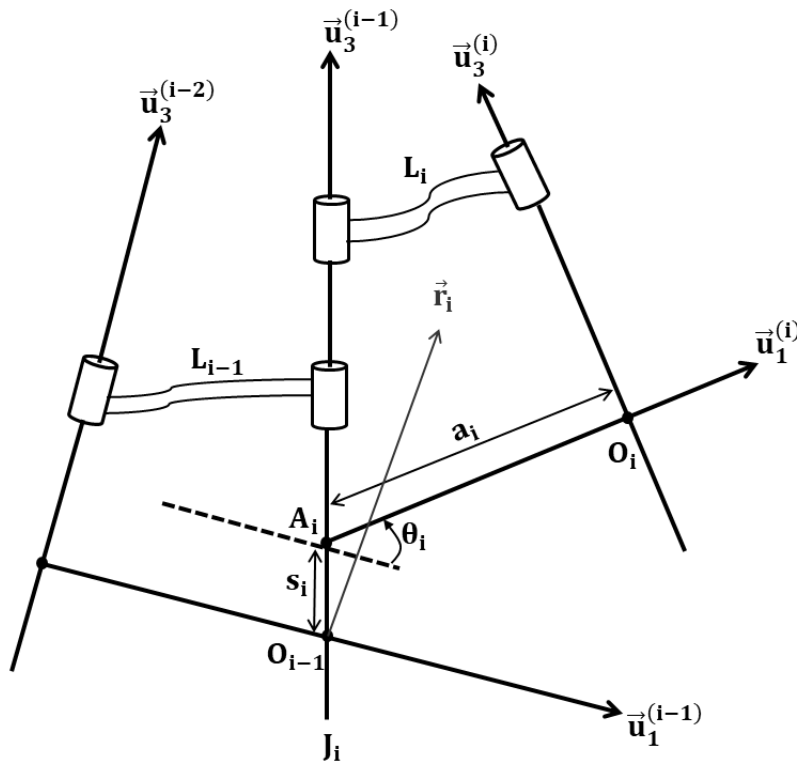


Figure 2.11. Mass Center Position of Link  $i$

Similar to the link origin locations, there is a small difference during the calculation of the mass center positions. This time,  $\vec{r}_i$  vector, defined in the corresponding link frame, is added to link  $i$ 's origin (rather than link  $i-1$ ). Hence, the calculations are performed for the parallel links as given below.

Link 2a

$${}^c\bar{P}_{2a} = \bar{P}_{2a} + \hat{C}^{(0,2)}\bar{r}_{2a} \quad (2.31)$$

Link 3a

$${}^c\bar{P}_{3a} = \bar{P}_{3a} + \hat{C}^{(0,3)}\bar{r}_{3a} \quad (2.32)$$

### 2.3.5. Velocity of the Link Origins

Link origin velocities are obtained by differentiating equation (2.24).

$$D_0(\vec{P}_i) = D_0(\vec{P}_{i-1}) + D_0(s_i\vec{u}_3^{(i-1)}) + D_0(a_i\vec{u}_1^{(i)}) \quad (2.33)$$

where  $D_0$  denotes the vector differentiation in the Base Frame.

The left-hand side of equation (2.33) is equal to  $\vec{V}_i$ , i.e.,

$$D_0(\vec{P}_i) = \vec{V}_i \quad (2.34)$$

The terms on the right-hand side of equation (2.33), on the other hand, can be expressed as follows.

$$\begin{aligned} D_0(\vec{P}_{i-1}) &= \vec{V}_{i-1} \\ D_0(s_i\vec{u}_3^{(i-1)}) &= \dot{s}_i\vec{u}_3^{(i-1)} + s_i\vec{\omega}_{i-1} \times \vec{u}_3^{(i-1)} \\ D_0(a_i\vec{u}_1^{(i)}) &= a_i\vec{\omega}_i \times \vec{u}_1^{(i)} \end{aligned} \quad (2.35)$$

Since there is no prismatic joint in the three and six DOF configurations,  $s_i$  is a constant parameter, which makes  $\dot{s}_i$  zero. Thus, the link origin velocity equation is given by

$$\vec{V}_i = \vec{V}_{i-1} + s_i \vec{\omega}_{i-1} \times \vec{u}_3^{(i-1)} + a_i \vec{\omega}_i \times \vec{u}_1^{(i)} \quad (2.36)$$

When equation (2.36) is rewritten in the Base Frame, one obtains

$$\bar{V}_i = \bar{V}_{i-1} + s_i \tilde{\omega}_{i-1} \hat{C}^{(0,i-1)} \bar{u}_3 + a_i \tilde{\omega}_i \hat{C}^{(0,i)} \bar{u}_1 \quad (2.37)$$

The origin velocity of each link is given by equation (2.37) where the velocity of the stationary base is taken to be zero and  $i$  changes from 1 to 6.

Similarly, the velocity of the origins for link 2a and link 3a are obtained as follows.

Link 2a

$$\bar{V}_{2a} = \bar{V}_2 + \ell_{3a} \tilde{\omega}_3 \hat{C}^{(0,3)} \bar{u}_3 \quad (2.38)$$

Link 3a

$$\bar{V}_{3a} = \bar{V}_{2a} - \ell_{2a} \tilde{\omega}_2 \hat{C}^{(0,2)} \bar{u}_1 \quad (2.39)$$

### 2.3.6. Velocity of the Link Mass Centers

By proceeding similarly, equation (2.40) is obtained by taking derivative of equation (2.29) in order to obtain the mass center velocities.

$${}^c\vec{V}_i = \vec{V}_{i-1} + \vec{\omega}_i \times \vec{r}_i \quad (2.40)$$

Equation (2.40) can be rewritten in the Base Frame as

$${}^c\bar{V}_i = \bar{V}_{i-1} + \tilde{\omega}_i \hat{C}^{(0,i)} \bar{r}_i \quad (2.41)$$

Therefore, each mass center velocity can be obtained via equation (2.41) by changing  $i$  from 1 to 6.

For parallel links, the following formulas must be considered.

Link 2a

$${}^c\bar{V}_{2a} = \bar{V}_{2a} + \tilde{\omega}_2 \hat{C}^{(0,2)} \bar{r}_{2a} \quad (2.42)$$

Link 3a

$${}^c\bar{V}_{3a} = \bar{V}_{3a} + \tilde{\omega}_3 \hat{C}^{(0,3)} \bar{r}_{3a} \quad (2.43)$$

## 2.4. Dynamic Analysis

In order to obtain the equations of motion that reflect manipulator dynamics, Lagrangian Dynamic formulation is used [29]. Firstly, the Lagrangian is constructed by taking the difference of total kinetic and potential energies of the manipulator system.

The kinetic energy of link  $i$  is expressed as

$$k_i = \frac{1}{2} m_i {}^c\bar{V}_i^T {}^c\bar{V}_i + \frac{1}{2} \bar{\omega}_i^T \hat{C}^{(0,i)} \hat{I}_i^{(i)} \hat{C}^{(i,0)} \bar{\omega}_i \quad (2.44)$$

where  ${}^c\bar{V}_i$  and  $\bar{\omega}_i$  are functions of  $\theta_i$  and  $\dot{\theta}_i$ .

The total kinetic energy is the sum of the kinetic energies of the individual links, i.e.,

$$K = \sum_{i=1}^n k_i \quad (2.45)$$

The potential energy of link  $i$  is given by

$$u_i = u_{\text{ref}_i} - m_i \bar{\mathbf{g}}^T {}^C \bar{\mathbf{P}}_i \quad (2.46)$$

where  $\bar{\mathbf{g}}^T = [0 \ 0 \ -g]$ ,  $u_{\text{ref}_i} = 0$  and  ${}^C \bar{\mathbf{P}}_i$  is function of  $\theta_i$ . Also, note that the direction of the gravitational acceleration is along the  $\vec{u}_3^{(0)}$  axis.

The total potential energy of the system is found by summing the individual potential energies of the links, i.e.,

$$U = \sum_{i=1}^n u_i \quad (2.47)$$

The Lagrangian, on the other hand, is defined by

$$\mathcal{L} = K - U \quad (2.48)$$

Hence, the equations of motion of the manipulator can be obtained via the equation

$$\frac{d}{dt} \frac{\partial \mathcal{L}}{\partial \dot{\theta}_k} - \frac{\partial \mathcal{L}}{\partial \theta_k} = \tau_k \quad (2.49)$$

where  $k$  changes from 1 to 3 for the three DOF configuration and 1 to 6 for the six DOF configuration.

By using equation (2.49), the equations of motion are obtained to be

$$\bar{H}(\theta)\ddot{\theta} + \bar{C}(\theta)\dot{\theta}^2 + \bar{G}(\theta) = \bar{\tau} \quad (2.50)$$

where

$N$  : Manipulator's DOF

$\bar{\theta}$  :  $N \times 1$  column matrix of joint variables

$\bar{H}(\theta)$  :  $N \times N$  mass matrix

$H(i,j)$  : The element of  $\bar{H}(\theta)$  in the  $i^{\text{th}}$  row and  $j^{\text{th}}$  column

$\bar{C}(\theta)$  :  $N \times ((N^2 + N)/2)$  matrix of Coriolis and Centrifugal Forces

$C(i,j)$  : The element of  $\bar{C}(\theta)$  in the  $i^{\text{th}}$  row and  $j^{\text{th}}$  column

$\dot{\theta}^2$  :  $((N^2 + N)/2) \times 1$  vector composed of  $\dot{\theta}_1\dot{\theta}_1, \dot{\theta}_1\dot{\theta}_2, \dots, \dot{\theta}_1\dot{\theta}_N, \dot{\theta}_2\dot{\theta}_2, \dot{\theta}_2\dot{\theta}_3, \dots, \dot{\theta}_2\dot{\theta}_N, \dot{\theta}_3\dot{\theta}_3, \dot{\theta}_3\dot{\theta}_4, \dots, \dot{\theta}_N\dot{\theta}_N$

$\bar{G}(\theta)$  :  $N \times 1$  column matrix of gravity terms

$G(i)$  : The  $i^{\text{th}}$  element of  $\bar{G}(\theta)$

$\bar{\tau}$  :  $N \times 1$  actuator torque column matrix

The three components of the actuator torque column matrix (namely  $\tau_1, \tau_2$  and  $\tau_3$ ) of the equations of motion of the three DOF haptic device are presented in Appendix A.1. The six components of the actuator torque column matrix (namely  $\tau_1, \tau_2, \tau_3, \tau_4, \tau_5$  and  $\tau_6$ ) of the equations of motion of the six DOF haptic device are also calculated. These results are obtained by implementing equation (2.49) using the software MATHEMATICA.

After the derivation of the dynamic equations, it is necessary to check their validities. In order to check, at least partially, the derived equations of motion, firstly, equation (2.50) is converted into the form given below.

$$\bar{H}(\theta)\ddot{\theta} + \bar{C}_{cvt}(\theta, \dot{\theta})\dot{\theta} + \bar{G}(\theta) = \bar{\tau} \quad (2.51)$$

In the representation above, the Coriolis and Centrifugal Forces matrix ( $\bar{C}_{cvt}$ ) is defined as an  $N \times N$  matrix elements of which are complex functions of  $\theta$  and  $\dot{\theta}$ . Recall that matrix  $\bar{C}$  is a function of  $\theta$  only.

Note that the elements of  $\bar{C}_{cvt}$  can be expressed in terms of the elements of the  $\bar{C}$  matrix via the equation

$$C_{cvt}(i, j) = C(i, j)\dot{\theta}_j + \sum_{\substack{k=1 \\ k \neq i}}^N C(i, k) \frac{\dot{\theta}_k}{2} \quad (2.52)$$

The following two properties related to the equations of motion are checked in order to check, at least partially, the validity of the obtained results.

- $\bar{H}(\theta)$  should be positive-definite.
- $(\bar{H}(\theta) - 2\bar{C}_{cvt}(\theta, \dot{\theta}))$  should be skew-symmetric.

The first property is derived from the definition of the inertia matrix and the fact that the kinetic energy of the system is zero only if the system is at rest. On the other hand, the second property, usually referred to as the passivity property, is due to the fact that the net energy of the manipulator is conserved in the absence of friction [30].

The results, given in Appendix A.2, indicate that the derived equations of motions satisfy the above two properties.

The derived equations of motion of the three DOF configuration are also compared with the equations of motion given in [25]. In order to compare the results obtained in this study with the ones given in [25], the differences in the joint angle conventions and the definitions of the link reference frames should be tackled with.

Firstly, the joint variables used in this study are converted into the form given in [25] via the equations

$$\begin{aligned}\theta_2 &= -\theta'_{2\text{ref}} \\ \theta_3 &= \theta'_{2\text{ref}} - \theta'_{3\text{ref}}\end{aligned}\tag{2.53}$$

where,  $\theta'_{\dots\text{ref}}$  are the joint angles used in [25].

Secondly, transformation matrix that transforms reference frames attached to Link 1, Link 2 and Link 2a to the reference frame used in [25] are given as

$$\hat{\mathbf{C}}^{(\text{ref\_frame\_set\_1,literature})} = \hat{\mathbf{R}}_1(\pi)\hat{\mathbf{R}}_2(-\pi/2)\tag{2.54}$$

where reference frame set 1 refers to the reference frame attached to Link 1, Link 2 or Link 2a.

Lastly, transformation matrix that transforms reference frames attached to Link 3 and Link 3a to the reference frame used in [25] are given as

$$\hat{\mathbf{C}}^{(\text{ref\_frame\_set\_2,literature})} = \hat{\mathbf{R}}_3(\pi/2)\hat{\mathbf{R}}_1(\pi/2)\tag{2.55}$$

where reference frame set 2 refers to the reference frame attached to Link 3 or Link 3a.

The converted results given in Appendix A.3 indicate that the equations of motion obtained in this study are identical with the equations of motion obtained in [25].



## CHAPTER 3

### OPTIMIZATION OF HAPTIC INTERFACES

In this chapter, the optimization procedure used to render the manipulator dynamics as linear as possible is explained. Section 3.1 starts with the introduction of the LN concept that is an indicator of the degree of linearity of a manipulator. Then, LNs of the three and six DOF configurations are calculated. In Section 3.2, LN of the three DOF case is optimized by using both analytical and numerical methods. As a result of the optimization, it is shown that the three DOF haptic manipulator with a parallelogram mechanism can be fully linearized. To the author's knowledge, this is a novel finding which does not appear in the literature. Manipulators having different degrees of linearity are also obtained in this section. In the last section, Section 3.3, the optimization procedure is applied to the six DOF haptic manipulator and it is shown that complete linearization of this configuration is not possible.

#### 3.1. Definition and Calculation of the Linearity Number

In Section 2.4, the equations of motion that define the manipulator dynamics have been derived in the form given by equation (2.50). Referring to the notation used in equation (2.50), the manipulator will be fully linear if the following conditions are satisfied [12].

- $\bar{H}(\theta)$  is a constant matrix.
- $\bar{C}(\theta)$  is a null matrix.
- $\bar{G}(\theta)$  is a constant column matrix.

Hence, LN of a manipulator is defined via the equation given below [12].

$$LN = \left\{ \sum_{j=1}^N \sum_{i=1}^N H_{ij} E[H(i,j), H(i,j)_{av}] + \sum_{j=1}^{(N^2+N)/2} \sum_{i=1}^N C_{ij} E[C(i,j), 0] + \sum_{i=1}^N G_i E[G(i), G(i)_{av}] \right\} / V \quad (3.1)$$

where

$N$  : DOF of the manipulator

$E[. . . ]$  : Error function that is defined in equation (3.2)

$H(i,j)$  : The element of  $\bar{H}(\theta)$  in the  $i^{\text{th}}$  row and  $j^{\text{th}}$  column

$H(i,j)_{av}$  : Average value of  $H(i,j)$  over the region  $R$

$C(i,j)$  : The element of  $\bar{C}(\theta)$  in the  $i^{\text{th}}$  row and  $j^{\text{th}}$  column

$G(i)$  : The  $i^{\text{th}}$  element of  $\bar{G}(\theta)$

$G(i)_{av}$  : Average value of  $G(i)$  over the region  $R$

$H_{ij}$  : Weighting coefficient of the error function related to  $H(i,j)$

$C_{ij}$  : Weighting coefficient of the error function related to  $C(i,j)$

$G_i$  : Weighting coefficient of the error function related to  $G(i)$

$V$  : Volume of the reachable region  $R$  defined in the joint space

The error function, defined for a scalar function  $f(q)$ , is defined via the equation

$$E(f, f_{av}) = \iint_R [f(q) - f_{av}]^2 dV_q \quad (3.2)$$

where, the average value of the function  $f(q)$  can be calculated via the equation

$$f_{av} = \frac{\iint_R f(q) dV_q}{V} \quad (3.3)$$

The weighting coefficients are user selected parameters and they can be used to define different LNs for different purposes. In this study, for all calculations related to LN, the weighting coefficients are chosen to be unity.

Besides the weighting coefficients, the region  $R$  needs to be specified as well. Since the manipulators that are under consideration are only composed of revolute joints, the region  $R$  is defined as in equation (3.4) by assuming that there are no rotation limitations on the joints.

$$R = \{(\theta_i): 0 \leq \theta_i \leq 2 \pi\} \quad (3.4)$$

for all  $i$ , where  $i = 1, 2, \dots, N$ .

Note that LN is equal to zero when the equations of motion of the manipulator are completely linear. If the degree of linearity of the manipulator decreases, in other words, nonlinearity increases, LN increases as well. LNs of the three and six DOF haptic interfaces are presented in Appendix B.1 and Appendix B.2. Note that these LNs are obtained by using MATHEMATICA.

### **3.2. Optimization of the Three Degrees of Freedom Configuration**

For the three DOF configuration, minimization of LN is realized analytically and numerically. Firstly, the analytical method is used to investigate whether the haptic device can be fully linearized or not. Secondly, the numerical method is applied in order to obtain manipulators to be used in the simulations. In Chapter 4, these manipulators will be employed to investigate the relationship between LN and performance of haptic interfaces.

The three DOF configuration contains totally 55 parameters in its dynamic equations. These parameters are listed below.

- 5 link lengths
- 5 link masses
- $5 \times 3 = 15$  mass center positions
- $5 \times 6 = 30$  inertial parameters

Recall from Section 2.2.1 that the length of the five links has already been fixed. Therefore, there are only 50 design parameters to be utilized during the optimization. These parameters are listed in Table 3.1.

Table 3.1. *Design Parameters of the Three DOF Haptic Device*

Mass	Mass Center Positions	Inertia Tensor
$m_1$	$r_{x_1}, r_{y_1}, r_{z_1}$	$XX_1, XY_1, XZ_1, YY_1, YZ_1, ZZ_1$
$m_2$	$r_{x_2}, r_{y_2}, r_{z_2}$	$XX_2, XY_2, XZ_2, YY_2, YZ_2, ZZ_2$
$m_{2a}$	$r_{x_{2a}}, r_{y_{2a}}, r_{z_{2a}}$	$XX_{2a}, XY_{2a}, XZ_{2a}, YY_{2a}, YZ_{2a}, ZZ_{2a}$
$m_3$	$r_{x_3}, r_{y_3}, r_{z_3}$	$XX_3, XY_3, XZ_3, YY_3, YZ_3, ZZ_3$
$m_{3a}$	$r_{x_{3a}}, r_{y_{3a}}, r_{z_{3a}}$	$XX_{3a}, XY_{3a}, XZ_{3a}, YY_{3a}, YZ_{3a}, ZZ_{3a}$

### 3.2.1. Analytical Method

Consider an n-dimensional constrained minimization problem where the objective function to be minimized is given by

$$f(x_1, x_2, \dots, x_n) \quad (3.5)$$

where  $x_1, x_2, \dots, x_n$  denote the n design variables.

Let the equality and inequality constraints be given by

$$g_i(x_1, x_2, \dots, x_n) = 0 \quad \text{where } i = 1, 2, 3, \dots, m \quad (3.6)$$

$$(x_i)_{\min} \leq x_i \leq (x_i)_{\max} \quad \text{where } i = 1, 2, 3, \dots, r \quad (3.7)$$

$$h_i(x_1, x_2, \dots, x_n) \geq 0 \quad \text{where } i = 1, 2, 3, \dots, p \quad (3.8)$$

Now, the Lagrangian function  $f_l(x_1, x_2, \dots, x_n, \lambda_1, \lambda_2, \dots, \lambda_m)$  may be defined via the equation

$$\begin{aligned} f_l(x_1, x_2, \dots, x_n, \lambda_1, \lambda_2, \dots, \lambda_m) \\ = f(x_1, x_2, \dots, x_n) + \sum_{i=1}^m \lambda_i g_i(x_1, x_2, \dots, x_n) \end{aligned} \quad (3.9)$$

where  $\lambda_i$  denotes the  $i^{\text{th}}$  Lagrange multiplier ( $i = 1, 2, \dots, m$ ).

The critical points of the function  $f(x_1, x_2, \dots, x_n)$  may then be obtained by solving the  $(n + m)$  equations given by

$$\frac{\partial f_l}{\partial x_1} = \frac{\partial f_l}{\partial x_2} = \dots = \frac{\partial f_l}{\partial x_n} = \frac{\partial f_l}{\partial \lambda_1} = \frac{\partial f_l}{\partial \lambda_2} = \dots = \frac{\partial f_l}{\partial \lambda_m} = 0 \quad (3.10)$$

It should be noted that the critical points could correspond to a minimum, a maximum, or an inflection point of the objective function. Furthermore, some of the critical points may lie outside the feasible region defined by the inequalities (3.7) and (3.8). Clearly, such infeasible critical points should be discarded since they do not satisfy the inequality constraints.

Next, one evaluates  $f(x_1, x_2, \dots, x_n)$  at each of the “feasible” critical points. The minimum of the  $f(x_1, x_2, \dots, x_n)$  values thus obtained will correspond to the minimum of the objective function (if it exists) “inside” the region defined by inequalities (3.7) and (3.8). In order to determine the minimum of the objective function “inside” the region and “on” the boundaries of the feasible region defined

by inequalities (3.7) and (3.8), one needs to evaluate the objective function “on” the boundaries of the feasible region defined by inequalities (3.7) and (3.8) as well.

Now, consider the minimization of LN of the three DOF manipulator. The objective function,  $f(x_1, x_2, \dots, x_n)$ , in this case will be the expression for LN which is presented in Appendix B.1. Hence, there will be 50 design variables (i.e.,  $n = 50$ ) which are presented in Table 3.1. Since there are no equality constraints [see equation (3.6)] to be considered, equation (3.9) yields

$$f_1(x_1, x_2, \dots, x_n, \lambda_1, \lambda_2, \dots, \lambda_m) = f(x_1, x_2, \dots, x_n) \quad (3.11)$$

In order to obtain the critical points of the function  $f(x_1, x_2, \dots, x_n)$ , one needs to solve the  $n$  nonlinear equations given by equation (3.10), where  $n = 50$ . To achieve this task, the REDUCE command of MATHEMATICA, which yields a single solution set for the design variables, has been utilized. The obtained solution is presented below.

$$r_{x_2} = -\frac{\ell_2 m_{2a} + \ell_2 m_3 + m_{2a} r_{x_{2a}}}{m_2} \quad (3.12)$$

$$r_{y_2} = 0 \quad (3.13)$$

$$r_{z_2} = \frac{-XZ_2 - XZ_{2a} - \ell_2 m_{2a} r_{z_{2a}} - m_{2a} r_{x_{2a}} r_{z_{2a}} + \ell_2 m_3 r_{y_3}}{m_2 r_{x_2}} \quad (3.14)$$

$$r_{y_{2a}} = 0 \quad (3.15)$$

$$r_{x_3} = 0 \quad (3.16)$$

$$r_{y_3} = \frac{-YZ_3 - YZ_{3a} + \ell_{3a} m_{2a} r_{z_{2a}} - \ell_{3a} m_{3a} r_{y_{3a}} - m_{3a} r_{y_{3a}} r_{z_{3a}}}{m_3 r_{z_3}} \quad (3.17)$$

$$r_{z_3} = -\frac{\ell_{3a} m_{2a} + \ell_{3a} m_{3a} + m_{3a} r_{z_{3a}}}{m_3} \quad (3.18)$$

$$r_{x_{3a}} = 0 \quad (3.19)$$

$$r_{z_{3a}} = \frac{-\ell_2 \ell_{3a} m_{3a} + \ell_{3a} m_{2a} r_{x_{2a}}}{\ell_2 m_{3a}} \quad (3.20)$$

$$YY_{2a} = XX_2 + XX_{2a} - YY_2 - \ell_2^2 m_{2a} - \ell_2^2 m_3 - 2\ell_2 m_{2a} r_{x_{2a}} - m_{2a} r_{x_{2a}}^2 - m_2 r_{x_2}^2 \quad (3.21)$$

$$ZZ_{3a} = XX_3 + XX_{3a} - ZZ_3 + \ell_4^2 m_{2a} + \ell_{3a}^2 m_{3a} + 2\ell_{3a} m_{3a} r_{z_{3a}} + m_{3a} r_{z_{3a}}^2 + m_3 r_{z_3}^2 \quad (3.22)$$

$$XY_2 = -XY_{2a} \quad (3.23)$$

$$YZ_2 = -YZ_{2a} \quad (3.24)$$

$$XY_3 = -XY_{3a} \quad (3.25)$$

$$XZ_3 = -XZ_{3a} \quad (3.26)$$

The solution set given by equations (3.12)-(3.26) indicates that only 15 design variables are restricted. Therefore, the remaining 35 design variables can be selected arbitrarily without disturbing the linearity of the haptic interface. These free design variables are listed in Table 3.2.

Table 3.2. Free Design Parameters of the Three DOF Haptic Device

Mass	Mass Center Positions	Inertia Tensor
$m_1$	$r_{x_1}, r_{y_1}, r_{z_1}$	$XX_1, XY_1, XZ_1, YY_1, YZ_1, ZZ_1$
$m_2$	-	$XX_2, XZ_2, YY_2, ZZ_2$
$m_{2a}$	$r_{x_{2a}}, r_{z_{2a}}$	$XX_{2a}, XY_{2a}, XZ_{2a}, YZ_{2a}, ZZ_{2a}$
$m_3$	-	$XX_3, YY_3, YZ_3, ZZ_3$
$m_{3a}$	$r_{y_{3a}}$	$XX_{3a}, XY_{3a}, XZ_{3a}, YY_{3a}, YZ_{3a}$

After assigning the design parameters provided through equations (3.12)-(3.26), the absolute minimum of LN of the three DOF haptic manipulator becomes zero which yields a fully linear manipulator. The linear equations of motion of the three DOF configuration are given by equation (3.27) given below.

$$\begin{bmatrix} \tau_1 \\ \tau_2 \\ \tau_3 \end{bmatrix} = \begin{bmatrix} K_{11} & 0 & 0 \\ 0 & K_{22} & K_{23} \\ 0 & K_{32} & K_{33} \end{bmatrix} \begin{bmatrix} \ddot{\theta}_1 \\ \ddot{\theta}_2 \\ \ddot{\theta}_3 \end{bmatrix} \quad (3.27)$$

where the “constant” inertia matrix elements  $K_{11}$ ,  $K_{22}$ ,  $K_{23}$ ,  $K_{32}$  and  $K_{33}$  are given by

$$K_{11} = \frac{1}{\ell_2^2 m_3 m_{3a}} \left( 2 \ell_2 \ell_{3a}^2 m_{2a}^2 m_{3a} r_{x_{2a}} + \ell_{3a}^2 m_{2a}^2 r_{x_{2a}}^2 (m_3 + m_{3a}) + \ell_2^2 m_{3a} \left( \ell_{3a}^2 m_{2a} (m_{2a} + m_3) + m_3 (XX_2 + XX_{2a} + XX_3 + XX_{3a} + YY_1 + m_1 r_{x_1}^2 + m_1 r_{z_1}^2 + m_{2a} r_{z_{2a}}^2 + m_2 r_{z_2}^2 + m_{3a} r_{y_{3a}}^2 + m_3 r_{y_3}^2) \right) \right)$$

$$K_{22} = \frac{1}{\ell_2^2 m_2 m_3 m_{3a}} \left( \ell_2^4 m_3 m_{3a} (m_2 m_{2a} + m_{2a}^2 + m_2 m_3 + 2 m_{2a} m_3 + m_3^2) + 2 \ell_2 \ell_{3a}^2 m_2 m_{2a}^2 m_{3a} r_{x_{2a}} + 2 \ell_2^3 m_{2a} m_3 m_{3a} r_{x_{2a}} (m_2 + m_{2a} + m_3) + \ell_{3a}^2 m_2 m_{2a}^2 r_{x_{2a}}^2 (m_3 + m_{3a}) + \ell_2^2 m_{3a} \left( \ell_{3a}^2 m_2 m_{2a} (m_{2a} + m_3) + m_3 (YY_3 m_2 + YY_{3a} m_2 + ZZ_2 m_2 + ZZ_{2a} m_2 + m_2 m_{2a} r_{x_{2a}}^2 + m_{2a}^2 r_{x_{2a}}^2) \right) \right)$$

$$K_{23} = K_{32} = \frac{1}{\ell_2^2 m_3 m_{3a}} \left( \ell_2^2 m_{3a} (YY_3 m_3 + YY_{3a} m_3 + \ell_{3a}^2 m_{2a} (m_{2a} + m_3)) + 2 \ell_2 \ell_{3a}^2 m_{2a}^2 m_{3a} r_{x_{2a}} + \ell_{3a}^2 m_{2a}^2 r_{x_{2a}}^2 (m_3 + m_{3a}) \right)$$

$$K_{33} = \frac{1}{\ell_2^2 m_3 m_{3a}} \left( \ell_2^2 m_{3a} (YY_3 m_3 + YY_{3a} m_3 + \ell_{3a}^2 m_{2a} (m_{2a} + m_3)) + 2 \ell_2 \ell_{3a}^2 m_{2a}^2 m_{3a} r_{x_{2a}} + \ell_{3a}^2 m_{2a}^2 r_{x_{2a}}^2 (m_3 + m_{3a}) \right)$$

While using the design conditions given by equations (3.12)-(3.26), one should note the following remarks.

- The inertial parameters of link 1 (namely,  $m_1$ ,  $r_{1x}$ ,  $r_{1y}$ ,  $r_{1z}$ ,  $XX_1$ ,  $XY_1$ ,  $XZ_1$ ,  $YY_1$ ,  $YZ_1$  and  $ZZ_1$ ) have no effect on the linearity of the three DOF haptic interface. Hence, they can be selected arbitrarily.
- The mass of link 2, link 2a, link 3 and link 3a (namely,  $m_2$ ,  $m_{2a}$ ,  $m_3$  and  $m_{3a}$ ) are also “set” as free design parameters. Hence, they can be selected freely such that the physical realizability conditions are satisfied.
- The mass center positions are given by equations (3.12)-(3.20). If the component of the mass center position vector of a link (i.e.  $r_x$ ,  $r_y$  or  $r_z$ ) does not lie along the link length or the corresponding link’s rotation axis, it must be assigned to zero. In Figure 3.1, the components of the mass center position vector of link 2 are presented.

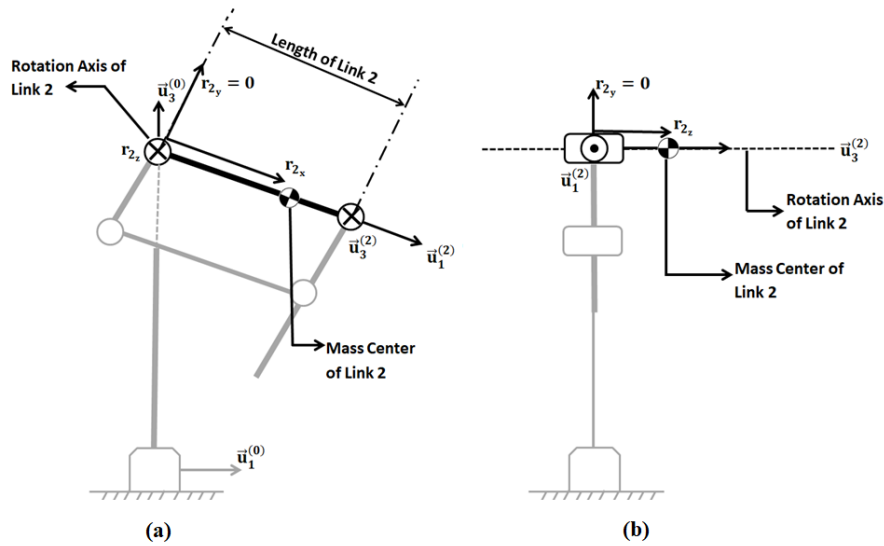


Figure 3.1. Mass Center Position Vector of Link 2 a) Side View b) Front View

As it can be seen from Figure 3.1, the component of the mass center position vector that lies along the link length is  $r_{2x}$ . Furthermore, the component of

the mass center position vector that lies along link 2's rotation axis is  $r_{2z}$ . Therefore, the remaining component (namely  $r_{2y}$ ) is assigned to zero in order to obtain linear equations of motion.

- It should be noted that when equations (3.12)-(3.20) are satisfied, the overall mass center of link 2, link 2a, link 3 and link 3a lies along the  $\vec{u}_3^{(1)}$  axis. This line is defined as the rotation axis of the parallelogram mechanism (see Figure 3.2).

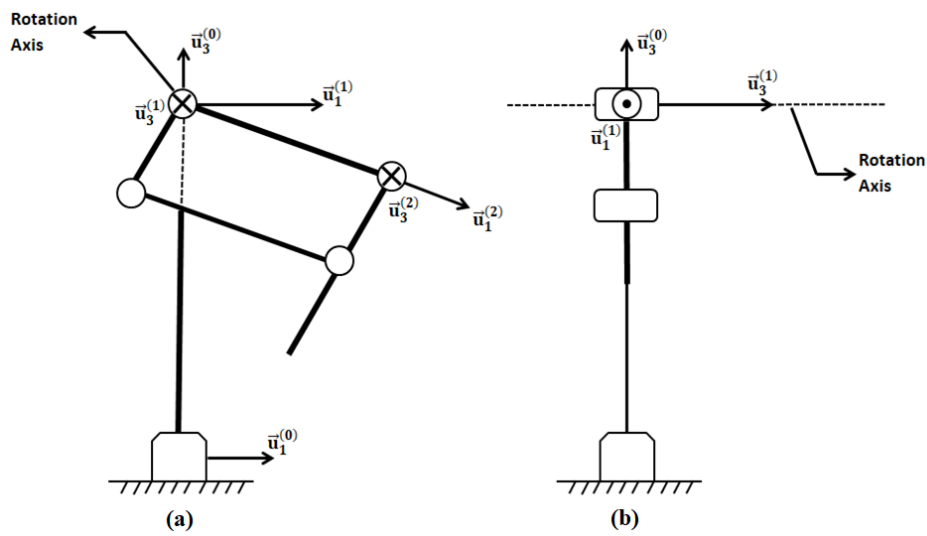


Figure 3.2. Rotation Axis of the Parallelogram Mechanism a) Side View b) Front View

- Limitations on the moments of inertia terms are given by equations (3.21) and (3.22). Although there are additional restrictions on the elements of the inertia tensor due to the inequality constraints, it is always possible to find a physically realizable manipulator set with the available free parameters at the right-hand side of the corresponding equations [free parameters  $XX_2$ ,  $XX_{2a}$ , and  $YY_2$  in equation (3.21) and free parameters  $XX_3$ ,  $XX_{3a}$ , and  $ZZ_3$  in equation (3.22)]. Inequality constraints will be examined later in this section.
- Limitations on the products of inertia terms are given by equations (3.23)-(3.26). If links which have symmetrical cross-sections are used in the design,

the restrictions regarding the products of inertia terms will always be satisfied.

In the remaining parts of this section, the inequality constraints that must be satisfied for a physically realizable manipulator will be determined and the critical points will be checked against these inequality constraints.

The 50 design parameters to be determined during the optimization are the link masses, mass center positions and elements of the inertia tensor. Since they are physical properties, these values cannot be selected arbitrarily if one wants to design a physically realizable manipulator. In order to construct a physically realizable manipulator, the following constraints, derived from the positive definiteness property of the inertia tensor, have to be satisfied (see [12]).

$$\begin{aligned}
& XX_i > 0 \\
& XX_i YY_i - XY_i^2 > 0 \\
& XX_i YY_i ZZ_i - XX_i YZ_i^2 - XY_i^2 ZZ_i - 2XY_i XZ_i YZ_i - XZ_i^2 YY_i > 0
\end{aligned} \tag{3.28}$$

In addition to the constraints regarding the positive definiteness property of the inertia tensor, the upper and lower boundaries for the masses, the mass center positions and the elements of the inertia tensor have been defined in order to design a practical haptic device for the given link lengths.

There are two different limitations on the masses since link 2a and link 3 are considerably lighter than link 2 and link 3a [25]. These limitations are given below.

$$\begin{aligned}
0.15 \leq m_2 \leq 0.30 \text{ [kg]} \\
0.15 \leq m_{3a} \leq 0.30 \text{ [kg]}
\end{aligned} \quad \text{for link 2 and link 3a} \tag{3.29}$$

$$\begin{aligned}
0.02 \leq m_{2a} \leq 0.15 \text{ [kg]} \\
0.02 \leq m_3 \leq 0.15 \text{ [kg]}
\end{aligned} \quad \text{for link 2a and link 3} \tag{3.30}$$

Lower and upper boundaries defined for the mass center positions and for the inertia terms are given below.

$$-0.25 \leq r_i \leq 0.25 \text{ [m]} \quad \text{for the x-y-z directions} \quad (3.31)$$

$$10^{-5} \leq I_i \leq 10^{-2} \text{ [kg m}^2\text{]} \quad \text{for all elements} \quad (3.32)$$

It has been observed that there exists many (actually infinitely many) solutions for the design variables which yields the absolute minimum of LN (which is 0) while satisfying the inequality constraints (3.28)-(3.32). In order to check the critical points given via the 15 equations (3.12)-(3.26) against the inequality constraints (3.28)-(3.32), the FindInstance command of MATHEMATICA, which attempts to find a specified number of numerical solutions to a given system of equations and inequalities, has been employed. One of the solutions thus obtained is given below (for the link lengths fixed as in Table 2.1). The mass center positions of the obtained solution are also presented in Figure 3.3.

$$m_1 = 0.25, m_2 = 0.156, m_{2a} = 0.026, m_3 = 0.031, m_{3a} = 0.242,$$

$$r_{x_1} = 0, r_{y_1} = 0, r_{z_1} = 0.15,$$

$$r_{x_2} = -0.091, r_{y_2} = 0, r_{z_2} = 0,$$

$$r_{x_{2a}} = 0.078, r_{y_{2a}} = 0, r_{z_{2a}} = 0,$$

$$r_{x_3} = 0, r_{y_3} = 0, r_{z_3} = -0.036,$$

$$r_{x_{3a}} = 0, r_{y_{3a}} = 0, r_{z_{3a}} = -0.031,$$

$$XX_1 = 0.009, \quad XY_1 = 0, \quad XZ_1 = 0, \quad YY_1 = 0.009, \quad YZ_1 = 0,$$

$$ZZ_1 = 0.00015,$$

$$XX_2 = 0.00982641, \quad XY_2 = 0, \quad XZ_2 = 0, \quad YY_2 = 0.00488281,$$

$$YZ_2 = 0, ZZ_2 = 0.00488281,$$

$$\begin{aligned}
XX_{2a} &= 0.00488281, & XY_{2a} &= 0, & XZ_{2a} &= 0, & YY_{2a} &= 0.00488281, \\
YZ_{2a} &= 0, & ZZ_{2a} &= 0.00488281, \\
XX_3 &= 0.00481407, & XY_3 &= 0, & XZ_3 &= 0, & YY_3 &= 0.00488281, \\
YZ_3 &= 0, & ZZ_3 &= 0.00488281, \\
XX_{3a} &= 0.00488281, & XY_{3a} &= 0, & XZ_{3a} &= 0, & YY_{3a} &= 0.00488281, \\
YZ_{3a} &= 0, & ZZ_{3a} &= 0.00488281
\end{aligned} \tag{3.33}$$

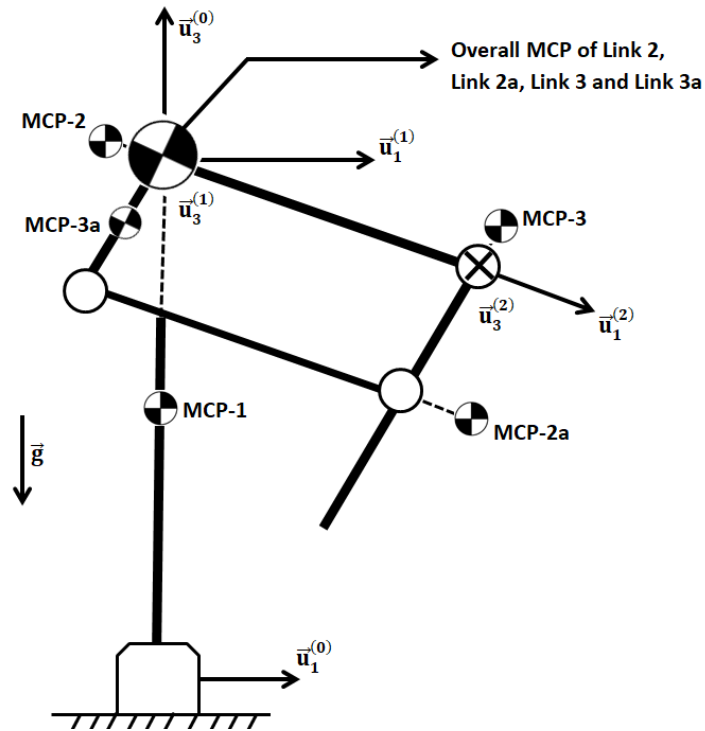


Figure 3.3. Mass Center Positions of the Example Solution

Note that mass values are in [kg], inertia values are in [kg m<sup>2</sup>] and mass center positions are in [m].

### 3.2.2. Numerical Method

One of the objectives of this study is to investigate the relationship between LN and the performance of a haptic device. Therefore, it is necessary to obtain manipulator

sets that possess a specified value of LN. In order to obtain these manipulator sets, the procedure explained below is followed.

Firstly, a set of manipulators with LN equals zero is obtained via the “Differential Evolution Method”, a numerical algorithm that is used for constrained global optimization. Although this method requires more computational power, it is suitable for problems with many local minima. In order to implement the “Differential Evolution Method”, NMINIMIZE command of MATHEMATICA has been used with the options explained as below.

- In this thesis, a set of initial points are automatically generated by default settings of NMINIMIZE. When it is desired to initiate the algorithm with a different set of initial points, the “RandomSeed” option is used. On the other hand, the set of initial points can also be directly defined by the “InitialPoints” option; however, this method is not preferred in this research.
- Size of the population used for evolution is defined by the “SearchPoints” option. Using the default settings of “SearchPoints”, MATHEMATICA generates a population of 50 points if the number of variables used during optimization is greater than 5. However, if the number of variables used during the optimization is less than or equal to 5, then, a population composed of  $10 \times n$  points, where  $n$  is the number of variables used during the optimization, is generated. In this thesis, the default value is selected for the “SearchPoints” option, therefore the size of each population is set to 50.
- In the “Differential Evolution” algorithm, the mutations are obtained by the mutation scheme defined via equation (3.34).

$$x_s = x_w + s(x_u - x_v) \quad (3.34)$$

where  $x_w$ ,  $x_u$  and  $x_v$  are the members of the old population and  $s$  is the scale applied to the difference vector. In this thesis,  $s$  is set to 1 by the “ScalingFactor” option.

- The probability of crossover is defined by the “CrossProbability” option. In this thesis, the default value of 0.5 is used.

Secondly, similar to Section 3.2.1, it is necessary to define additional constraints for the masses, the mass center locations and for the inertia tensors. The upper and lower boundaries associated with these constraints are provided in equations (3.35)-(3.38). While determining these boundaries, the dynamic properties of Phantom Premium 1.5 have been considered [25].

Two separate upper and lower boundaries have been defined for the masses. The upper boundary corresponding to the heavier links (i.e., link 2 and link 3a) is chosen to be five times greater than link 2, the heaviest link of the commercial product. Similarly, the upper boundary corresponding to the lighter links (i.e., link 2a and link 3) is determined to be five times greater than link 3, the lightest link of the commercial product. The lower boundaries corresponding to the heavier and lighter links are chosen to be close to masses of link 3a and link 3 respectively.

$$\begin{aligned} 0.15 \leq m_2 \leq 0.30 \text{ [kg]} \\ 0.15 \leq m_{3a} \leq 0.30 \text{ [kg]} \end{aligned} \quad \text{for link 2 and link 3a} \quad (3.35)$$

$$\begin{aligned} 0.02 \leq m_{2a} \leq 0.15 \text{ [kg]} \\ 0.02 \leq m_3 \leq 0.15 \text{ [kg]} \end{aligned} \quad \text{for link 2a and link 3} \quad (3.36)$$

The upper and lower boundaries corresponding to the mass center positions are chosen to be close to the longest link length, yielding

$$-0.25 \leq r_i \leq 0.25 \text{ [m]} \quad \text{for the x-y-z directions} \quad (3.37)$$

The boundaries of the inertia tensor are taken to be 10 times greater and 10 times smaller than the order of magnitude of the commercial product, yielding

$$10^{-5} \leq I_i \leq 10^{-2} \text{ [kg m}^2\text{]} \quad \text{for all elements} \quad (3.38)$$

One hundred different manipulators, with  $LN = 0$ , are then obtained by seeding random initial points to the optimization algorithm.

In order to obtain a set of manipulators with  $LN = LN_{\text{desired}}$ , the additional constraint

$$LN \geq LN_{\text{desired}} \quad (3.39)$$

is added to the minimization problem. Then, the optimization algorithm is run by seeding random initial points until one obtains 100 manipulators with  $LN = LN_{\text{desired}}$ .

Utilizing the above procedure, and taking  $LN_{\text{desired}}$  to be 0, 0.001, 0.01, 0.1, 1, and 2; a total of 600 manipulators have been obtained. Design parameters of five manipulators yielding a certain  $LN_{\text{desired}}$  are presented in Appendix C (see Table 3.3).

Table 3.3. *Manipulator with Different Degrees of Linearity*

Number of Manipulators	LN	Parameters
100	0	Appendix C.1
100	0.001	Appendix C.2
100	0.01	Appendix C.3
100	0.1	Appendix C.4
100	1	Appendix C.5
100	2	Appendix C.6

### 3.3. Optimization of the Six Degrees of Freedom Configuration

For the six DOF haptic interface, link lengths are also fixed as in Section 3.2. Thus, remaining 80 design parameters listed in Table 3.4 are used during the optimization. The minimization procedure is almost the same as the one explained in Section 3.2.1.

First of all, the constraints from the positive definiteness property of the inertia tensors are defined [see equation (3.28)]. Furthermore, the upper and lower limits for the masses, the mass center positions and the elements of inertia tensor are selected. However, these limits are chosen as coarse as possible this time in order to see whether the equations of motion can be fully linearized regardless of any practical constraint. The imposed constraints are presented below.

Table 3.4. *Design Parameters of the Six DOF Haptic Device*

Mass	Mass Center Positions	Inertia Tensor
$m_1$	$r_{x_1}, r_{y_1}, r_{z_1}$	$XX_1, XY_1, XZ_1, YY_1, YZ_1, ZZ_1$
$m_2$	$r_{x_2}, r_{y_2}, r_{z_2}$	$XX_2, XY_2, XZ_2, YY_2, YZ_2, ZZ_2$
$m_{2a}$	$r_{x_{2a}}, r_{y_{2a}}, r_{z_{2a}}$	$XX_{2a}, XY_{2a}, XZ_{2a}, YY_{2a}, YZ_{2a}, ZZ_{2a}$
$m_3$	$r_{x_3}, r_{y_3}, r_{z_3}$	$XX_3, XY_3, XZ_3, YY_3, YZ_3, ZZ_3$
$m_{3a}$	$r_{x_{3a}}, r_{y_{3a}}, r_{z_{3a}}$	$XX_{3a}, XY_{3a}, XZ_{3a}, YY_{3a}, YZ_{3a}, ZZ_{3a}$
$m_4$	$r_{x_4}, r_{y_4}, r_{z_4}$	$XX_4, XY_4, XZ_4, YY_4, YZ_4, ZZ_4$
$m_5$	$r_{x_5}, r_{y_5}, r_{z_5}$	$XX_5, XY_5, XZ_5, YY_5, YZ_5, ZZ_5$
$m_6$	$r_{x_6}, r_{y_6}, r_{z_6}$	$XX_6, XY_6, XZ_6, YY_6, YZ_6, ZZ_6$

Link masses:

$$10^{-15} \leq m_i \leq 10^{15} \text{ [kg]} \quad \text{for all links} \quad (3.40)$$

Mass center positions:

$$-10^{15} \leq r_i \leq 10^{15} \text{ [m]} \quad \text{for the x-y-z directions} \quad (3.41)$$

Inertia tensor elements:

$$10^{-15} \leq I_i \leq 10^{15} \text{ [kg m}^2\text{]} \quad \text{for all elements} \quad (3.42)$$

Secondly, the Lagrangian function is formed similar to equation (3.5) where the number of design variables is 80.

In order to obtain the critical points of the function  $f(x_1, x_2, \dots, x_n)$ , one needs to solve the  $n$  nonlinear equations given by equation (3.10), where  $n = 80$ . To achieve this task, firstly, the SOLVE command of MATHEMATICA, which attempts to solve a system of nonlinear equations in closed form, has been utilized. Unfortunately, SOLVE has not yielded a closed form solution. MATHEMATICA could not complete its operation when the SOLVE command is evaluated (even though a long computation time have been provided). Hence, it was necessary to resort to a numerical solution via the command FindInstance of MATHEMATICA.

In order to minimize the LN of the six DOF manipulator, FindInstance has been utilized to solve the nonlinear equations [obtained via equation (3.10)] and the inequality constraints that must be satisfied for a physical realizable manipulator. FindInstance has returned an empty set as the solution (see Appendix D) which implies that full linearization of the six DOF haptic interface is not possible (when the link lengths are fixed as in Section 3.2).

## CHAPTER 4

### PERFORMANCE SIMULATIONS OF HAPTIC INTERFACES

In this chapter, simulations, in order to investigate the relationship between the selected performance criteria and the LN of three DOF haptic interface, are performed. Details of the simulations (with respect to the two performance criteria of the haptic manipulator, the stable impedance range and the transparency bandwidth) are explained in two sections.

In Section 4.1, firstly, the mathematical model constructed for the stable impedance range simulations and its implementation on MATLAB Simulink<sup>®</sup> are introduced. Secondly, the calculation methodology of the stable impedance range is explained. The simulation conditions and the adopted assumptions are also summarized in this section. In the last part of Section 4.1, the simulation results are presented and the relationship between the stable impedance range and the LN is examined.

Similar to the previous section, the first part of Section 4.2 contains the mathematical model of the haptic interface and its Simulink implementation for the transparency bandwidth simulations. In the second part of Section 4.2, the calculation procedure, in order to obtain the transparency bandwidth of the haptic manipulator, is explained. Furthermore, the simulation conditions and the assumptions that are used for the transparency bandwidth simulations are provided. Lastly, the simulation results are presented and a correlation is sought between the transparency bandwidth and the LN.

#### 4.1. Stable Impedance Range Simulations

A haptic display is a device that transfers kinesthetic information (e.g., body pose and movement) or tactile stimuli (e.g., texture and temperature) to the user. There are two types of haptic display. The first type, which measures movement and

displays force, is called an impedance display. The other type, which measures force and displays movement, is called an admittance display.

Whether the haptic interface is impedance or admittance, the most important feature of the haptic interface is its interaction with a virtual environment. The virtual environment, which responds to the user's action, is a computer-generated environment of the physical environment. It can be modeled exactly the same as the physical environment or can be a highly simplified model. An ideal haptic interface should represent the virtual environment in exactly the same way.

Regardless of the complexity of the virtual environment, there are two different interaction types between the haptic interface and the virtual environment. A virtual environment may behave as if impedance, i.e., taking the velocity and position as inputs and representing the force, determined based on the physical model, as an output. On the other hand, a virtual environment may behave as if an admittance, i.e., taking the force as an input and representing the velocity or position as an output [31]. In this study, an impedance haptic display (namely, Phantom Premium 1.5), which can render the impedance type of virtual environment, is examined.

The mechanical impedance of the virtual environment is defined as the ratio of force to velocity. During the reflection of the virtual environment to the user, maintaining stability is important. Impedances (of a virtual environment) that a haptic device can reflect to the user without compromising the system stability are defined as the range of stable impedances. The conditions adopted in this study, which provide stable haptic interaction, are given in Section 4.1.2.

The stable impedance range of a haptic interface is obtained via simulations. Before performing the simulations, a proper model has to be formed; a procedure in order to calculate the stable impedance range has to be developed and the simulation conditions have to be determined. In the following sections, the haptic interaction model, the calculation methodology, and the simulation conditions are explained.

Besides, the simulation results and the assessments regarding stable impedance range simulations are given at the end.

#### **4.1.1. Simulation Model**

The three main parts of the simulation model are listed below.

- The three DOF haptic interface
- The compensator
- The virtual environment

##### **4.1.1.1. Model of the Haptic Interface**

Firstly, the equations of motion, which represent the motion of the three DOF haptic interface, are constructed by using Simscape Multibody™ in Simulink. Simscape Multibody is a widely used and approved simulation environment for 3D mechanical systems. Although the design can be made parametrically, the equations of motions are obtained and solved numerically at the background. Since the equations of motion are not explicitly shown to the user, Simscape Multibody cannot be used for the optimization procedure followed in Chapter 3. On the other hand, it is preferred in this section because of being less error-prone due to the usage of blocks (rather than the complicated equations).

Simulink model of the three DOF haptic interface is shown in Figure 4.1. This part of the model refers to the physical manipulator and it is responsible for the forward dynamics computations. Each degree of freedom can be actuated at any desired torque value. Moreover, their angular positions, velocities, and accelerations can be measured via the joint sensors.

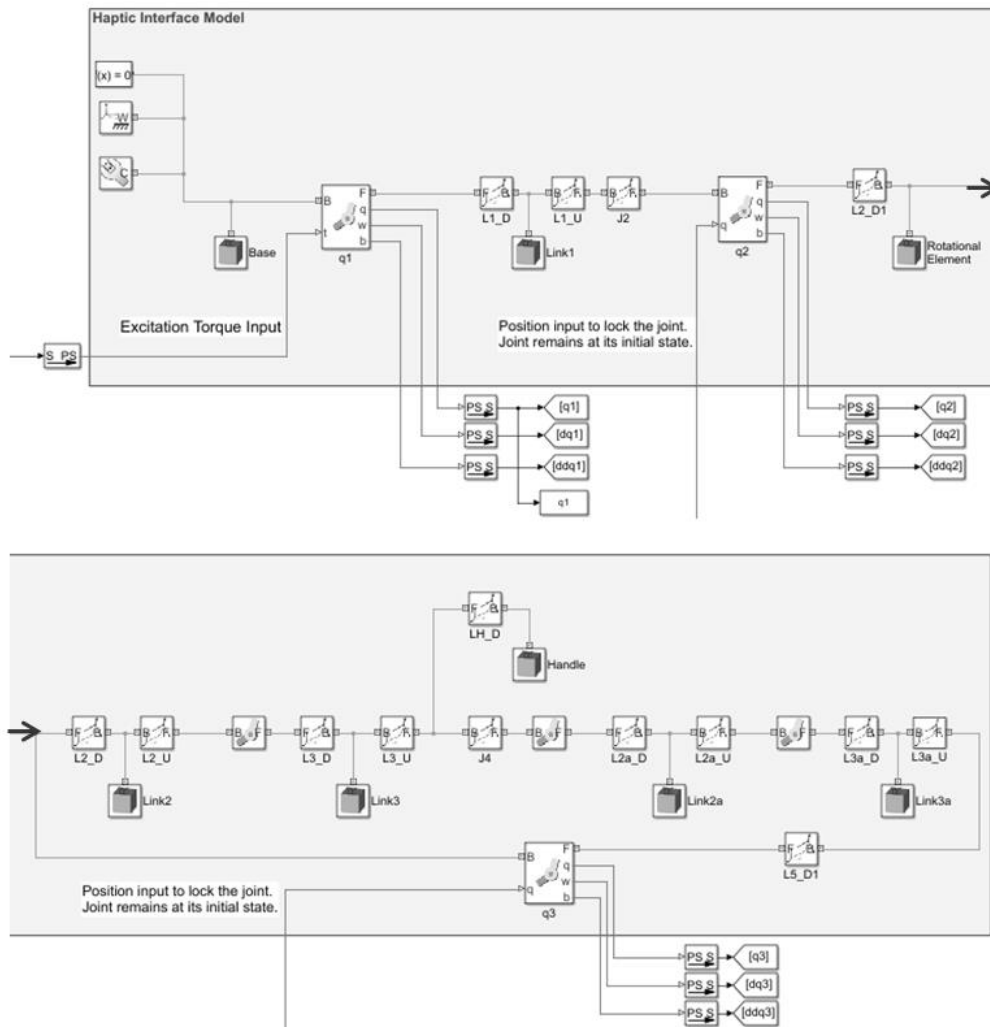


Figure 4.1. Haptic Interface Model for the Stable Impedance Range Simulations

#### 4.1.1.2. Model of the Compensator

The compensator, which is responsible for eliminating the undesirable intrinsic dynamics, is a mathematical model of the physical haptic manipulator. The model-based compensator, implemented for the three DOF haptic interface, is shown in Figure 4.2 and Figure 4.3.

Its block formation is similar to the haptic interface model provided in Figure 4.1. However, a parameter called error percentage, which is used to reflect modeling

errors, multiplies each design variable (i.e., mass, inertia terms and mass center positions) in the compensator. In this way, an error can be introduced if it is desired to see the effects of an imperfect compensator. For instance, the selected mass values will be 90 percent less than the values specified in the haptic interface model (see Section 4.1.1.1), if the error percentage is set as 90.

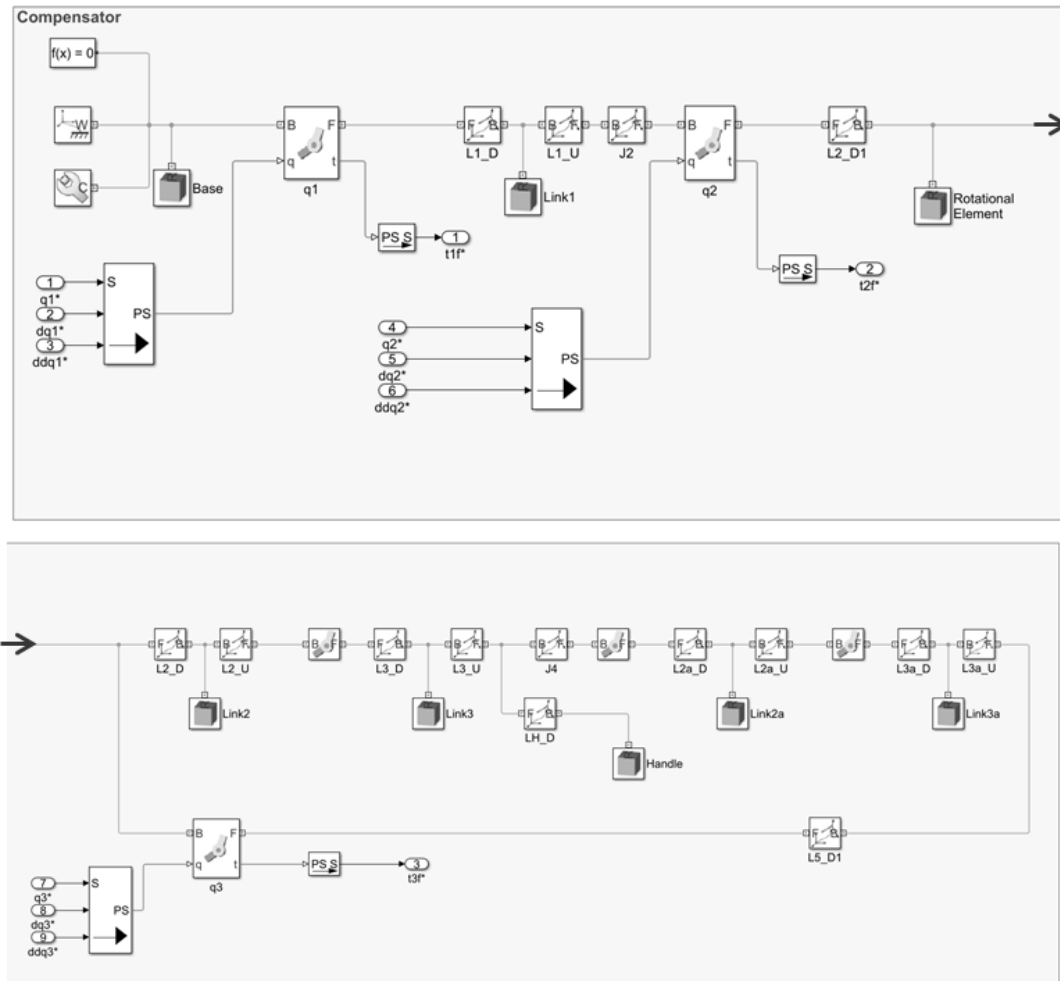


Figure 4.2. Layout of the Compensator Block for the Stable Impedance Range Simulations

This part of the model is related to the controller and it is responsible for the inverse dynamics computations. It calculates the torque to be compensated with respect to the joints' instantaneous angular position, velocity, and acceleration.

An important point that has to be considered in this section is the simulation time step. While the model, which represents the physical manipulator, runs at continuous time domain in the physical world, the compensator is operated in discrete time. Therefore, the sensed quantities such as joint positions, velocities and, accelerations must be sampled. On the other hand, the torque calculated by the compensator must be fed back with zero-order hold (i.e., ZOH). The zero-order hold is a mathematical model that creates the effect of the digital-to-analog converter (i.e., DAC) by holding each sample along the single sample interval.

These actions are implemented in Simulink as given in Figure 4.3.

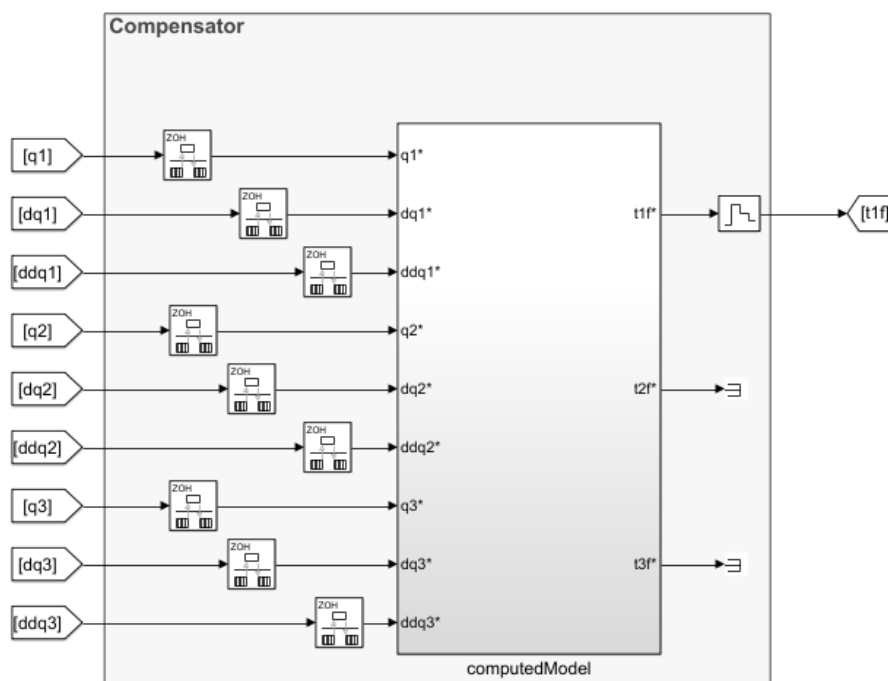


Figure 4.3. Compensator Block for the Stable Impedance Range Simulations

#### 4.1.1.3. Model of the Virtual Environment

Lastly, the virtual environment to be rendered by the haptic interface is introduced into the simulation model. In this study, an elastic virtual wall, modeled as a single freedom spring applied to the joint axis that is to be excited by the user, is chosen as the virtual environment. The spring constant of the virtual wall is initially set to 1 Nm/rad. At each simulation step, this spring constant will be increased by 1 Nm/rad. One can refer to Section 4.1.2 for more details.

According to the difference between the angular position of the connected joint and the equilibrium position of the spring, a torque is applied proportional to the spring constant, in other words, proportional to the impedance of the virtual environment. Similar to the compensator, the sensed joint position is discretized and the torque applied to the joint is turned into an analog signal by using ZOH since the virtual environment is also at the digital side.

The modeled virtual environment is given in Figure 4.4.

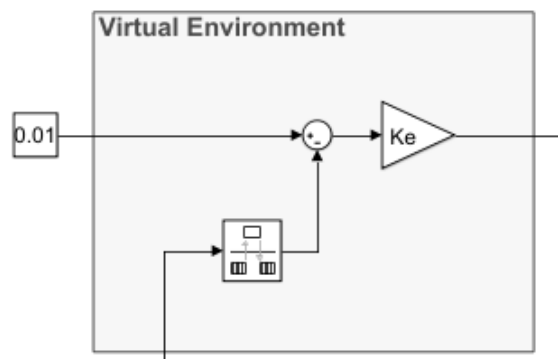


Figure 4.4. Virtual Environment Block for the Stable Impedance Range Simulations

#### 4.1.1.4. Composition of the Simulation Model

In Section 4.1, the three main parts of the simulation model (i.e., the haptic interface, the compensator and the virtual environment) have been explained. In order to generate the haptic interaction, these parts are combined as described below.

Phantom Premium 1.5, the haptic device to be simulated in this study, is an impedance display that does not contain any torque sensor. Therefore, Open-Loop Impedance Control strategy, shown in Figure 4.5, is implemented on its controller [32].

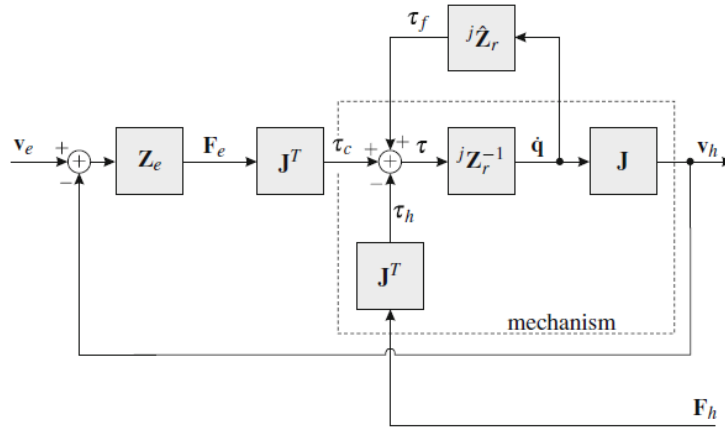


Figure 4.5. Open-Loop Impedance Control Scheme of a Haptic Interface [32]

The parameters used in Figure 4.5 are listed below.

${}^jZ_r$  : The impedance of the haptic display in the joint space. It is defined as the ratio of the joint torque (i.e.,  $\tau$ ) to the joint velocity (i.e.,  $\dot{q}$ ).

${}^j\hat{Z}_r$  : The modeled impedance of the haptic display in the joint space. Due to an estimation error, the modeled impedance can differ from the actual impedance.

$\tau$  : The resulting joint torque applied to the manipulator

$\dot{q}$  : The actual joint velocity of the haptic interface

$\tau_f$  : The feedforward torque which is introduced in order to compensate the device's intrinsic dynamics.

$J$  : The Jacobian Matrix of the haptic display that defines the relationship between the joint velocity and the end-effector velocity

$v_h$  : The resulting velocity of the end-effector (i.e., hand) defined in the task space

$F_h$  : The force that is applied by the user to the end-effector of the haptic display

$\tau_h$  : The joint torque resulting from the force applied by the user to the end-effector of the haptic display

$Z_e$  : The impedance of the virtual environment

$v_e$  : The desired velocity of the end-effector defined in the task space

$F_e$  : The desired force at the haptic display's end-effector defined in the task space

$\tau_c$  : The joint torque resulting from the desired force at the haptic display's end-effector

By adopting the Open-Loop Impedance control scheme explained above and by combining the three sub-components of the model, the complete layout of the simulation environment may be formed in Simulink as shown in Figure 4.6.

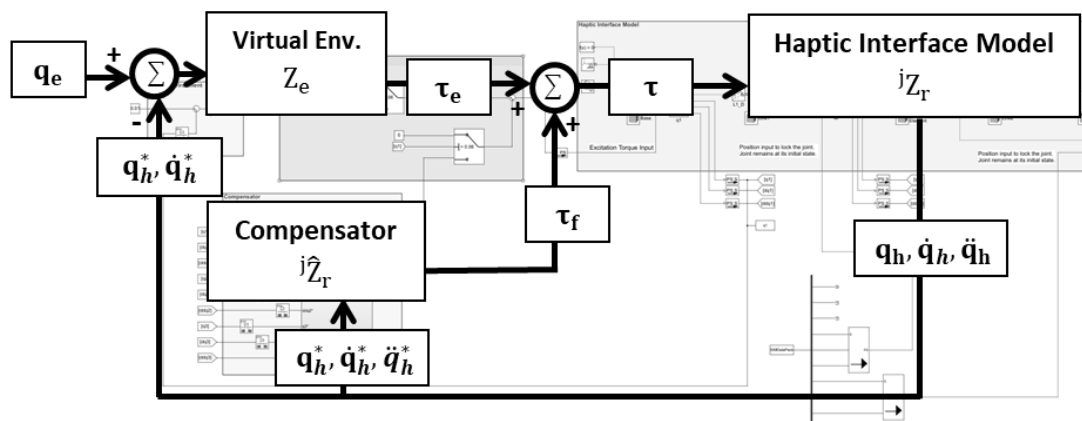


Figure 4.6. Complete Layout of the Simulation Model for the Stable Impedance Range Simulations

The parameters of the block scheme used in Figure 4.6 are listed below.

${}^jZ_r$  : The impedance of the haptic display in the joint space. For the stable impedance range simulations, it corresponds to the haptic interface model given in Section 4.1.1.1.

${}^j\hat{Z}_r$  : The modeled impedance of the haptic display in the joint space. For the stable impedance range simulations, it corresponds to the compensator model given in 4.1.1.2.

$\tau_f$  : The feedforward torque which is calculated by the compensator considering the manipulator's instantaneous motion

$\tau$  : The resulting joint torque, which acts on the manipulator

$q_h$  : The actual joint position of the haptic interface

$\dot{q}_h$  : The actual joint velocity of the haptic interface

$\ddot{q}_h$  : The actual joint acceleration of the haptic interface

$q_h^*$  : The sensed (quantized) joint position of the actual joint position,  $q_h$

$\dot{q}_h^*$  : The sensed (quantized) joint velocity of the actual joint velocity,  $\dot{q}_h$

$\ddot{q}_h^*$  : The sensed (quantized) joint acceleration of the actual joint acceleration,  $\ddot{q}_h$

$Z_e$  : The impedance of the virtual environment. For the stable impedance range simulations, it corresponds to the virtual environment model given in 4.1.1.3.

$q_e$  : The desired joint position

$\tau_e$  : The desired joint torque which acts on the haptic device due to the virtual environment

There is a difference between the block schemes provided in Figure 4.5 and Figure 4.6. The first difference is regarding the workspace that is used. In reference [32], the desired forces and motions are defined in the task space; while the joint space is preferred in this study (in order to see the effect of linearization on each DOF). Thus, the joint velocities and torques given in Figure 4.6 are not converted into the velocities and forces defined in the task space by using the Jacobian Matrix (i.e.,  $J$ ).

#### **4.1.2. Stable Impedance Range Calculation Methodology**

The stable impedance range is defined as the range of impedances of the virtual environment that can be rendered by the haptic device without disturbing stability. This stable impedance range is not unique over the entire workspace of a haptic manipulator. It depends on the position and orientation (i.e., pose) of a haptic manipulator. For different poses, the haptic manipulator may have different stable impedance ranges. Besides the pose of a haptic manipulator, the dynamics due to the interaction with other joints may also change the stable impedance range of the haptic manipulator. For instance, the stable impedance range of the first DOF may vary with respect to the instantaneous position and velocity of the other DOFs (even for the same initial condition of the first DOF).

In order to obtain the range of stable impedance and observe the effect of linearization, two different types of stable impedance range simulations have been performed.

In the first simulation type, a virtual wall is implemented on the first DOF of the three DOF haptic interface. Therefore, a disturbance is only introduced to the first DOF while the second and third DOFs are locked at their initial positions and remain stationary during the simulation. In the second simulation type, the virtual wall is again implemented only on the first DOF of the three DOF haptic interface. Similar to the first simulation type, a disturbance is introduced to the first DOF; however, this time, the second and third DOFs are moved on a predefined path with a predefined velocity.

For both simulation types, the steps of the method are listed below.

- The iteration starts with the impedance value of the virtual environment at 1Nm/rad. The impedance is increased by 1 Nm/rad for the next iteration; therefore, the range of the stable impedances is calculated with the resolution of 1 Nm/rad. This resolution is chosen in order to complete the simulations in a moderate time.
- A torque is applied to the first DOF by the virtual environment due to the initial condition of the virtual spring. The value of the applied torque changes with respect to the angular position of the excited joint. While for the first simulation type, the second and the third DOFs remain stationary at their initial positions during the simulation; for the second simulation type, the second and third DOFs are moved on a desired path with a desired velocity.
- The simulation time is set to be long enough such that the system reaches to steady-state.
- If the observed overshoot is less than 0.012 radian and the system reaches steady-state at the end of the simulation time, the iterated impedance value is taken as stable. 0.012 radian value is chosen heuristically and it is taken to be the same for all simulation cases. Although its value affects the stable impedance range, it is not critical as long as the same condition is applied to all simulation cases (since the purpose of this study is to seek a relationship between the stable impedance range and LN rather than finding the haptic interface's exact stable impedance range).
- The impedance of the virtual environment is increased by one for the next iteration until the overshoot exceeds 0.012 radian or an unstable behavior is observed.
- At the iteration step that the simulated impedance value is considered to be unstable (according to the conditions mentioned above), the value of the previous iteration is taken as the maximum stable impedance. Hence, the

range between 1 Nm/rad and the maximum stable impedance corresponds to the stable impedance range.

Note that, for the impedance values that make the system unstable, the simulations are terminated by MATLAB due to the violation of simulation tolerances. If the simulation is interrupted once, the remaining cases will not be simulated. Therefore, in order to maintain the simulations, the structure shown in Figure 4.7 is employed.

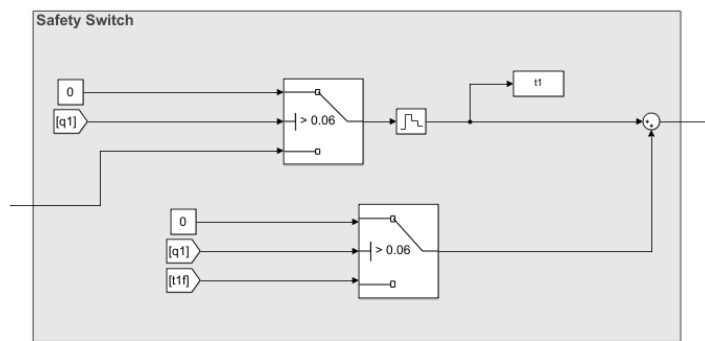


Figure 4.7. Safety Switch Block

The safety switch block is responsible for cutting the applied torque acting on the virtual environment and the compensator off when the simulated joint rotates 0.06 radians (5 times greater than the overshoot) at any direction from its reference point. Therefore, the violation of the simulation tolerances is prevented. Furthermore, if the safety switch block becomes active, the corresponding impedance value will be considered to be unstable.

#### 4.1.3. Simulation Conditions

The specified conditions and the adopted assumptions for the stable impedance range simulations are listed below.

- i. For the stable haptic interaction, the system must contain some amount of physical damping. Therefore, damping is introduced to the joints actuated by the motors.

The value of the inherent damping of each DOF, shown in Table 4.1, is set after trial simulations in order to provide a sensible stable impedance range to the system. These values remain the same throughout all simulation cases. In real applications, virtual couplings are used to arrange the performance of the haptic device [33].

Table 4.1. *Inherent Damping of the Manipulator*

DOF	Value	Unit
1	0.50	Nm/(rad/s)
2	0.50	
3	0.35	

In Figure 4.8, the way the damping is defined for the first DOF in the simulation environment is presented. Note that, in order not to eliminate the required damping of the system, no damping is introduced to the compensator.

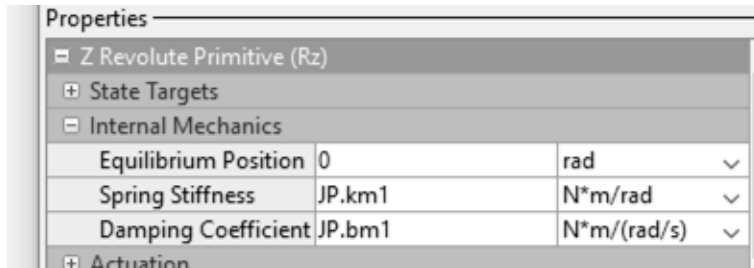


Figure 4.8. Damping at Joint 1

- ii. The virtual wall, modeled with a single spring, is implemented as the virtual environment (see Section 4.1.1.3). During the calculation of the stable impedance range, the initial position of the spring is selected differently than

the equilibrium position of the spring in order to initiate the motion of the haptic interface. The equilibrium position of the spring and the initial condition of the joint position are given in Table 4.2.

Table 4.2. *Initial Condition of the Virtual Wall*

DOF	Equilibrium Position of the Spring	Initial Position of the Joints
1 <sup>st</sup>	0.01 [rad]	0 [rad]
2 <sup>nd</sup>	No Virtual Wall	0 [rad]
3 <sup>rd</sup>	No Virtual Wall	0 [rad]

- iii. Two different types of simulations are performed in order to obtain the stable impedance range and observe the effects of linearization. For both simulation types, stable impedance range of the first DOF is calculated. In the first simulation type, the second and third DOFs remain stationary during the simulation. In the second simulation type, the second and third DOFs are moved on a predefined path with a predefined velocity given in Table 4.3.

Table 4.3. *Conditions of the Simulation Types*

Simulation Type	DOF	Desired Path of the Joints	Desired Velocity of the Joints
1	1 <sup>st</sup>	Disturbance generated by the virtual environment	Disturbance generated by the virtual environment
	2 <sup>nd</sup>	0	0
	3 <sup>rd</sup>	0	0
2	1 <sup>st</sup>	Disturbance generated by the virtual environment	Disturbance generated by the virtual environment
	2 <sup>nd</sup>	$0.52 \times \sin(3\pi \times t)$ [rad]	$1.57\pi \times \cos(3\pi \times t)$ [rad]
	3 <sup>rd</sup>	$0.52 \times \sin(3\pi \times t)$ [rad]	$1.57\pi \times \cos(3\pi \times t)$ [rad]

- iv. In the simulations, the haptic interface (see Section 4.1.1.1) represents the physical world; while the compensator (see Section 4.1.1.2) and the virtual environment (see Section 4.1.1.3) stay at the digital side. Thus, it is necessary to use two different time frames, namely, continuous and discrete.  
Continuous time implies an infinitely small sampling time. However, in the simulation environment, the physical world can only be reflected by selecting the simulation time step small enough. As a result, the time step of the simulation is taken as  $10^{-4}$  seconds by considering the cost of computations. On the other hand, during the conversion of the real world to the virtual one, sensor signals are quantized with 1 kHz sampling rate [34]. Therefore, the calculated torques by the compensator and the virtual environment have to be held and applied at the same value for 10 simulation time steps until new measurements are collected.
- v. The total simulation time is set to 5 seconds, which is enough to reach steady-state conditions.
- vi. In the simulations it is assumed that there is no modeling error in the compensator. However, although the compensator is perfectly modeled, an error still exists in the feedforward torque (applied by the compensator) due to the quantization of the sensor data and the usage of ZOH (see Section 4.1.1.3 for detail).
- vii. The user's hand is not modeled and the hand dynamics, which widens the stable impedance range, is ignored.
- viii. The impedance value is increased by one for every iteration step which limits the resolution of the obtained stable impedance range to 1 Nm/rad.

- ix. All sensors used in the simulations are assumed to be perfect. There are no noise and delay on the measurement of the joint positions, velocities and accelerations.
- x. All links are considered as rigid and friction between the elements is neglected.

#### **4.1.4. Simulation Results and Assessments**

The stable impedance range simulations are performed for the 600 different manipulators given in Table 3.3. In order to investigate the effects of linearization, two different simulation types are realized. Therefore, a total of  $600 \times 2 = 1200$  different simulation cases have been realized. In the first simulation type, the maximum stable impedance values of the first DOF of the three DOF haptic manipulator are obtained. During these simulations, the second and third DOFs are kept stationary at their initial positions. In the second simulation type, similar to the first one, the maximum stable impedance values of the first DOF of the three DOF haptic manipulator are obtained. However, during these simulations, the second and third DOFs are moved on a previously defined path with a previously defined velocity.

In the first part of this section, beeswarm plots are provided for the first simulation type. The x-axis of the graphs corresponds to the six LN values given in Table 3.3. The y-axis of the graphs corresponds to the maximum stable impedance value, the maximum value in the stable impedance range, obtained via the simulations.

In these graphs, the maximum stable impedance values are grouped with respect to the six LNs given in the x-axis and jitter is added (along the x-axis) to the overlapped values in the y-axis (in order to see the distribution of the maximum stable impedance values). Each circle in the graph represents the result of a single simulation. Each LN set contains 100 circles and, a total of 600 circles are plotted in

a single graph. Furthermore, mean values and standard deviations of the maximum stable impedances are also calculated and represented (for each LN) in the graphs.

In the second part of this section, the maximum stable impedance values of the first and second simulation types are presented on the same plot in order to see the difference in the performance of the haptic interface when the remaining joints are not stationary. In these graphs, while the x-axis of the graphs corresponds to the simulation number (performed with 100 different haptic manipulators given in Table 3.3), the y-axis of the graphs corresponds to the maximum stable impedance value. Six separate plots, each containing the maximum stable impedance values of 100 different haptic manipulators, are provided for each LN separately. At the end, the number of haptic manipulators whose performance varies and the number of haptic manipulators whose performance remains the same through the two different simulation types are presented using a bar graph.

#### **4.1.4.1. Results of Simulation Type 1**

In Figure 4.9, the maximum stable impedance values obtained via the stable impedance range simulations for the first simulation type are given with respect to the LN of the three DOF haptic manipulator. The results are summarized in Table 4.4 by providing the highest and the lowest value of the maximum stable impedances for each LN. Furthermore, the mean value and the standard deviation of the maximum stable impedances are also listed for each linearity level.

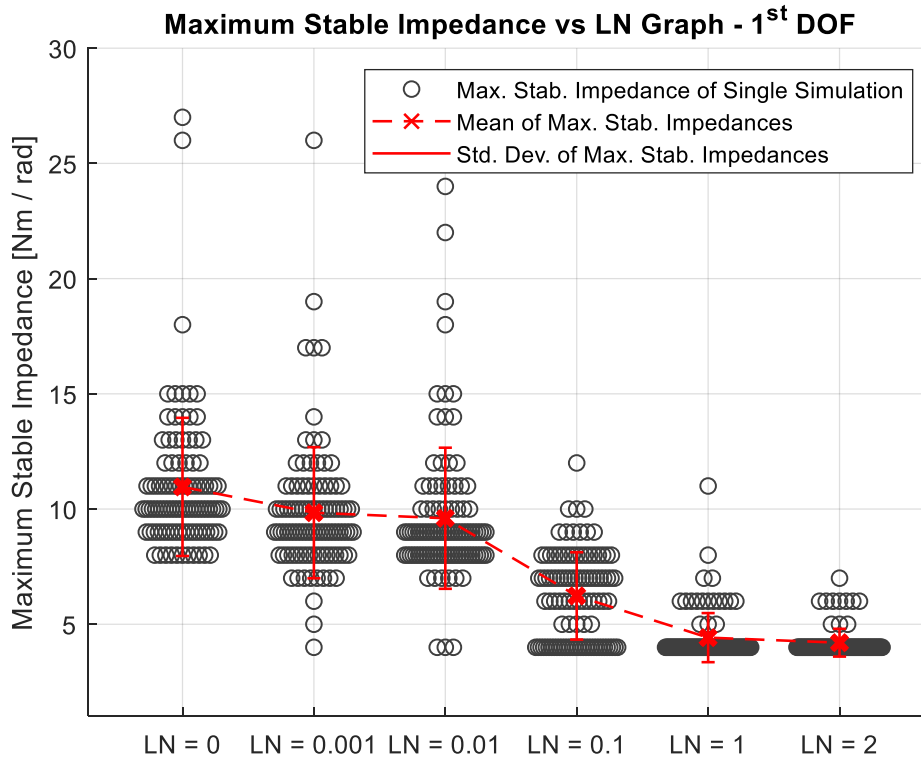


Figure 4.9. Maximum Stable Impedance vs LN Graph for the First DOF – Simulation Type 1

Table 4.4. Results of the Stable Impedance Range Simulations for the First DOF – Simulation Type 1

LN	Maximum Stable Impedance [Nm/rad]	Mean [Nm/rad]	Standard Deviation $1\sigma$ [Nm/rad]
0	8 - 27	10.96	2.99
0.001	4 - 26	9.84	2.85
0.01	4 - 24	9.60	3.06
0.1	4 - 12	6.23	1.89
1	4 - 11	4.42	1.07
2	4 - 7	4.20	0.60

It can be observed from Figure 4.9 and Table 4.4 that the maximum stable impedances which correspond to the same LN fall into a wide range. For instance,

the maximum stable impedance of the haptic interface changes between 8 Nm/rad and 27 Nm/rad for  $LN = 0$ . The magnitude of these deviations decreases, except for the region between  $LN = 0.001$  and  $LN = 0.01$ , when the manipulator becomes less linear. However, the standard deviations are above the resolution of the stable impedance range calculations (i.e., 1 Nm/rad) for  $LN = 0$ ,  $LN = 0.001$  and  $LN = 0.01$ .

Furthermore, the mean value of the maximum stable impedances decreases, which is undesirable for the haptic performance, when the manipulator becomes less linear. In other words, it appears that linearization affects haptic performance positively.

#### **4.1.4.2. Results of Simulation Type 2**

In Figure 4.10, the maximum stable impedance values obtained via the stable impedance range simulations both for the first and second simulation types are given on the same plot with respect to the  $LN$  of the three DOF haptic manipulator.

It can be observed from Figure 4.10 that the maximum stable impedance values obtained from the first and second simulation types are exactly same when haptic interface has completely linear dynamics. With increasing non-linearity in the manipulator dynamics, the maximum stable impedance values obtained for the first and second simulation types begin to differ from each other.

### Maximum Stable Impedance vs LN Graph - Simulation Type 1 and Type 2

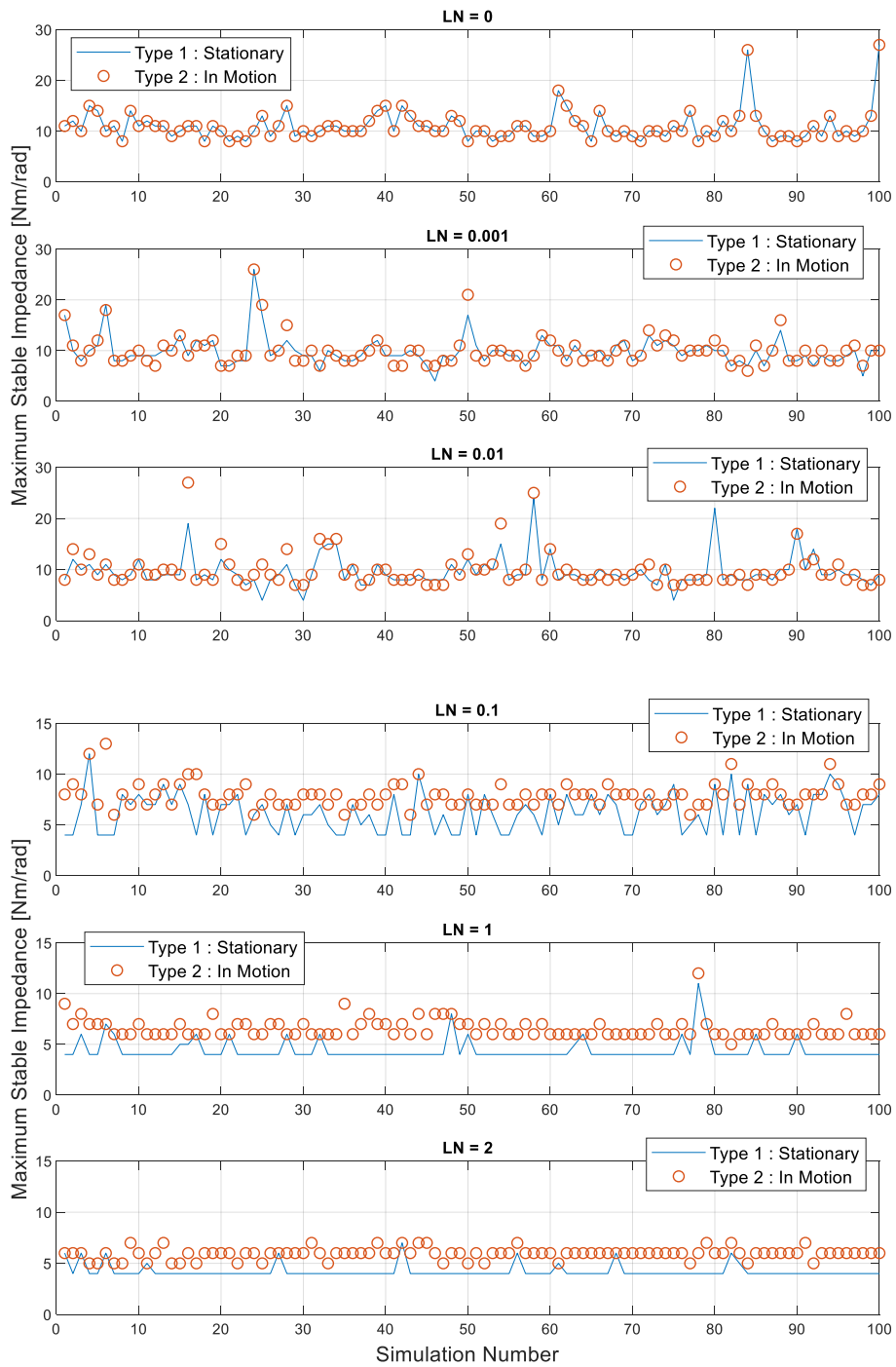


Figure 4.10. Maximum Stable Impedance vs LN Graph – Simulation Type 1 and Type 2

The bar graph, given in Figure 4.11, represents the number of haptic manipulators (among the 100 haptic manipulators for each LN) with different and same maximum stable impedance values when the results of the first simulation type are compared with the results of the second simulation type. It can be observed from Figure 4.11 that when the haptic interface has completely linear dynamics (i.e., LN = 0), two simulation types have exactly the same stable impedance range for 100 haptic manipulators. However, the percentage of haptic manipulators having the same stable impedance range in both simulation types decreases from 54% to 8% while LN increases from 0.001 to 2.

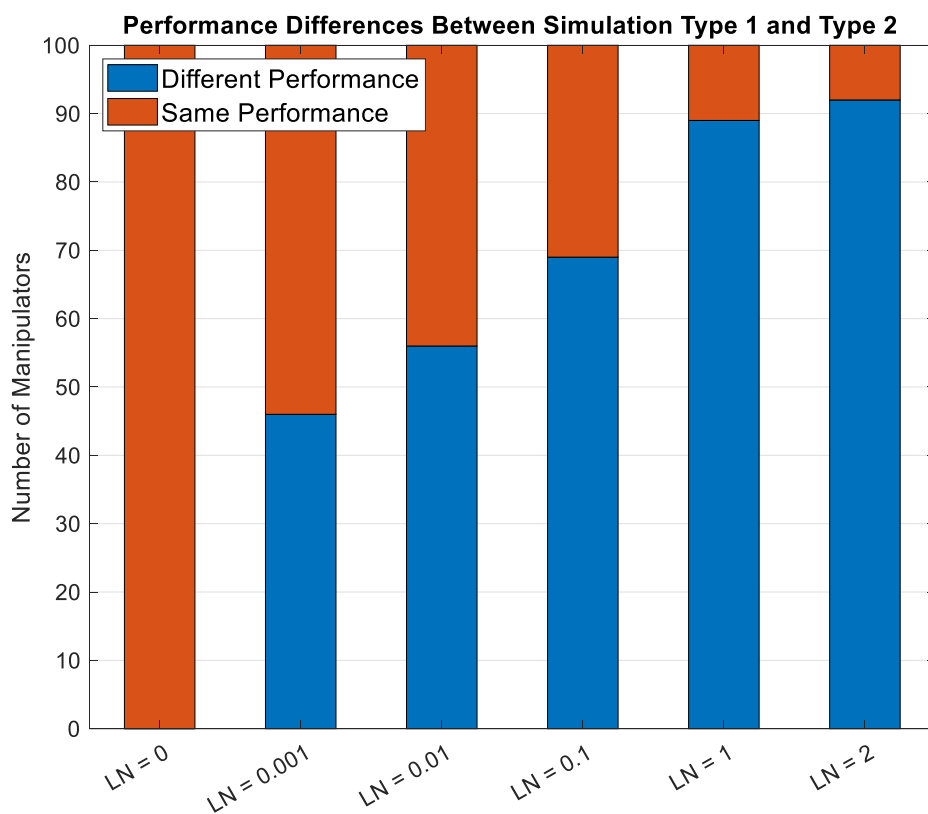


Figure 4.11. Stable Impedance Range Differences Between Simulation Type 1 and Type 2

#### **4.1.4.3. Assessments of Stable Impedance Range Simulations**

In the first simulation type, different manipulators with same degrees of linearity have been compared for six different LNs. From the results provided in Section 4.1.4.1, a clear relationship between stable impedance range and LN cannot be stated. In fact, even haptic manipulators at the same linearity level may have different maximum stable impedance values. However, these results have been obtained from the simulations realized under ideal conditions, which partially reflects the real-world conditions given in Section 4.1.3.

The real effect of the linearization of the equations of motion, however, would possibly appear in practical applications. For instance, avoiding modeling error is impossible in practice; but, in the simulations, no modeling error has been introduced to the compensator. It is expected that the modeling error will be much less for the linear configurations since many parameters do not contribute to the manipulator dynamics after the linearization.

In the simulation environment, the required time for the computations realized in the compensator is not taken into account. The inverse dynamics calculations are performed in the compensator and modeling linear (or more linear) equations of motions in the compensator would, definitely, require much less computation time. Clearly, for a sampling rate, which is as high as 1 kHz, a small delay in the computations will deteriorate the manipulator performance. Therefore, the time spent in the compensator in order to solve the equations of motions is very important. In addition to this, cheaper and less powerful processors can be used as the compensator, if the computations are not extremely time consuming.

In the second simulation type, the performance of same haptic manipulators has been compared under different simulation conditions. From the results provided in Section 4.1.4.2, it can be observed that the haptic manipulators with complete linear equations of motion have exactly the same performance (both for the first and second simulation types) regardless of pose of the manipulator and instantaneous

dynamics of the other links. On the other hand, as the non-linearity increases, the difference in the results of two different simulation types increases as well.

Therefore, linearization of the manipulator dynamics eliminates (for fully linear manipulator dynamics) or reduces (for partially linearized manipulator dynamics) the effects of initial conditions and instantaneous dynamics of the other DOFs on the performance of the haptic interface. Hence, it appears that the more linear haptic interface is, the more uniform (over the workspace) the performance of the haptic interface will become.

## **4.2. Transparency Bandwidth Simulations**

Transparency is a concept that shows how the forces resulting from the virtual environment are conveyed to the user. It is dependent on both the magnitude and frequency of the force desired to be reflected. For instance, the device dynamics is more dominant when the virtual environment has low impedance and applies smaller forces to the manipulator compared to the device dynamics. Conversely, the transparency is affected less from the device's intrinsic dynamics while rendering higher impedances, which applies larger forces to the manipulator compared to the device dynamics. On the other hand, lower frequencies are reflected with a higher transparency, but the transparency value decreases when higher frequencies are transmitted.

Transparency is the transfer function between the transmitted impedance and the desired impedance. This transfer function is defined as the ratio of the transmitted impedance, impedance value sensed by the user, and the actual impedance of the virtual environment. If the haptic device is perfectly transparent, the impedance of the virtual environment and the impedance sensed by the user are identical, which makes the value of the transfer function unity [23].

Since transparency is a frequency dependent property, the concept of transparency bandwidth has been introduced in order to determine the frequency range that a haptic device is considered as transparent. For the perfectly transparent haptic

interface, the magnitude of frequency response of the transparency transfer function is 0 dB. However, a haptic device is also considered as transparent as long as the magnitude of the transparency transfer function remains within  $\pm 3$  dB. Therefore, transparency bandwidth is defined as the frequency value that the magnitude of transparency transfer function crossovers  $\pm 3$  dB [23]. Detailed conditions for a haptic interaction to be considered as transparent can be found in Section 4.2.2.

In an ideal case, the transparency bandwidth has to be evaluated throughout the stable impedance range. However, in order to see the relationship between LN and transparency bandwidth, a single impedance value is selected and the corresponding transparency bandwidth is calculated for manipulators with different LNs. If a meaningful relationship is detected between them, additional simulations need to be performed for the whole stable impedance range.

The layout of Section 4.2 is similar to Section 4.1. In this section, a model constructed for the simulations, transparency bandwidth calculations, simulation conditions, adopted assumptions, obtained results and assessments are presented. Since there are several common subjects for both the stable impedance range and the transparency bandwidth simulations, by considering the information given in Section 4.1, only the differences between them are explained in the following sections.

#### **4.2.1. Simulation Model**

Similar to Section 4.1.1, the three main parts of the simulation model are listed below.

- The three DOF haptic interface
- The compensator
- The virtual environment

While the model constructed for the compensator is exactly the same, the haptic interface and the virtual environment models contain some differences.

#### 4.2.1.1. Model of the Haptic Interface

In stable impedance range simulations, a single joint (the first DOF) is excited with the torque resulting from the virtual environment while the remaining joints are either locked at their initial positions or rotated with specified velocities according to the selected simulation type. For the transparency bandwidth simulations, a predefined path is defined for the first DOF. Similar to the stable impedance range simulations, the remaining joints either remain stationary at their initial positions or move with specified velocities according to the selected simulation type. The block scheme of the haptic interface model is presented in Figure 4.12.

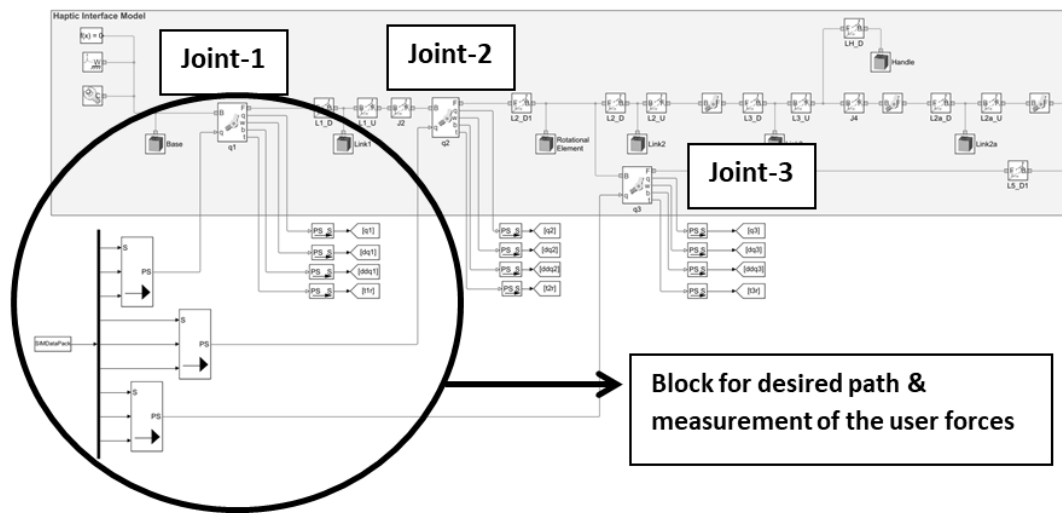


Figure 4.12. Haptic Interface Model for the Transparency Bandwidth Simulations

The haptic interface model, provided in Figure 4.12, is similar to the one given in Figure 4.1. However, in this case the manipulator follows a desired path for the transparency bandwidth simulations. The desired path is defined in Simulink as presented in Figure 4.13.

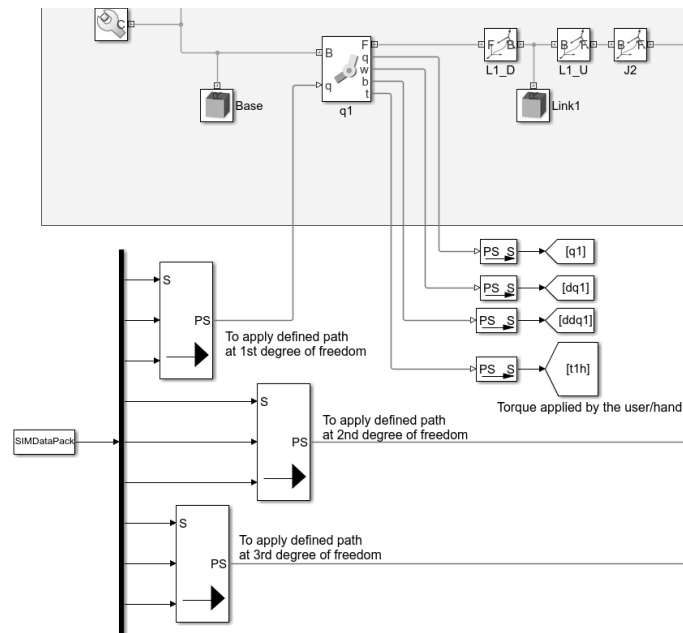


Figure 4.13. Application of the Desired Path and Measurement of the User Forces

Additionally, the force, generated by the user while moving the haptic interface and interacting with the virtual environment, must be measured in order to compute the difference between the actual force transmitted to the user and the desired force that the user must apply at a certain position of the virtual environment.

The measurement of the user force in the simulation environment is also presented in Figure 4.13.

#### 4.2.1.2. Model of the Compensator

The compensator model used for the transparency bandwidth simulation is identical with the one given in Section 4.1.1.2.

#### 4.2.1.3. Model of the Virtual Environment

Two separate virtual environment models are constructed for transparency bandwidth simulations.

The ideal virtual environment model, given in Figure 4.14, is only utilized in order to obtain the desired impedance value. It uses the actual sensor position and applies the force at the actual simulation time step.

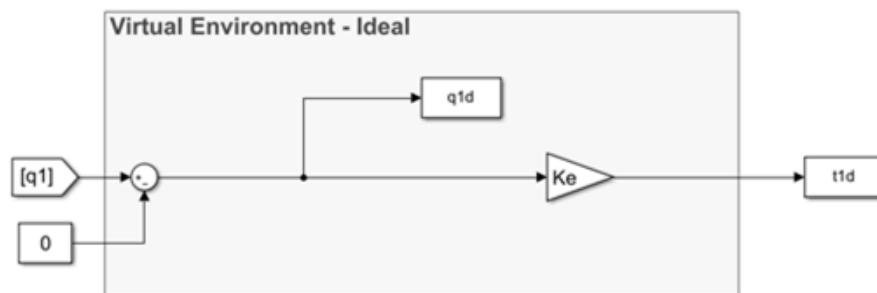


Figure 4.14. Ideal Virtual Environment Model for the Transparency Bandwidth Simulations

The implemented virtual environment model, given in Figure 4.15, is constructed similar to the virtual environment model explained for the stable impedance range simulations in Section 4.1.1.3.

Different from the ideal virtual environment model, the implemented one uses quantized data obtained from the sensors and ZOH during the force reflection, which may cause an error, depends on the frequency of the hand movement, between the desired force and the transmitted force.

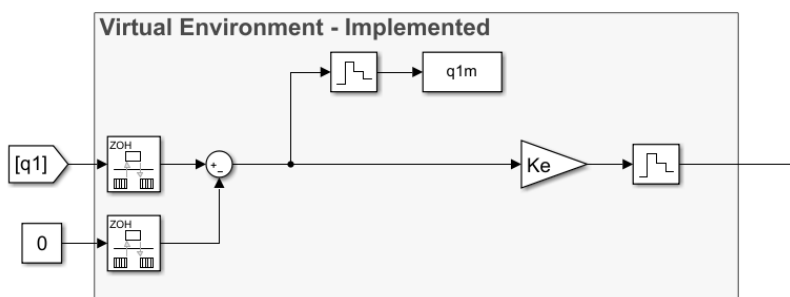


Figure 4.15. Implemented Virtual Environment Model for the Transparency Bandwidth Simulations

#### 4.2.1.4. Composition of the Simulation Model

Similar to Section 4.1.1.4, the complete layout of the simulation model is shown in Figure 4.16.

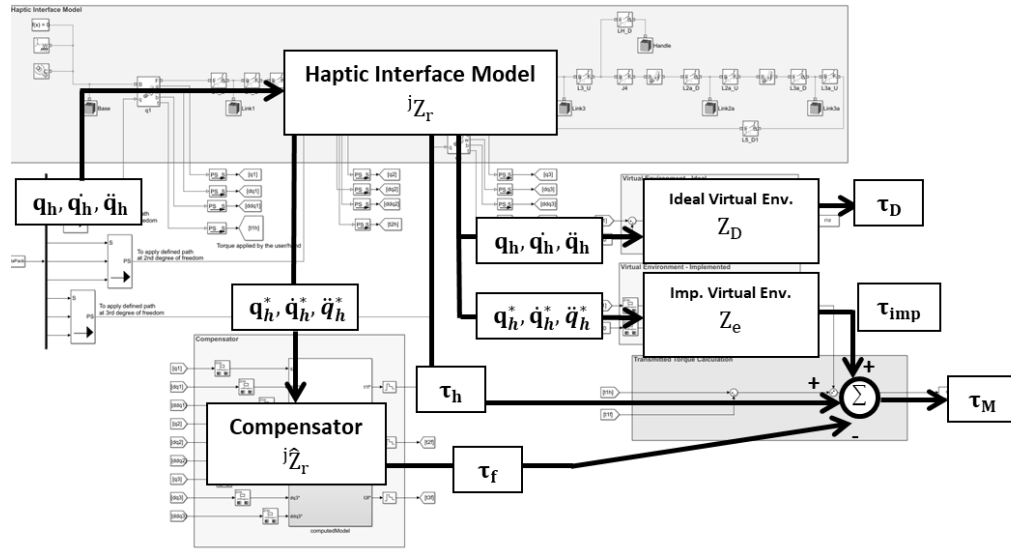


Figure 4.16. Complete Layout of the Simulation Model for the Transparency Bandwidth Simulations

The parameters of the block scheme used in Figure 4.16 are listed below.

$jZ_r$  : The impedance of the haptic display in the joint space. For the transparency bandwidth simulations, it corresponds to the haptic interface model given in Section 4.2.1.1.

$j\hat{Z}_r$  : The modeled impedance of the haptic display in the joint space. For the transparency bandwidth simulations, it corresponds to the compensator model given in 4.2.1.2.

$\tau_f$  : The feedforward torque which is calculated by the compensator considering the manipulator's instantaneous motion.

$\tau_h$  : The joint torque resulting from the force applied by the user to the end-effector of the haptic display

$q_h$  : The actual joint position of the haptic interface

$\dot{q}_h$  : The actual joint velocity of the haptic interface

$\ddot{q}_h$  : The actual joint acceleration of the haptic interface

$q_h^*$  : The sensed (quantized) joint position of the actual joint position,  $q_h$

$\dot{q}_h^*$  : The sensed (quantized) joint velocity of the actual joint velocity,  $\dot{q}_h$

$\ddot{q}_h^*$  : The sensed (quantized) joint acceleration of the actual joint acceleration,  $\ddot{q}_h$

$Z_D$  : The impedance of the ideal virtual environment. For the transparency bandwidth simulations, it corresponds to the ideal virtual environment model given in 4.2.1.3.

$\tau_D$  : The joint torque calculated by the ideal virtual environment

$Z_e$  : The impedance of the implemented virtual environment. For the transparency bandwidth simulations, it corresponds to the implemented virtual environment model given in 4.2.1.3.

$\tau_{imp}$  : The joint torque calculated by the implemented virtual environment

$\tau_M$  : The torque transmitted to the user

During the haptic interaction, the user applies torque to the haptic manipulator in order to move the device to the desired position (i.e.,  $\tau_h$ ) and at the same time, the user resists the virtual environment torques (i.e.,  $\tau_{imp}$ ). The compensator of the haptic device generates the feedforward torque (i.e.,  $\tau_f$ ) in order to eliminate the torque resulting from the inherent dynamics of the haptic interface. The resultant of the three torques mentioned above is equal to the transmitted torque (i.e.,  $\tau_M$ ), which is to be compared with the desired torque (i.e.,  $\tau_D$ ) in order to calculate the transparency bandwidth of the haptic manipulator.

Detailed calculation procedure of the transmitted and desired torque and the transparency bandwidth of the haptic interface are explained in the following section.

#### **4.2.2. Transparency Bandwidth Calculation Methodology**

The transparency bandwidth is defined as frequency range of the motion input that a haptic device is considered as transparent. However, transparency bandwidth is not uniform over the entire workspace of a haptic manipulator. It varies with the pose of the manipulator. It also varies due to the dynamics resulting from the joint interactions.

Similar to the stable impedance range simulations, in order to observe the effects of linearization, two different types of transparency bandwidth simulations have been performed.

In the first simulation type, a virtual wall is implemented on the first DOF of the three DOF haptic interface. Therefore, the transparency bandwidth of the haptic manipulator is obtained only for the first DOF by introducing an excitation to the first DOF while the second and third DOFs remain stationary at their initial positions. In the second simulation type, the virtual wall is again implemented on the first DOF of the three DOF haptic interface. Similar to the first simulation type, the transparency bandwidth is only obtained for the first DOF. However, this time, an excitation acts on the remaining two DOFs of the haptic manipulator.

For both simulation types, the calculations are performed as described below.

- In the first simulation type, only the first DOF of the haptic manipulator is excited with a varying velocity and acceleration by using a chirp signal that corresponds to the joint displacement. A chirp signal is a cosine signal with a constant amplitude, where the frequency is increased from the selected initial frequency to the target swept-frequency along the desired swept time. An example chirp signal is shown in Figure 4.17. Besides the first DOF, the

second and third DOFs remain stationary at their initial positions for the first simulation type.

- In the second simulation type, the chirp signal which is used in the first simulation type in order to excite the first DOF is used for all DOFs of the haptic manipulator.
- The joint velocities (i.e.,  $\dot{q}$ ) and accelerations (i.e.,  $\ddot{q}$ ) are obtained by differentiating the chirp signal, which represents the joint position (i.e.,  $q$ ), with respect to the simulation time.

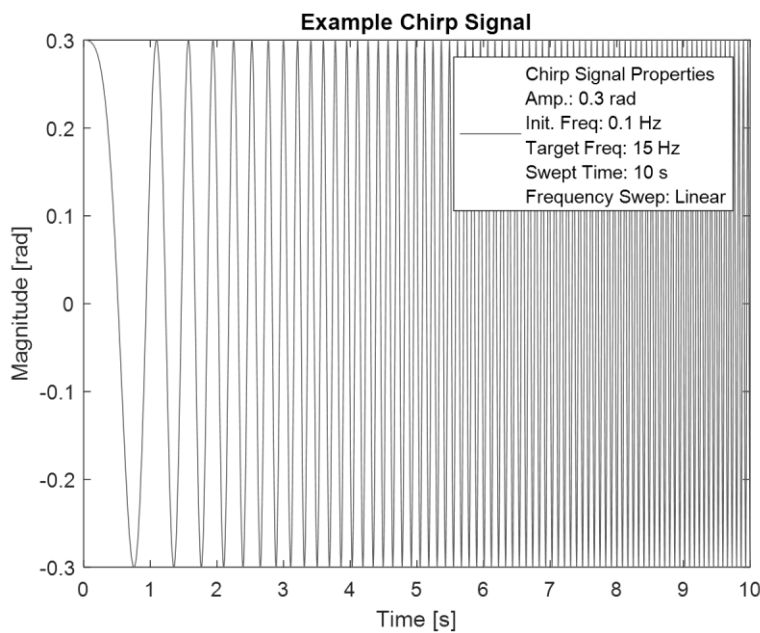


Figure 4.17. Example Chirp Signal

- The torque (i.e.,  $\tau_h$ ) that moves the manipulator in the specified path is measured using the model given in Figure 4.13. This torque is only due to the internal dynamics of the haptic interface as if there is no virtual environment and compensation.
- The compensator torque (i.e.,  $\tau_f$ ) is calculated from the compensator model. Ideally,  $\tau_f$  should be equal to  $\tau_h$  and the compensator should perfectly

eliminate the device dynamics. However, this is not possible due to the quantization error.

- The desired torque (i.e.,  $\tau_D$ ) is measured using the ideal virtual environment model shown in Figure 4.14.
- The desired impedance (i.e.,  $Z_D$ ) is estimated as a function of frequency after dividing of the cross power spectral density between the displacement (i.e.,  $q$ ) and the desired torque output (i.e.,  $\tau_D$ ) by the power spectral density of the displacement input (i.e.,  $q$ ) [35], [36]. The calculation method is approved by observing a constant amplitude across the whole frequency range, which is equal to the impedance, set for the simulations.
- The transmitted torque (i.e.,  $\tau_M$ ) is calculated from the formula given by equation (4.1). The torque applied by the virtual environment (i.e.,  $\tau_{imp}$ ) is evaluated by using the model given in Figure 4.15.

$$\tau_M = \tau_h + \tau_{imp} - \tau_f \quad (4.1)$$

- Similar to the desired impedance, the transmitted impedance (i.e.,  $Z_M$ ) is evaluated as a function of frequency by dividing the cross power spectral density between the position input (i.e.,  $q$ ) and the transmitted torque output (i.e.,  $\tau_M$ ) by the power spectral density of the position (i.e.,  $q$ ).
- The transparency, which is defined as the ratio of transmitted impedances to desired impedances [23], can be computed via equation (4.2). Note that the transfer function is equal to unity when the haptic interface is perfectly transparent.

$$G_T = \frac{Z_M}{Z_D} \quad (4.2)$$

- The transparency bandwidth is obtained from the frequency response of the transparency transfer function given in equation (4.2). A haptic device is

considered as transparent if the magnitude of frequency response of the transparency transfer function lies within  $\pm 3$  dB [23]. Hence, the frequency value that the magnitude of the transparency transfer function crossovers  $\pm 3$  dB band is defined as the transparency bandwidth of the haptic interface (see Figure 4.18).

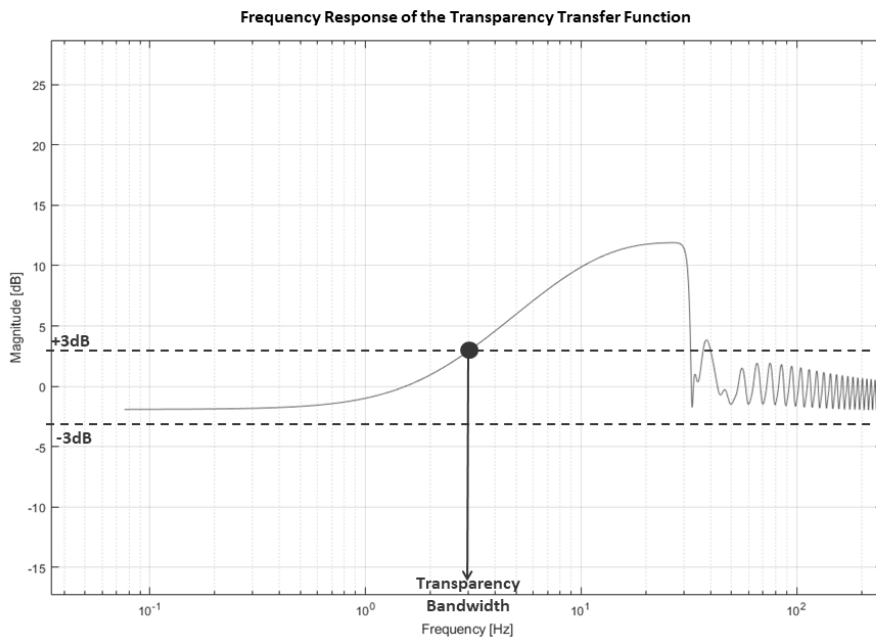


Figure 4.18. Frequency Response of the Transparency Transfer Function

### 4.2.3. Simulation Conditions

The simulation conditions stated in Section 4.1.3, except for the conditions (v) and (viii), are also valid in this section. Additional considerations regarding the transparency bandwidth simulations are given below.

ii. Properties of the chirp signal used in order to excite the joint are listed below.

- Amplitude : 0.3 radians
- Initial Frequency : 0.1 Hz
- Target Frequency : 15 Hz
- Swept Time : 10 seconds
- Frequency Sweep : Linear

According to the simulation type, the related joints are excited with chirp signal defined in Table 4.5.

Table 4.5. *Conditions of the Simulation Types*

Simulation Type	DOF	Desired Path of the Joints	Desired Velocity of the Joints
1	1 <sup>st</sup>	Excited with chirp signal	Excited with chirp signal
	2 <sup>nd</sup>	0	0
	3 <sup>rd</sup>	0	0
2	1 <sup>st</sup>	Excited with chirp signal	Excited with chirp signal
	2 <sup>nd</sup>	Excited with chirp signal	Excited with chirp signal
	3 <sup>rd</sup>	Excited with chirp signal	Excited with chirp signal

In Simscape Multibody, position, velocity, and acceleration values are required in order to actuate a joint. The properties of the chirp signal given above are used to define the desired joint positions of each DOF. The joint velocities and accelerations are calculated by simply differentiating two successive positions/velocities and dividing it by the time step of the simulation. Equation (4.3) shows the basic formulation for the joint velocity and acceleration derivation. Note that only a single joint is actuated during a simulation.

$$\begin{aligned}\dot{q}_{t_1} &= \frac{(q_{t_1} - q_{t_0})}{t_1 - t_0} \\ \ddot{q}_{t_1} &= \frac{(\dot{q}_{t_1} - \dot{q}_{t_0})}{t_1 - t_0}\end{aligned}\tag{4.3}$$

where

$q_{t_1}$  : The joint position at the current time step

$q_{t_0}$  : The joint position at the previous time step (The initial conditions of joint positions are set to zero for all joints.)

$\dot{q}_{t_1}$  : The joint velocity at the current time step

$\dot{q}_{t_0}$  : The joint velocity at the previous time step (The initial conditions of joint velocities are set to zero for all joints.)

$\ddot{q}_{t_1}$  : The joint acceleration at the current time step. (The initial conditions of joint accelerations are set to zero for all joints.)

$t_1-t_0$  : Timestep of the simulation

- iii. The impedance of the virtual environment is set to 4 Nm/rad for the first DOF. It is the only impedance value (obtained from the stable impedance simulations) that can be rendered stably by all haptic manipulators used in this study.
- iv. The total simulation time is set to 10 seconds in all transparency bandwidth simulations.

#### 4.2.4. Simulation Results and Assessments

Similar to the stable impedance range simulations, the transparency bandwidth simulations are performed for the 600 different manipulators given in Table 3.3. In order to investigate the effects of the linearization, two different simulation types are realized. Therefore, a total of  $600 \times 2 = 1200$  different simulation cases have been realized. In the first simulation type, the transparency bandwidth values of the first DOF of the three DOF haptic manipulator are obtained. During these simulations, the second and third DOFs are kept stationary at their initial positions. In the second simulation type, similar to the first one, the transparency bandwidth values of the first DOF of the three DOF haptic manipulator are obtained. However, during these simulations, the second and third DOFs are moved on a previously defined path with a previously defined velocity.

In the first part of this section, beeswarm plots are provided for the first simulation type. The x-axis of the graphs corresponds to the six LN values given in Table 3.3. The y-axis of the graphs corresponds to the transparency bandwidth.

In these graphs, the transparency bandwidth values are grouped with respect to the six LNs given in the x-axis and jitter is added (along the x-axis) to the overlapped values in the y-axis (in order to see the distribution of the transparency bandwidth values). Each circle in the graph represents the result of a single simulation. Each LN set contains 100 circles and a total of 600 circles are plotted in a single graph. Furthermore, mean values and standard deviations of the transparency bandwidth are also calculated and represented (for each LN) in the graphs.

In the second part of this section, the transparency bandwidth values of the first and second simulation types are presented on the same plot in order to see the difference in performance of the haptic interface when the remaining joints are not stationary. In these graphs, while the x-axis of the graphs corresponds to the simulation number (performed with 100 different haptic manipulators given in Table 3.3), the y-axis of the graphs corresponds to the transparency bandwidth value. Six separate plots, each

containing the transparency bandwidth values of 100 different haptic manipulators, are provided for each LN separately. At the end, the number of haptic manipulators whose performance varies and the number of haptic manipulators whose performance remains the same through the two different simulation types are presented using a bar graph.

#### 4.2.4.1. Results of Simulation Type 1

In Figure 4.19, the transparency bandwidth values obtained via the transparency bandwidth simulations of the first DOF are given with respect to the LN of the three DOF haptic manipulator. The results are summarized in Table 4.6 by providing the highest and the lowest value of the transparency bandwidth for each LN. Furthermore, the mean value and the standard deviation of the transparency bandwidth are also listed for each linearity level.

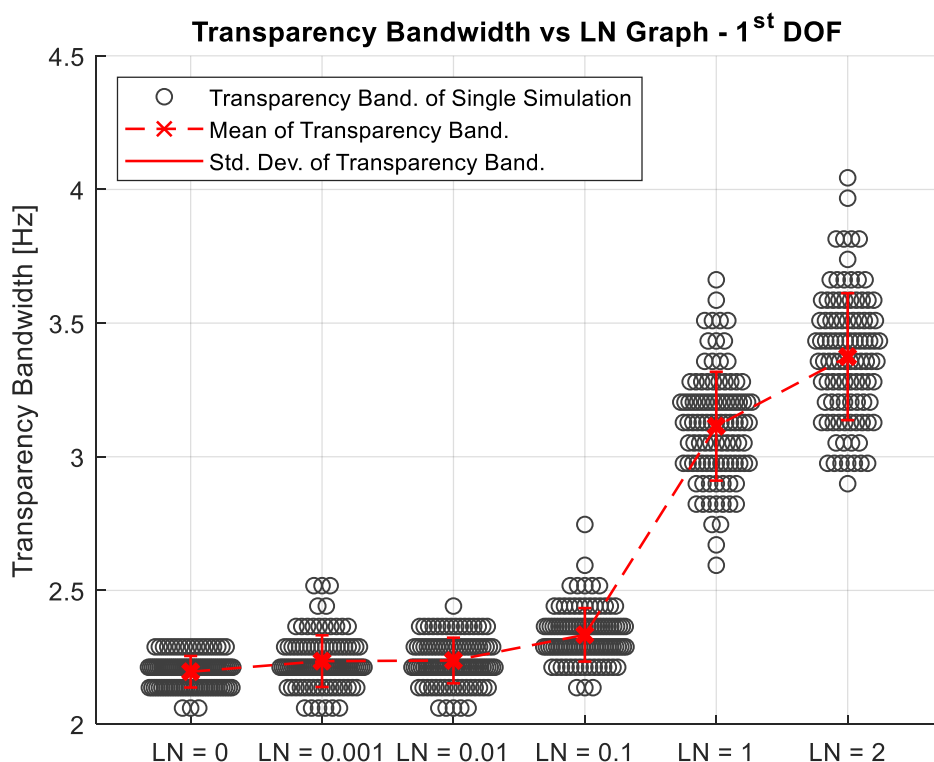


Figure 4.19. Transparency Bandwidth vs LN Graph for the First DOF – Simulation Type 1

Table 4.6. Results of the Transparency Bandwidth Simulations for the First DOF – Simulation Type 1

LN	Transparency Bandwidth [Hz]	Mean [Hz]	Standard Deviation $1\sigma$ [Hz]
0	2.1 - 2.3	2.2	0.1
0.001	2.1 - 2.5	2.2	0.1
0.01	2.1 - 2.4	2.2	0.1
0.1	2.1 - 2.8	2.3	0.1
1	2.6 - 3.7	3.1	0.2
2	2.9 - 4.0	3.4	0.2

It can be observed from Figure 4.19 and Table 4.6 that the transparency bandwidth values, corresponding to the same LN, lie in a wide range. For instance, the transparency bandwidth of the haptic interface changes between 2.9 Hz and 4.0 Hz for LN = 2. The magnitude of these deviations increases, when the manipulator becomes less linear.

Furthermore, the mean value of the transparency bandwidth increases, which is desirable for the haptic performance, when the manipulator becomes less linear. In other words, it appears that linearization affects haptic performance negatively.

#### 4.2.4.2. Results of Simulation Type 2

In Figure 4.20, the transparency bandwidth values obtained via the transparency bandwidth simulations both for the first and second simulation types are given on the same plot with respect to the LN of the three DOF haptic manipulator.

It can be observed from Figure 4.20 that the transparency bandwidth values obtained for the first and second simulation types are exactly same when the haptic interface has completely linear dynamics. With increasing non-linearity in the manipulator dynamics, the transparency bandwidth values obtained for the first and second simulation types begin to differ from each other.

### Transparency Bandwidth vs LN Graph - Simulation Type 1 and Type 2

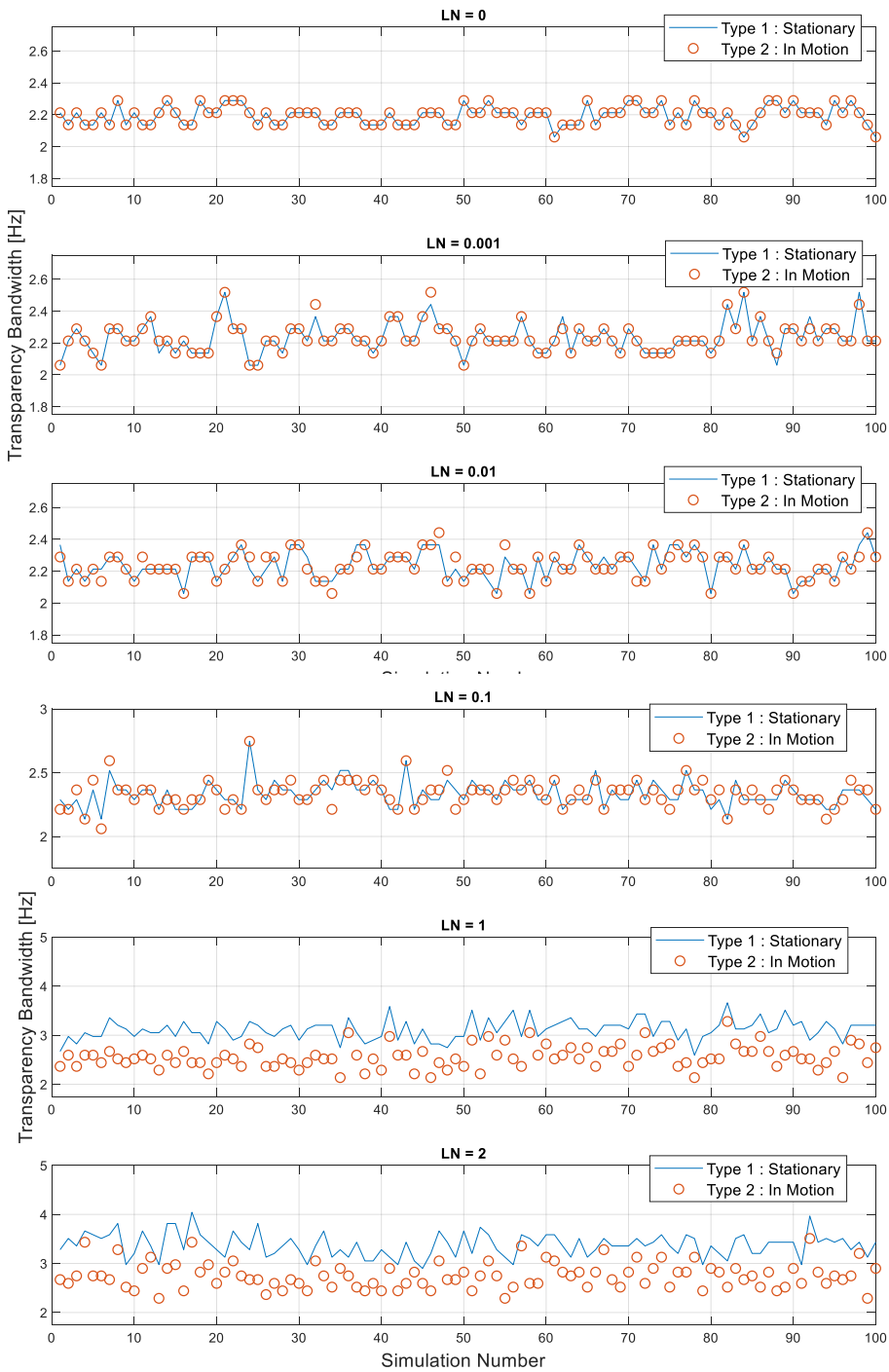


Figure 4.20. Transparency Bandwidth vs LN Graph – Simulation Type 1 and Type 2

The bar graph, given in Figure 4.21, represents the number of haptic manipulators (among the 100 haptic manipulators for each LN) with different and same transparency bandwidth values when the results of the first simulation type are compared with the results of the second simulation type. It can be observed from Figure 4.21 that when the haptic interface has completely linear dynamics (i.e., LN = 0), the two simulation types have exactly the same transparency bandwidth for 100 haptic manipulators. However, the percentage of haptic manipulators having the same transparency bandwidth in both simulation types decreases from 93% to 0% while LN increases from 0.001 to 2.

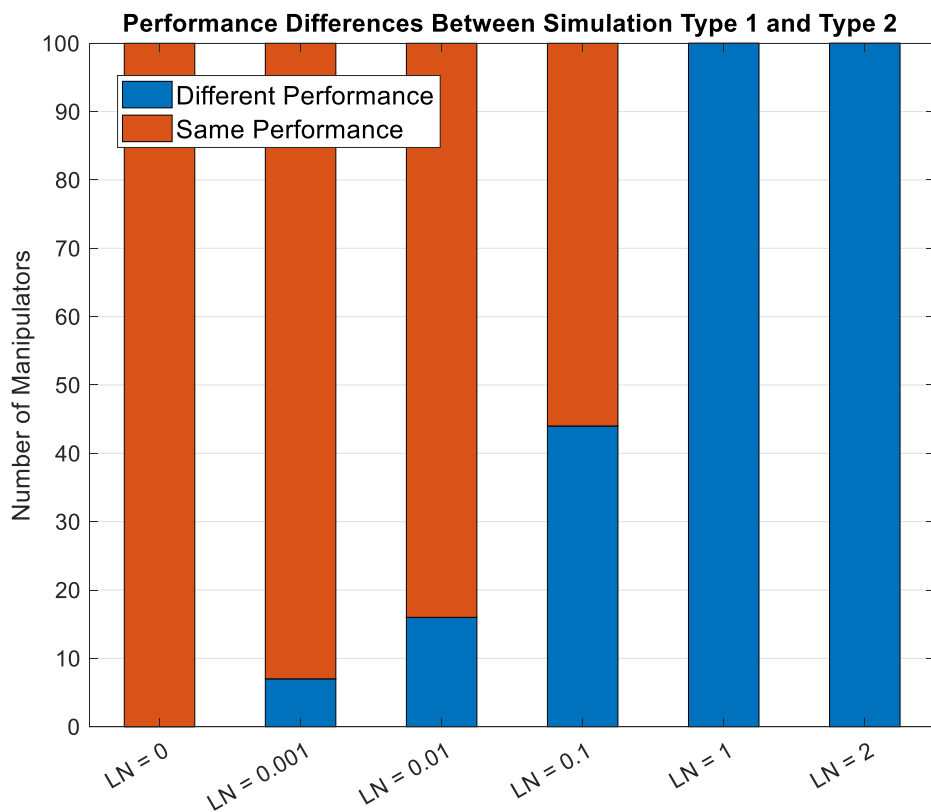


Figure 4.21. Transparency Bandwidth Differences Between Simulation Type 1 and Type 2

#### **4.2.4.3. Assessments of Transparency Bandwidth Simulations**

Similar to the results of the stable impedance range simulations given in Section 4.1.4, in the first simulation type, different manipulators with same degrees of linearity have been compared for six different LNs. From the results provided in Section 4.2.4.1, a clear relationship between transparency bandwidth and LN cannot be deduced. In fact, even haptic manipulators at the same linearity level may have different transparency bandwidth values. However, these results are obtained from the simulations realized under ideal conditions, which partially reflects the real-world conditions given in Section 4.2.3.

As mentioned in Section 4.1.4, the real effect of the linearization of the equations of motion, however, would possibly appear in practical applications. For instance, avoiding modeling error is impossible in practice; but, in the simulations, no modeling error has been introduced to the compensator. It is expected that the modeling error will be much less for the linear configurations since many parameters do not contribute to the manipulator dynamics after the linearization.

In the simulation environment, the required time for the computations realized in the compensator is not taken into account. The inverse dynamics calculations are performed in the compensator and modeling linear (or more linear) equations of motions in the compensator would, definitely, require much less computation time. Clearly, for a sampling rate, which is as high as 1 kHz, a small delay in the computations will deteriorate the manipulator performance. Therefore, the time spent in the compensator in order to solve the equations of motions is very important. In addition to this, cheaper and less powerful processors can be used as the compensator, if the computations are not extremely time consuming.

In the second simulation type, the performance of same haptic manipulators has been compared under different simulation conditions. From the results provided in Section 4.2.4.2, it can be observed that the haptic manipulators with complete linear equations of motion have exactly the same performance (both for the first and

second simulation types) regardless of the pose of the manipulator and the instantaneous velocity of other links. On the other hand, as the non-linearity increases, the difference in the results of two different simulation types increases as well.

Therefore, linearization of the manipulator dynamics eliminates (for fully linear manipulator dynamics) or reduces (for partially linearized manipulator dynamics) the effects of initial conditions and instantaneous dynamics of the other DOFs on the performance of the haptic interface. Hence, it appears that the more linear haptic interface is, the more uniform (over the workspace) the performance of the haptic interface will become.



## CHAPTER 5

### CONCLUSION AND FUTURE WORK

In this thesis, manipulator dynamics of two selected haptic interfaces and the effects of manipulator dynamics on the performance of haptic interfaces are investigated in detail. As the haptic interface, the three and six DOF configurations of Phantom Premium 1.5 are preferred due to their reputations in the research area.

Firstly, the equations of motion of the selected haptic interfaces are derived in symbolic form. A generic computer code, which obtains the equations of motion of a hybrid manipulator composed of revolute and prismatic joints, is developed. The equations of motion of the three and six DOF configurations of Phantom Premium 1.5 are successfully derived. The equations of motion of the three DOF haptic interface have been compared against the derived equations of motion in [25].

Secondly, linearization of the obtained equations of motion of the three and six DOF configurations has been attempted via the concept of LN.

The three DOF haptic interface has 55 parameters, consisting of link lengths, masses, mass center positions and elements of inertia tensor, that affect the equations of motion. After fixing the five link lengths in order not to affect the workspace of the manipulator, 50 inertial parameters are left for design. Additionally, two different types of constraints are imposed on the design parameters in order to construct a physically realizable and practical manipulator.

By using the method of Lagrange Multiplier, the conditions that the 50 design variables must satisfy in order to minimize LN have been obtained in closed form. As a result, the equations of motion of the three DOF haptic interface are completely linearized. Although, complete linearization of a three DOF serial manipulator has already been realized in previous studies; in this study, linearization of a three DOF

hybrid manipulator that contains a loop is achieved. To the author's knowledge, such a linearization does not exist in literature.

A similar optimization procedure is also utilized for the six DOF haptic interface. After fixing the eight link lengths, among the 88 parameters that affect the equations of motion, 80 inertial parameters are left for design. As opposed to the three DOF haptic interface, only one type of constraint is defined for the six DOF configuration. While the constraints for obtaining a physically realizable manipulator are conserved, the constraints for designing a practical manipulator are kept extremely loose in order to observe whether complete linearization can be achieved. By using the method of Lagrange Multiplier, it is shown that complete linearization of the equations of motion of six DOF haptic interface is not possible (for the specified set of kinematic dimensions).

Lastly, simulations are performed, by utilizing the three DOF haptic interface, in order to observe the effects of linearization of manipulator dynamics of a haptic device on the stable impedance range and the transparency bandwidth properties. Six manipulator sets are constructed for six different LN values. Each manipulator set contains 100 different manipulators at the same degree of linearity.

For the stable impedance range and the transparency bandwidth simulations, a distinct mathematical model of the haptic interface, a virtual environment model and a compensator model have been built. Two different types of simulations have been performed both for stable impedance range and transparency bandwidth performance criteria. In the first simulation type, the performance of the first DOF of the haptic interface is obtained while the second and third DOFs are stationary. On the other hand, in the second simulation type, the performance of the first DOF of the haptic interface has been obtained while the second and third DOFs are moved on a predefined path with a predefined velocity. A total of 1200 different cases, per performance criteria, have been simulated for the first DOF of the 600 different manipulators. At the end of the simulations, the obtained results have been

investigated both for the stable impedance range and the transparency bandwidth simulations.

Using the results of the first simulation type, a strong relationship between the two performance criteria (i.e., stable impedance range and transparency bandwidth) and LN cannot be stated. Even for haptic manipulators with the same degrees of linearity, the simulation results considerably vary to be able to declare a correlation. For instance, the maximum stable impedances of the three DOF haptic device change from 8 Nm/rad to 27 Nm/rad, for the first DOF, when  $LN = 0$ . On the other hand, the transparency bandwidth of the three DOF haptic device changes from 2.9 Hz to 4.0 Hz, for the first DOF, when  $LN = 2$ .

For the stable impedance range simulations, the mean value of maximum stable impedances decreases as non-linearity increases. On the other hand, the mean value of transparency bandwidth increases as non-linearity increases. Therefore, when the stable impedance range of the three DOF haptic interface is considered, linearization affects the system performance positively. Conversely, linearization seems to be harmful for the transparency bandwidth of the three DOF haptic interface.

Although a strong correlation between the performance of a haptic device and LN cannot be deduced from the simulation results, the simulations that have been performed under ideal conditions may conceal the real effects of linearization on the stable impedance range and transparency bandwidth. For instance, the modeling error of a haptic interface, implemented in the compensator, is neglected. However, when the haptic manipulator has linear equations of motion, fewer design variables contribute to the manipulator dynamics. Thus, modeling error will be less even if the design variables are identified incorrectly. In addition to the modeling error, delays due to computations realized in the compensator have also been neglected. When the manipulator has linear dynamics, it has simpler equations of motion and solving them requires less computation power, which leads to faster computations.

Using the results of second simulation type, it can be observed that there is no difference (both for the stable impedance range and transparency bandwidth simulations) between the results of simulation type 1 and simulation type 2 when the haptic manipulators have completely linear equations of motion. Furthermore, among the 100 different manipulators for each LN, the difference between the results of simulation type 1 and simulation type 2 of the stable impedance range simulations increases from 0% to 92% as the non-linearity increases. Similar to the stable impedance range simulations, in transparency bandwidth simulations, the difference between the results of simulation type 1 and simulation type 2 increases from 0% to %100 as the non-linearity of the manipulator dynamics increases.

Therefore, it appears that linearization of the equations of motion provides the haptic manipulator a more uniform performance over its workspace by eliminating the performance (considering two performance criteria; stable impedance range and transparency bandwidth) difference of the haptic interface resulting from the initial conditions of the manipulator and the instantaneous dynamics of the remaining DOFs.

Lastly, as future work, a new simulation environment, which reflects the physical world conditions better, can be constructed and additional simulations can be performed in order to observe the practical effects of linearization on the stable impedance range and the transparency bandwidth.

In addition to this, also as future work, requirements for a stable haptic interaction (both for linear and non-linear configurations), can be derived analytically (rather than directly obtaining the maximum stable impedance value via simulations) in terms of design parameters of the haptic manipulator, parameters of the virtual environment and simulation conditions (i.e., sampling time). Therefore, the effect of each parameter on the stable haptic interaction can be observed separately and the relationship between linearization and performance of the haptic interface can be evaluated more clearly.

## REFERENCES

- [1] K. Youcef-Toumi, “Analysis and Design of Manipulators With Decoupled and Configuration-Invariant Inertia Tensors Using Remote Actuation,” *J. Dyn. Syst. Meas. Control*, vol. 114, no. 2, p. 204, 2008.
- [2] V. Arakelian and S. Sargsyan, “On the design of serial manipulators with decoupled dynamics,” in *Mechatronics*, 2012, vol. 22, no. 6, pp. 904–909.
- [3] H. S. Kim, Y. M. Cho, and K. I. Lee, “Robust nonlinear task space control for 6 DOF parallel manipulator,” *Automatica*, vol. 41, no. 9, pp. 1591–1600, 2005.
- [4] V. Duchaine, S. Bouchard, and C. M. Gosselin, “Computationally efficient predictive robot control,” in *IEEE/ASME Transactions on Mechatronics*, 2007, vol. 12, no. 5, pp. 570–578.
- [5] I. Davliakos and E. Papadopoulos, “Model-based control of a 6-dof electrohydraulic Stewart-Gough platform,” *Mech. Mach. Theory*, vol. 43, no. 11, pp. 1385–1400, 2008.
- [6] J. L. Chen and W. Der Chang, “Feedback linearization control of a two-link robot using a multi-crossover genetic algorithm,” *Expert Syst. Appl.*, vol. 36, no. 2 PART 2, pp. 4154–4159, 2009.
- [7] C. Yang, Q. Huang, and J. Han, “Decoupling control for spatial six-degree-of-freedom electro-hydraulic parallel robot,” *Robot. Comput. Integr. Manuf.*, vol. 28, no. 1, pp. 14–23, 2012.
- [8] H. Asada, “A Geometrical Representation of Manipulator Dynamics and Its Application to Arm Design,” *J. Dyn. Syst. Meas. Control*, vol. 105, no. 3, p. 131, 2009.

- [9] D. C. H. Yang and S. W. Tzeng, "Simplification and Linearization of Manipulator Dynamics by the Design of Inertia Distribution," *Int. J. Rob. Res.*, vol. 5, no. 3, pp. 120–128, 1986.
- [10] H. S. Park and H. S. Cho, "General design conditions for an ideal robotic manipulator having simple dynamics," *Int. J. Rob. Res.*, vol. 10, no. 1, pp. 21–29, 1991.
- [11] K. Youcef-Toumi and H. Asada, "The Design of Open-Loop Manipulator Arms With Decoupled and Configuration-Invariant Inertia Tensors," *J. Dyn. Syst. Meas. Control*, vol. 109, no. 3, p. 268, 2009.
- [12] R. Soylu and A. Sarrafi, "Linearization and optimization of robot dynamics via inertial parameter design," *J. Robot. Syst.*, vol. 13, no. 8, pp. 527–538, 1996.
- [13] M. Mihelj and J. Podobnik, "Introduction to Haptics," in *Haptics for Virtual Reality and Teleoperation*, vol. 64. Dordrecht: Springer Netherlands, 2012, ch. 2, p. 37.
- [14] R. E. Ellis, O. M. Ismaeil, and M. G. Lipsett, "Design and evaluation of a high-performance haptic interface," *Robotica*, vol. 14, no. 03, p. 321, 2009.
- [15] V. Hayward and O. R. Astley, "Performance Measures for Haptic Interfaces," in *Robotics Research*, 2011, pp. 195–206.
- [16] D. A. Lawrence, "Stability and Transparency in Bilateral Teleoperation," *IEEE Trans. Robot. Autom.*, vol. 9, no. 5, pp. 624–637, 1993.
- [17] B. Hannaford and J. H. Ryu, "Time-domain passivity control of haptic interfaces," *IEEE Trans. Robot. Autom.*, vol. 18, no. 1, pp. 1–10, 2002.

- [18] J. S. Mehling, J. E. Colgate, and M. A. Peshkin, "Increasing the impedance range of a haptic display by adding electrical damping," in *Proceedings - 1st Joint Eurohaptics Conference and Symposium on Haptic Interfaces for Virtual Environment and Teleoperator Systems; World Haptics Conference, WHC 2005*, 2005, pp. 257–262.
- [19] H.-S. Ahn, J. Ryu, and Y.-A. Lim, "Analogue input shaper for haptic interfaces," *IET Control Theory Appl.*, vol. 3, no. 12, pp. 1553–1564, 2009.
- [20] K. Lee and D. Y. Lee, "Adjusting output-limiter for stable haptic rendering in virtual environments," *IEEE Trans. Control Syst. Technol.*, vol. 17, no. 4, pp. 768–779, 2009.
- [21] J. P. Kim, S. Y. Baek, and J. Ryu, "A force bounding approach for stable haptic interaction," in *2011 IEEE World Haptics Conference, WHC 2011*, 2011, pp. 397–402.
- [22] M. Franken, S. Stramigioli, S. Misra, C. Secchi, and A. MacChelli, "Bilateral telemanipulation with time delays: A two-layer approach combining passivity and transparency," *IEEE Trans. Robot.*, vol. 27, no. 4, pp. 741–756, 2011.
- [23] O. Baser, H. Gurocak, and E. I. Konukseven, "Hybrid control algorithm to improve both stable impedance range and transparency in haptic devices," *Mechatronics*, vol. 23, no. 1, pp. 121–134, 2013.
- [24] B. Siciliano and O. Khatib, "Kinematics," in *Handbook on Robotics*, 2008, ch. 1, pp. 11-25.
- [25] M. Cenk Cavusoglu and D. Feygin, "Kinematics and Dynamics of Phantom(TM) model 1.5 Haptic Interface," 2001.
- [26] O. Baser and E. I. Konukseven, "Kinematic Calibration of PHANTOM Premium 1.5/6DOF Haptic Device," *Key Eng. Mater.*, vol. 486, pp. 205–208, 2011.

- [27] J. J. Craig, “Manipulator kinematics,” in *Introduction to robotics : mechanics and control*, Upper Saddle River, N.J: Pearson/Prentice Hall, 2005, ch. 3, pp. 73-76.
- [28] J. J. Craig, “Jacobians: velocities and static forces,” in *Introduction to robotics : mechanics and control*, Upper Saddle River, N.J: Pearson/Prentice Hall, 2005, ch. 5, pp. 135-149.
- [29] J. J. Craig, “Manipulator dynamics,” in *Introduction to robotics : mechanics and control*, Upper Saddle River, N.J: Pearson/Prentice Hall, 2005, ch. 6, pp. 182-185.
- [30] R. M. Murray, Z. Li, and S. Shankar Sastry, “Dynamics of Open-Chain Manipulators,” in *A mathematical introduction to robotic manipulation*, CRC Press, 1994, ch. 3, pp. 171-172.
- [31] M. Mihelj and J. Podobnik, “Introduction to Haptics,” in *Haptics for Virtual Reality and Teleoperation*, vol. 64. Dordrecht: Springer Netherlands, 2012, ch. 2, pp. 38-39.
- [32] M. Mihelj and J. Podobnik, “Control of Haptic Interfaces,” in *Haptics for Virtual Reality and Teleoperation*, vol. 64. Dordrecht: Springer Netherlands, 2012, ch. 7, pp. 121-123.
- [33] M. Mihelj and J. Podobnik, “Stability Analysis of Haptic Interfaces,” in *Haptics for Virtual Reality and Teleoperation*, vol. 64, Dordrecht: Springer Netherlands, 2012, ch. 8, pp. 140-145.
- [34] J. J. Gil, A. Avello, ac A. Rubio, and J. Flórez, “Stability analysis of a 1 DOF haptic interface using the Routh-Hurwitz criterion,” *IEEE Trans. Control Syst. Technol.*, vol. 12, no. 4, pp. 583–588, 2004.
- [35] K. B. Fite, L. Shao, and M. Goldfarb, “Loop shaping for transparency and stability robustness in bilateral telemanipulation,” *IEEE Trans. Robot. Autom.*, vol. 20, no. 3, pp. 620–624, 2004.

- [36] A. Gupta and M. K. O'Malley, "Disturbance-Observer-Based Force Estimation for Haptic Feedback," *J. Dyn. Syst. Meas. Control*, vol. 133, no. 1, p. 014505, 2010.



## APPENDICES

### A. Results of Dynamic Analysis

Elements of actuator torque vector, validation results and comparison of the derived equations of motion with the ones that are obtained in [25] ones are presented in the following sections.

#### A.1. Elements of the Actuator Torque Vector

The first row ( $\tau_1$ ) :

$$\begin{aligned}
 & (1. I_{xz2} \cos[\theta_2[t]] + 1. I_{xz2a} \cos[\theta_2[t]] + \\
 & \quad 1. l_2 m_2 a r_{2az} \cos[\theta_2[t]] + 1. m_2 a r_{2ax} r_{2az} \cos[\theta_2[t]] + \\
 & \quad 1. m_2 r_{2x} r_{2z} \cos[\theta_2[t]] - 1. l_2 m_3 r_{3y} \cos[\theta_2[t]] - \\
 & \quad 1. I_{xy3} \cos[\theta_2[t] + \theta_3[t]] - 1. I_{xy3a} \cos[\theta_2[t] + \theta_3[t]] - \\
 & \quad 1. m_3 a r_{3ax} r_{3ay} \cos[\theta_2[t] + \theta_3[t]] - 1. m_3 r_{3x} r_{3y} \cos[\theta_2[t] + \theta_3[t]] - \\
 & \quad 1. (1. I_{yz2} + 1. I_{yz2a} + 1. m_2 a r_{2ay} r_{2az} + 1. m_2 r_{2y} r_{2z}) \sin[\theta_2[t]] + \\
 & \quad 1. (1. I_{yz3} + 1. I_{yz3a} - 1. l_3 a m_2 a r_{2az} + 1. l_3 a m_3 a r_{3ay} + 1. m_3 a r_{3ay} r_{3az} + 1. m_3 r_{3y} r_{3z}) \\
 & \quad \sin[\theta_2[t] + \theta_3[t]]) \theta_2'^2[t] - \\
 & 2. ((1. I_{xy3} + 1. I_{xy3a} + 1. m_3 a r_{3ax} r_{3ay} + 1. m_3 r_{3x} r_{3y}) \cos[\theta_2[t] + \theta_3[t]] + \\
 & \quad (-1. I_{yz3} - 1. I_{yz3a} + 1. l_3 a m_2 a r_{2az} - 1. l_3 a m_3 a r_{3ay} - 1. m_3 a r_{3ay} r_{3az} - 1. m_3 r_{3y} r_{3z}) \\
 & \quad \sin[\theta_2[t] + \theta_3[t]]) \theta_2'[t] \theta_3'[t] + \\
 & ((-1. I_{xy3} - 1. I_{xy3a} - 1. m_3 a r_{3ax} r_{3ay} - 1. m_3 r_{3x} r_{3y}) \cos[\theta_2[t] + \theta_3[t]] + \\
 & \quad (1. I_{yz3} + 1. I_{yz3a} - 1. l_3 a m_2 a r_{2az} + 1. l_3 a m_3 a r_{3ay} + 1. m_3 a r_{3ay} r_{3az} + 1. m_3 r_{3y} r_{3z}) \\
 & \quad \sin[\theta_2[t] + \theta_3[t]]) \theta_3'^2[t] + \theta_2'[t] \\
 & (((-2. I_{xy2} - 2. I_{xy2a} - 2. l_2 m_2 a r_{2ay} - 2. m_2 a r_{2ax} r_{2ay} - 2. m_2 r_{2x} r_{2y}) \cos[2 \theta_2[t]] + \\
 & \quad (-2. I_{xz3} - 2. I_{xz3a} - 2. l_3 a m_3 a r_{3ax} - 2. m_3 a r_{3ax} r_{3az} - 2. m_3 r_{3x} r_{3z}) \\
 & \quad \cos[2(\theta_2[t] + \theta_3[t])] - 2. l_2 l_3 a m_2 a \cos[2 \theta_2[t] + \theta_3[t]] - 2. l_3 a \\
 & \quad m_2 a r_{2ax} \cos[2 \theta_2[t] + \theta_3[t]] - 2. l_2 m_3 r_{3z} \cos[2 \theta_2[t] + \theta_3[t]] + \\
 & \quad 1. I_{xx2} \sin[2 \theta_2[t]] + 1. I_{xx2a} \sin[2 \theta_2[t]] - 1. I_{yy2} \sin[2 \theta_2[t]] - \\
 & \quad 1. I_{yy2a} \sin[2 \theta_2[t]] - 1. l_2^2 m_2 a \sin[2 \theta_2[t]] - 1. l_2^2 m_3 \sin[2 \theta_2[t]] - \\
 & \quad 2. l_2 m_2 a r_{2ax} \sin[2 \theta_2[t]] - 1. m_2 a r_{2ax}^2 \sin[2 \theta_2[t]] + 1. m_2 a r_{2ay}^2 \\
 & \quad \sin[2 \theta_2[t]] - 1. m_2 r_{2x}^2 \sin[2 \theta_2[t]] + 1. m_2 r_{2y}^2 \sin[2 \theta_2[t]] + \\
 & \quad 1. I_{xx3} \sin[2(\theta_2[t] + \theta_3[t])] + 1. I_{xx3a} \sin[2(\theta_2[t] + \theta_3[t])] - \\
 & \quad 1. I_{zz3} \sin[2(\theta_2[t] + \theta_3[t])] - 1. I_{zz3a} \sin[2(\theta_2[t] + \theta_3[t])] + \\
 & \quad 1. l_3 a^2 m_2 a \sin[2(\theta_2[t] + \theta_3[t])] + 1. l_3 a^2 m_3 a \\
 & \quad \sin[2(\theta_2[t] + \theta_3[t])] - 1. m_3 a r_{3ax}^2 \sin[2(\theta_2[t] + \theta_3[t])]) + \\
 & (1. I_{xz2} \cos[\theta_2[t]] + 1. I_{xz2a} \cos[\theta_2[t]] + \\
 & \quad 1. l_2 m_2 a r_{2az} \cos[\theta_2[t]] + 1. m_2 a r_{2ax} r_{2az} \cos[\theta_2[t]] + \\
 & \quad 1. m_2 r_{2x} r_{2z} \cos[\theta_2[t]] - 1. l_2 m_3 r_{3y} \cos[\theta_2[t]] - \\
 & \quad 1. I_{xy3} \cos[\theta_2[t] + \theta_3[t]] - 1. I_{xy3a} \cos[\theta_2[t] + \theta_3[t]] - \\
 & \quad 1. m_3 a r_{3ax} r_{3ay} \cos[\theta_2[t] + \theta_3[t]] - 1. m_3 r_{3x} r_{3y} \cos[\theta_2[t] + \theta_3[t]] - \\
 & \quad 1. (1. I_{yz2} + 1. I_{yz2a} + 1. m_2 a r_{2ay} r_{2az} + 1. m_2 r_{2y} r_{2z}) \sin[\theta_2[t]] + \\
 & \quad 1. (1. I_{yz3} + 1. I_{yz3a} - 1. l_3 a m_2 a r_{2az} + 1. l_3 a m_3 a r_{3ay} + 1. m_3 a r_{3ay} r_{3az} + 1. m_3 r_{3y} r_{3z}) \\
 & \quad \sin[\theta_2[t] + \theta_3[t]]) \theta_2'^2[t] - \\
 & 2. ((1. I_{xy3} + 1. I_{xy3a} + 1. m_3 a r_{3ax} r_{3ay} + 1. m_3 r_{3x} r_{3y}) \cos[\theta_2[t] + \theta_3[t]] + \\
 & \quad (-1. I_{yz3} - 1. I_{yz3a} + 1. l_3 a m_2 a r_{2az} - 1. l_3 a m_3 a r_{3ay} - 1. m_3 a r_{3ay} r_{3az} - 1. m_3 r_{3y} r_{3z}) \\
 & \quad \sin[\theta_2[t] + \theta_3[t]]) \theta_2'[t] \theta_3'[t] + \\
 & (((-1. I_{xy3} - 1. I_{xy3a} - 1. m_3 a r_{3ax} r_{3ay} - 1. m_3 r_{3x} r_{3y}) \cos[\theta_2[t] + \theta_3[t]] + \\
 & \quad (1. I_{yz3} + 1. I_{yz3a} - 1. l_3 a m_2 a r_{2az} + 1. l_3 a m_3 a r_{3ay} + 1. m_3 a r_{3ay} r_{3az} + 1. m_3 r_{3y} r_{3z}) \\
 & \quad \sin[\theta_2[t] + \theta_3[t]]) \theta_3'^2[t] + \theta_2'[t] \\
 & (((-2. I_{xy2} - 2. I_{xy2a} - 2. l_2 m_2 a r_{2ay} - 2. m_2 a r_{2ax} r_{2ay} - 2. m_2 r_{2x} r_{2y}) \cos[2 \theta_2[t]] +
 \end{aligned}$$

Figure 0.1. First Actuator Torque

$$\begin{aligned}
& (-2. Ixz3 - 2. Ixz3a - 2. l3a m3a r3ax - 2. m3a r3ax r3az - 2. m3 r3x r3z) \\
& \cos[2(\theta_2[t] + \theta_3[t])] - 2. l2 l3a m2a \cos[2\theta_2[t] + \theta_3[t]] - 2. l3a \\
& m2a r2ax \cos[2\theta_2[t] + \theta_3[t]] - 2. l2 m3 r3z \cos[2\theta_2[t] + \theta_3[t]] + \\
& 1. Ixx2 \sin[2\theta_2[t]] + 1. Ixx2a \sin[2\theta_2[t]] - 1. Iyy2 \sin[2\theta_2[t]] - \\
& 1. Iyy2a \sin[2\theta_2[t]] - 1. l2^2 m2a \sin[2\theta_2[t]] - 1. l2^2 m3 \sin[2\theta_2[t]] - \\
& 2. l2 m2a r2ax \sin[2\theta_2[t]] - 1. m2a r2ax^2 \sin[2\theta_2[t]] + 1. m2a r2ay^2 \\
& \sin[2\theta_2[t]] - 1. m2 r2x^2 \sin[2\theta_2[t]] + 1. m2 r2y^2 \sin[2\theta_2[t]] + \\
& 1. Ixx3 \sin[2(\theta_2[t] + \theta_3[t])] + 1. Ixx3a \sin[2(\theta_2[t] + \theta_3[t])] - \\
& 1. Izz3 \sin[2(\theta_2[t] + \theta_3[t])] - 1. Izz3a \sin[2(\theta_2[t] + \theta_3[t])] + \\
& 1. l3a^2 m2a \sin[2(\theta_2[t] + \theta_3[t])] + 1. l3a^2 m3a \\
& \sin[2(\theta_2[t] + \theta_3[t])] - 1. m3a r3ax^2 \sin[2(\theta_2[t] + \theta_3[t])] + \\
& 1. l2 m3 r3x \sin[2\theta_2[t] + \theta_3[t]] \theta_3'[t] + \\
2 & (0.25 Ixx2 + 0.25 Ixx2a + 0.25 Ixx3 + 0.25 Ixx3a + 0.5 Iyy1 + 0.25 Iyy2 + \\
& 0.25 Iyy2a + 0.25 Izz3 + 0.25 Izz3a + 0.25 l2^2 m2a + \\
& 0.25 l3a^2 m2a + 0.25 l2^2 m3 + 0.25 l3a^2 m3a + 0.5 m1 r1x^2 + \\
& 0.5 m1 r1z^2 + 0.5 l2 m2a r2ax + 0.25 m2a r2ax^2 + \\
& 0.25 m2a r2ay^2 + 0.5 m2a r2az^2 + 0.25 m2 r2x^2 + \\
& 0.25 m2 r2y^2 + 0.5 m2 r2z^2 + 0.25 m3a r3ax^2 + \\
& 0.5 m3a r3ay^2 + 0.5 l3a m3a r3az + 0.25 m3a r3az^2 + \\
& 0.25 m3 r3x^2 + 0.5 m3 r3y^2 + 0.25 m3 r3z^2 + \\
& (-0.25 Ixx2 - 0.25 Ixx2a + 0.25 Iyy2 + 0.25 Iyy2a + 0.25 l2^2 m2a + 0.25 l2^2 m3 + \\
& 0.5 l2 m2a r2ax + 0.25 m2a r2ax^2 - 0.25 m2a r2ay^2 + 0.25 m2 r2x^2 - 0.25 m2 r2y^2) \\
& \cos[2\theta_2[t]] + (0.5 l3a m2a r2ay + 0.5 l2 m3 r3x) \cos[\theta_3[t]] - \\
& 0.25 Ixx3 \cos[2(\theta_2[t] + \theta_3[t])] - \\
& 0.25 Ixx3a \cos[2(\theta_2[t] + \theta_3[t])] + \\
& 0.25 Izz3 \cos[2(\theta_2[t] + \theta_3[t])] + \\
& 0.25 Izz3a \cos[2(\theta_2[t] + \theta_3[t])] - \\
& 0.25 l3a^2 m2a \cos[2(\theta_2[t] + \theta_3[t])] - \\
& 0.25 l3a^2 m3a \cos[2(\theta_2[t] + \theta_3[t])] + \\
& 0.25 m3a r3ax^2 \cos[2(\theta_2[t] + \theta_3[t])] - \\
& 0.5 l3a m3a r3az \cos[2(\theta_2[t] + \theta_3[t])] - \\
& 0.25 m3a r3az^2 \cos[2(\theta_2[t] + \theta_3[t])] + \\
& 0.25 m3 r3x^2 \cos[2(\theta_2[t] + \theta_3[t])] - \\
& 0.25 m3 r3z^2 \cos[2(\theta_2[t] + \theta_3[t])] - \\
& 0.5 l3a m2a r2ay \cos[2\theta_2[t] + \theta_3[t]] + \\
& 0.5 l2 m3 r3x \cos[2\theta_2[t] + \theta_3[t]] - \\
& 0.5 Ixy2 \sin[2\theta_2[t]] - 0.5 Ixy2a \sin[2\theta_2[t]] - \\
& 0.5 l2 m2a r2ay \sin[2\theta_2[t]] - 0.5 m2a r2ax r2ay \sin[2\theta_2[t]] - \\
& 0.5 m2 r2x r2y \sin[2\theta_2[t]] - 0.5 l2 l3a m2a \sin[\theta_3[t]] - \\
& 0.5 l3a m2a r2ax \sin[\theta_3[t]] - 0.5 l2 m3 r3z \sin[\theta_3[t]] - \\
& 0.5 Ixz3 \sin[2(\theta_2[t] + \theta_3[t])] - \\
& 0.5 Ixz3a \sin[2(\theta_2[t] + \theta_3[t])] - \\
& 0.5 l3a m3a r3ax \sin[2(\theta_2[t] + \theta_3[t])] - \\
& 0.5 m3a r3ax r3az \sin[2(\theta_2[t] + \theta_3[t])] - \\
& 0.5 m3 r3x r3z \sin[2(\theta_2[t] + \theta_3[t])] - \\
& 0.5 l2 l3a m2a \sin[2\theta_2[t] + \theta_3[t]] - \\
& 0.5 l3a m2a r2ax \sin[2\theta_2[t] + \theta_3[t]] - \\
& 0.5 l2 m3 r3z \sin[2\theta_2[t] + \theta_3[t]] \theta_3''[t] + \\
((1. Iyz2 + 1. Iyz2a + 1. m2a r2ay r2az + 1. m2 r2y r2z) \cos[\theta_2[t]] + \\
& (-1. Iyz3 - 1. Iyz3a + 1. l3a m2a r2az - 1. l3a m3a r3ay - 1. m3a r3ay r3az - 1. m3 r3y r3z) \\
& \cos[\theta_2[t] + \theta_3[t]] + 1. Ixz2 \sin[\theta_2[t]] + \\
& 1. Ixz2a \sin[\theta_2[t]] + 1. l2 m2a r2az \sin[\theta_2[t]] + \\
& 1. m2a r2ax r2az \sin[\theta_2[t]] + 1. m2 r2x r2z \sin[\theta_2[t]] - \\
& 1. l2 m3 r3y \sin[\theta_2[t]] - 1. Ixy3 \sin[\theta_2[t] + \theta_3[t]] - \\
& 1. Ixy3a \sin[\theta_2[t] + \theta_3[t]] - 1. m3a r3ax r3ay \sin[\theta_2[t] + \theta_3[t]] - \\
& 1. m3 r3x r3y \sin[\theta_2[t] + \theta_3[t]] \theta_2''[t] + \\
((-1. Iyz3 - 1. Iyz3a + 1. l3a m2a r2az - 1. l3a m3a r3ay - 1. m3a r3ay r3az - 1. m3 r3y r3z) \\
& \cos[\theta_2[t] + \theta_3[t]] + (-1. Ixy3 - 1. Ixy3a - 1. m3a r3ax r3ay - 1. m3 r3x r3y) \\
& \sin[\theta_2[t] + \theta_3[t]] \theta_3''[t]
\end{aligned}$$

Figure 0.1. Continued

The second row ( $\tau_2$ ) :

$$\begin{aligned}
& g \left( - \left( 12 (m2a + m3) + m2a r2ax + m2 r2x \right) \cos[\theta_2(t)] - (m3a r3ax + m3 r3x) \right. \\
& \quad \cos[\theta_2(t) + \theta_3(t)] + m2a r2ay \sin[\theta_2(t)] + m2 r2y \sin[\theta_2(t)] + \\
& \quad 13a m2a \sin[\theta_2(t) + \theta_3(t)] + 13a m3a \sin[\theta_2(t) + \theta_3(t)] + \\
& \quad \left. m3a r3az \sin[\theta_2(t) + \theta_3(t)] + m3 r3z \sin[\theta_2(t) + \theta_3(t)] \right) + \\
& \left( (1. Ixy2 + 1. Ixy2a + 1. 12 m2a r2ay + 1. m2a r2ax r2ay + 1. m2 r2x r2y) \cos[2 \theta_2(t)] + \right. \\
& \quad (1. Ixz3 + 1. Ixz3a + 1. 13a m3a r3ax + 1. m3a r3ax r3az + 1. m3 r3x r3z) \\
& \quad \cos[2 (\theta_2(t) + \theta_3(t))] + 1. 12 13a m2a \cos[2 \theta_2(t) + \theta_3(t)] + \\
& \quad 1. 13a m2a r2ax \cos[2 \theta_2(t) + \theta_3(t)] + 1. 12 m3 r3z \cos[2 \theta_2(t) + \theta_3(t)] - \\
& \quad 0.5 Ixx2 \sin[2 \theta_2(t)] - 0.5 Ixx2a \sin[2 \theta_2(t)] + 0.5 Iyy2 \sin[2 \theta_2(t)] + \\
& \quad 0.5 Iyy2a \sin[2 \theta_2(t)] + 0.5 12^2 m2a \sin[2 \theta_2(t)] + 0.5 12^2 m3 \sin[2 \theta_2(t)] + \\
& \quad 1. 12 m2a r2ax \sin[2 \theta_2(t)] + 0.5 m2a r2ax^2 \sin[2 \theta_2(t)] - \\
& \quad 0.5 m2a r2ay^2 \sin[2 \theta_2(t)] + 0.5 m2 r2x^2 \sin[2 \theta_2(t)] - \\
& \quad 0.5 m2 r2y^2 \sin[2 \theta_2(t)] - 0.5 Ixx3 \sin[2 (\theta_2(t) + \theta_3(t))] - \\
& \quad 0.5 Ixx3a \sin[2 (\theta_2(t) + \theta_3(t))] + 0.5 Izz3 \sin[2 (\theta_2(t) + \theta_3(t))] + \\
& \quad 0.5 Izz3a \sin[2 (\theta_2(t) + \theta_3(t))] - 0.5 13a^2 m2a \sin[2 (\theta_2(t) + \theta_3(t))] - \\
& \quad 0.5 13a^2 m3a \sin[2 (\theta_2(t) + \theta_3(t))] + \\
& \quad 0.5 m3a r3ax^2 \sin[2 (\theta_2(t) + \theta_3(t))] - 1. 13a m3a r3az \\
& \quad \sin[2 (\theta_2(t) + \theta_3(t))] - 0.5 m3a r3az^2 \sin[2 (\theta_2(t) + \theta_3(t))] + \\
& \quad 0.5 m3 r3x^2 \sin[2 (\theta_2(t) + \theta_3(t))] - 0.5 m3 r3z^2 \sin[2 (\theta_2(t) + \theta_3(t))] - \\
& \quad \left. 1. 13a m2a r2ay \sin[2 \theta_2(t) + \theta_3(t)] + 1. 12 m3 r3x \sin[2 \theta_2(t) + \theta_3(t)] \right) \\
& \theta_2(t)^2 + ((-2. 12 13a m2a - 2. 13a m2a r2ax - 2. 12 m3 r3z) \cos[\theta_3(t)] + \\
& \quad (-2. 13a m2a r2ay - 2. 12 m3 r3x) \sin[\theta_3(t)]) \theta_2'(t) \theta_3'(t) + \\
& \left( (-1. 12 13a m2a - 1. 13a m2a r2ax - 1. 12 m3 r3z) \cos[\theta_3(t)] + \right. \\
& \quad \left. (-1. 13a m2a r2ay - 1. 12 m3 r3x) \sin[\theta_3(t)] \right) \theta_2(t)^2 + \\
& \left( (1. Iyz2 + 1. Iyz2a + 1. m2a r2ay r2az + 1. m2 r2y r2z) \cos[\theta_2(t)] + \right. \\
& \quad (-1. Iyz3 - 1. Iyz3a + 1. 13a m2a r2az - 1. 13a m3a r3ay - 1. m3a r3ay r3az - 1. m3 r3y r3z) \\
& \quad \cos[\theta_2(t) + \theta_3(t)] + 1. Ixz2 \sin[\theta_2(t)] + 1. Ixz2a \sin[\theta_2(t)] + \\
& \quad 1. 12 m2a r2az \sin[\theta_2(t)] + 1. m2a r2ax r2az \sin[\theta_2(t)] + \\
& \quad 1. m2 r2x r2z \sin[\theta_2(t)] - 1. 12 m3 r3y \sin[\theta_2(t)] - \\
& \quad 1. Ixy3 \sin[\theta_2(t) + \theta_3(t)] - 1. Ixy3a \sin[\theta_2(t) + \theta_3(t)] - \\
& \quad \left. 1. m3a r3ax r3ay \sin[\theta_2(t) + \theta_3(t)] - 1. m3 r3x r3y \sin[\theta_2(t) + \theta_3(t)] \right) \\
& \theta_2(t)^2 + (1. Iyy3 + 1. Iyy3a + 1. Izz2 + 1. Izz2a + 1. 12^2 m2a + 1. 13a^2 m2a + \\
& \quad 1. 12^2 m3 + 1. 13a^2 m3a + 2. 12 m2a r2ax + 1. m2a r2ax^2 + 1. m2a r2ay^2 + \\
& \quad 1. m2 r2x^2 + 1. m2 r2y^2 + 1. m3a r3ax^2 + 2. 13a m3a r3az + 1. m3a r3az^2 + \\
& \quad 1. m3 r3x^2 + 1. m3 r3z^2 + (2. 13a m2a r2ay + 2. 12 m3 r3x) \cos[\theta_3(t)] + \\
& \quad (-2. 12 13a m2a - 2. 13a m2a r2ax - 2. 12 m3 r3z) \sin[\theta_3(t)]) \theta_2(t)^2 + \\
& (1. Iyy3 + 1. Iyy3a + 1. 13a^2 m2a + 1. 13a^2 m3a + 1. m3a r3ax^2 + 2. 13a m3a r3az + \\
& \quad 1. m3a r3az^2 + 1. m3 r3x^2 + 1. m3 r3z^2 + (1. 13a m2a r2ay + 1. 12 m3 r3x) \cos[\theta_3(t)] + \\
& \quad (-1. 12 13a m2a - 1. 13a m2a r2ax - 1. 12 m3 r3z) \sin[\theta_3(t)]) \theta_2(t)^2
\end{aligned}$$

Figure 0.2. Second Actuator Torque

The third row ( $\tau_3$ ) :

$$\begin{aligned}
& g \left( (-1. m3a r3ax - 1. m3 r3x) \cos[\theta_2[t] + \theta_3[t]] + \right. \\
& \quad (13a (m2a + m3a) + m3a r3az + m3 r3z) \sin[\theta_2[t] + \theta_3[t]] \left. + \right. \\
& \quad \left( (0.5 l2 l3a m2a + 0.5 l3a m2a r2ax + 0.5 l2 m3 r3z) \cos[\theta_3[t]] + \right. \\
& \quad (1. Ixz3 + 1. Ixz3a + 1. l3a m3a r3ax + 1. m3a r3ax r3az + 1. m3 r3x r3z) \\
& \quad \cos[2 (\theta_2[t] + \theta_3[t])] + 0.5 l2 l3a m2a \cos[2 \theta_2[t] + \theta_3[t]] + \\
& \quad 0.5 l3a m2a r2ax \cos[2 \theta_2[t] + \theta_3[t]] + \\
& \quad 0.5 l2 m3 r3z \cos[2 \theta_2[t] + \theta_3[t]] + 0.5 l3a m2a r2ay \sin[\theta_3[t]] + \\
& \quad 0.5 l2 m3 r3x \sin[\theta_3[t]] - 0.5 Ixx3 \sin[2 (\theta_2[t] + \theta_3[t])] - \\
& \quad 0.5 Ixx3a \sin[2 (\theta_2[t] + \theta_3[t])] + 0.5 Izz3 \sin[2 (\theta_2[t] + \theta_3[t])] + \\
& \quad 0.5 Izz3a \sin[2 (\theta_2[t] + \theta_3[t])] - 0.5 l3a^2 m2a \sin[2 (\theta_2[t] + \theta_3[t])] - \\
& \quad 0.5 l3a^2 m3a \sin[2 (\theta_2[t] + \theta_3[t])] + \\
& \quad 0.5 m3a r3ax^2 \sin[2 (\theta_2[t] + \theta_3[t])] - 1. l3a m3a r3az \\
& \quad \sin[2 (\theta_2[t] + \theta_3[t])] - 0.5 m3a r3az^2 \sin[2 (\theta_2[t] + \theta_3[t])] + \\
& \quad 0.5 m3 r3x^2 \sin[2 (\theta_2[t] + \theta_3[t])] - 0.5 m3 r3z^2 \sin[2 (\theta_2[t] + \theta_3[t])] - \\
& \quad 0.5 l3a m2a r2ay \sin[2 \theta_2[t] + \theta_3[t]] + \\
& \quad \left. \left. 0.5 l2 m3 r3x \sin[2 \theta_2[t] + \theta_3[t]] \right) \theta_1'[t]^2 + \right. \\
& \quad \left( (1. l2 l3a m2a + 1. l3a m2a r2ax + 1. l2 m3 r3z) \cos[\theta_3[t]] + \right. \\
& \quad (1. l3a m2a r2ay + 1. l2 m3 r3x) \sin[\theta_3[t]] \left. \right) \theta_2'[t]^2 + \\
& \quad \left( (-1. Iyz3 - 1. Iyz3a + 1. l3a m2a r2az - 1. l3a m3a r3ay - 1. m3a r3ay r3az - 1. m3 r3y r3z) \right. \\
& \quad \cos[\theta_2[t] + \theta_3[t]] + (-1. Ixy3 - 1. Ixy3a - 1. m3a r3ax r3ay - 1. m3 r3x r3y) \\
& \quad \left. \sin[\theta_2[t] + \theta_3[t]] \right) \theta_1''[t] + \\
& \quad (1. Iyy3 + 1. Iyy3a + 1. l3a^2 m2a + 1. l3a^2 m3a + 1. m3a r3ax^2 + 2. l3a m3a r3az + \\
& \quad 1. m3a r3az^2 + 1. m3 r3x^2 + 1. m3 r3z^2 + (1. l3a m2a r2ay + 1. l2 m3 r3x) \cos[\theta_3[t]] + \\
& \quad (-1. l2 l3a m2a - 1. l3a m2a r2ax - 1. l2 m3 r3z) \sin[\theta_3[t]] \left. \right) \theta_2''[t] + \\
& \quad (1. Iyy3 + 1. Iyy3a + 1. l3a^2 m2a + 1. l3a^2 m3a + 1. m3a r3ax^2 + 2. l3a m3a r3az + \\
& \quad 1. m3a r3az^2 + 1. m3 r3x^2 + 1. m3 r3z^2) \theta_3''[t]
\end{aligned}$$

Figure 0.3. Third Actuator Torque

## A.2. Validity Check of the Derived Equations of Motion

Positive definiteness of  $\bar{H}(\theta)$  and the skew-symmetric property of the matrix  $(\bar{H}(\theta) - 2\bar{C}_{\text{cvt}}(\theta, \dot{\theta}))$  are checked via the following MATHEMATICA codes.

### Construct Equations of Motion

```

M11 = D[tau1, theta1''[t]];
M12 = D[tau1, theta2''[t]];
M13 = D[tau1, theta3''[t]];
M21 = D[tau2, theta1''[t]];
M22 = D[tau2, theta2''[t]];
M23 = D[tau2, theta3''[t]];
M31 = D[tau3, theta1''[t]];
M32 = D[tau3, theta2''[t]];
M33 = D[tau3, theta3''[t]];

Tau1theta1dottheta1dot = D[D[tau1, theta1'[t]], theta1'[t]] / 2;
Tau1theta1dottheta2dot = D[D[tau1, theta1'[t]], theta2'[t]];
Tau1theta1dottheta3dot = D[D[tau1, theta1'[t]], theta3'[t]];
Tau1theta2dottheta2dot = D[D[tau1, theta2'[t]], theta2'[t]] / 2;
Tau1theta2dottheta3dot = D[D[tau1, theta2'[t]], theta3'[t]];
Tau1theta3dottheta3dot = D[D[tau1, theta3'[t]], theta3'[t]] / 2;

Tau2theta1dottheta1dot = D[D[tau2, theta1'[t]], theta1'[t]] / 2;
Tau2theta1dottheta2dot = D[D[tau2, theta1'[t]], theta2'[t]];
Tau2theta1dottheta3dot = D[D[tau2, theta1'[t]], theta3'[t]];
Tau2theta2dottheta2dot = D[D[tau2, theta2'[t]], theta2'[t]] / 2;
Tau2theta2dottheta3dot = D[D[tau2, theta2'[t]], theta3'[t]];
Tau2theta3dottheta3dot = D[D[tau2, theta3'[t]], theta3'[t]] / 2;

Tau3theta1dottheta1dot = D[D[tau3, theta1'[t]], theta1'[t]] / 2;
Tau3theta1dottheta2dot = D[D[tau3, theta1'[t]], theta2'[t]];
Tau3theta1dottheta3dot = D[D[tau3, theta1'[t]], theta3'[t]];
Tau3theta2dottheta2dot = D[D[tau3, theta2'[t]], theta2'[t]] / 2;
Tau3theta2dottheta3dot = D[D[tau3, theta2'[t]], theta3'[t]];
Tau3theta3dottheta3dot = D[D[tau3, theta3'[t]], theta3'[t]] / 2;

c11 = Tau1theta1dottheta1dot * theta1'[t] +
      Tau1theta1dottheta2dot / 2 * theta2'[t] + Tau1theta1dottheta3dot / 2 * theta3'[t];
c12 = Tau1theta2dottheta2dot * theta2'[t] + Tau1theta1dottheta2dot / 2 * theta1'[t] +
      Tau1theta2dottheta3dot / 2 * theta3'[t];
c13 = Tau1theta3dottheta3dot * theta3'[t] + Tau1theta1dottheta3dot / 2 * theta1'[t] +
      Tau1theta2dottheta3dot / 2 * theta2'[t];

c21 = Tau2theta1dottheta1dot * theta1'[t] +
      Tau2theta1dottheta2dot / 2 * theta2'[t] + Tau2theta1dottheta3dot / 2 * theta3'[t];
c22 = Tau2theta2dottheta2dot * theta2'[t] + Tau2theta1dottheta2dot / 2 * theta1'[t] +
      Tau2theta2dottheta3dot / 2 * theta3'[t];
c23 = Tau2theta3dottheta3dot * theta3'[t] + Tau2theta1dottheta3dot / 2 * theta1'[t] +
      Tau2theta2dottheta3dot / 2 * theta2'[t];

c31 = Tau3theta1dottheta1dot * theta1'[t] +
      Tau3theta1dottheta2dot / 2 * theta2'[t] + Tau3theta1dottheta3dot / 2 * theta3'[t];
c32 = Tau3theta2dottheta2dot * theta2'[t] + Tau3theta1dottheta2dot / 2 * theta1'[t] +
      Tau3theta2dottheta3dot / 2 * theta3'[t];
c33 = Tau3theta3dottheta3dot * theta3'[t] + Tau3theta1dottheta3dot / 2 * theta1'[t] +
      Tau3theta2dottheta3dot / 2 * theta2'[t];

```

Figure 0.4. Validity Check of the Derived Equations

```

Check matrix M symmetric
Check matrix (M_dot - 2C) is a skew-symmetric

Simplify[M12 - M21]
Simplify[M13 - M31]
Simplify[M23 - M32]

Simplify[D[M33, t] - 2 * c33]
Simplify[D[M22, t] - 2 * c22]
Simplify[D[M11, t] - 2 * c11]
Simplify[(D[M21, t] - 2 * c21) + (D[M12, t] - 2 * c12)]
Simplify[(D[M31, t] - 2 * c31) + (D[M13, t] - 2 * c13)]
Simplify[(D[M23, t] - 2 * c23) + (D[M32, t] - 2 * c32)]

0.
0
0.
0
0.
0.
0.
0.
0.
0.

```

*Figure 0.4. Continued*

### A.3. Comparison with the Available Equations of Motion given in [25]

In order to compare the results of dynamic analysis with the equations of motions given in [25], a conversion is applied to the derived equations of motion. The elements of the [M], [C] and [G] matrices thus obtained, in accordance with the convention given in [25], are presented below.

$$\begin{aligned}
 \mathbf{M11} = & 0.5 \text{IyyA} + 1. \text{IyyBase} + 0.5 \text{IyyC} + 0.5 \text{IyyDF} + 0.5 \text{IyyEB} + 0.5 \text{IzzA} + 0.5 \text{IzzC} + \\
 & 0.5 \text{IzzDF} + 0.5 \text{IzzEB} + 0.5 \text{I1}^2 \text{ma} + 0.125 \text{I2}^2 \text{ma} + 0.125 \text{I1}^2 \text{mc} + 0.5 \text{I3}^2 \text{mc} + \\
 & (0.5 \text{IyyC} + 0.5 \text{IyyEB} - 0.5 \text{IzzC} - 0.5 \text{IzzEB} + 0.5 \text{I1}^2 \text{ma} + 0.125 \text{I1}^2 \text{mc}) \text{Cos}[2 \text{theta}2\text{c}[t]] - \\
 & 0.5 \text{I3}^2 \text{mc} \text{Cos}[\text{theta}3\text{c}[t]]^2 + 0.5 \text{IyyA} \text{Cos}[2 \text{theta}3\text{c}[t]] + 0.5 \text{IyyDF} \text{Cos}[2 \text{theta}3\text{c}[t]] - \\
 & 0.5 \text{IzzA} \text{Cos}[2 \text{theta}3\text{c}[t]] - 0.5 \text{IzzDF} \text{Cos}[2 \text{theta}3\text{c}[t]] - \\
 & 0.125 \text{I2}^2 \text{ma} \text{Cos}[2 \text{theta}3\text{c}[t]] + 1. \text{I1} \text{I2} \text{ma} \text{Cos}[\text{theta}2\text{c}[t]] \text{Sin}[\text{theta}3\text{c}[t]] + \\
 & 1. \text{I1} \text{I3} \text{mc} \text{Cos}[\text{theta}2\text{c}[t]] \text{Sin}[\text{theta}3\text{c}[t]] + 0.5 \text{I3}^2 \text{mc} \text{Sin}[\text{theta}3\text{c}[t]]^2 \\
 \mathbf{M12} = & 0 \\
 \mathbf{M13} = & 0 \\
 \mathbf{M21} = & 0 \\
 \mathbf{M22} = & 1. \text{IxxC} + 1. \text{IxxEB} + 1. \text{I1}^2 \text{ma} + 0.25 \text{I1}^2 \text{mc} \\
 \mathbf{M23} = & -0.5 \text{I1} \text{I2} \text{ma} \text{Sin}[\text{theta}2\text{c}[t] - \text{theta}3\text{c}[t]] - 0.5 \text{I1} \text{I3} \text{mc} \text{Sin}[\text{theta}2\text{c}[t] - \text{theta}3\text{c}[t]] \\
 \mathbf{M31} = & 0 \\
 \mathbf{M32} = & -0.5 \text{I1} \text{I2} \text{ma} \text{Sin}[\text{theta}2\text{c}[t] - \text{theta}3\text{c}[t]] - 0.5 \text{I1} \text{I3} \text{mc} \text{Sin}[\text{theta}2\text{c}[t] - \text{theta}3\text{c}[t]] \\
 \mathbf{M33} = & 1. \text{IxxA} + 1. \text{IxxDF} + 0.25 \text{I2}^2 \text{ma} + 1. \text{I3}^2 \text{mc} \\
 \mathbf{C11} = & \frac{1}{2} ((-1. \text{IyyC} - 1. \text{IyyEB} + 1. \text{IzzC} + 1. \text{IzzEB} - 1. \text{I1}^2 \text{ma} - 0.25 \text{I1}^2 \text{mc}) \text{Sin}[2 \text{theta}2\text{c}[t]] + \\
 & \text{I1} (-1. \text{I2} \text{ma} - 1. \text{I3} \text{mc}) \text{Sin}[\text{theta}2\text{c}[t]] \text{Sin}[\text{theta}3\text{c}[t]]) \text{theta}2\text{c}'[t] + \\
 & \frac{1}{2} (\text{I1} (1. \text{I2} \text{ma} + 1. \text{I3} \text{mc}) \text{Cos}[\text{theta}2\text{c}[t]] \text{Cos}[\text{theta}3\text{c}[t]] + \\
 & (-1. \text{IyyA} - 1. \text{IyyDF} + 1. \text{IzzA} + 1. \text{IzzDF} + 0.25 \text{I2}^2 \text{ma} + 1. \text{I3}^2 \text{mc}) \\
 & \text{Sin}[2 \text{theta}3\text{c}[t]]) \text{theta}3\text{c}'[t] \\
 \mathbf{C12} = & \frac{1}{2} ((-1. \text{IyyC} - 1. \text{IyyEB} + 1. \text{IzzC} + 1. \text{IzzEB} - 1. \text{I1}^2 \text{ma} - 0.25 \text{I1}^2 \text{mc}) \text{Sin}[2 \text{theta}2\text{c}[t]] + \\
 & \text{I1} (-1. \text{I2} \text{ma} - 1. \text{I3} \text{mc}) \text{Sin}[\text{theta}2\text{c}[t]] \text{Sin}[\text{theta}3\text{c}[t]]) \text{theta}1'[t]
 \end{aligned}$$

Figure 0.5. Comparison with Available Equations

$$\begin{aligned}
\mathbf{C13} &= \\
&\frac{1}{2} \left( 11 (1.12 ma + 1.13 mc) \cos[\theta_{2c}[t]] \cos[\theta_{3c}[t]] + \right. \\
&\quad \left. (-1.1I_{yyA} - 1.1I_{yyDF} + 1.1I_{zzA} + 1.1I_{zzDF} + 0.25 12^2 ma + 1.13^2 mc) \right. \\
&\quad \left. \sin[2\theta_{3c}[t]] \right) \theta_{1'}[t] \\
\mathbf{C21} &= \\
&\left( 0.5 I_{yyC} + 0.5 I_{yyEB} - 0.5 I_{zzC} - 0.5 I_{zzEB} + 0.5 11^2 ma + 0.125 11^2 mc \right) \sin[2\theta_{2c}[t]] + \\
&\quad 11 (0.5 12 ma + 0.5 13 mc) \sin[\theta_{2c}[t]] \sin[\theta_{3c}[t]] \theta_{1'}[t] \\
\mathbf{C22} &= \\
&0 \\
\mathbf{C23} &= \\
&11 (0.5 12 ma + 0.5 13 mc) \cos[\theta_{2c}[t] - \theta_{3c}[t]] \theta_{3c}'[t] \\
\mathbf{C31} &= \\
&\left( 11 (-0.5 12 ma - 0.5 13 mc) \cos[\theta_{2c}[t]] \cos[\theta_{3c}[t]] + \right. \\
&\quad \left. (0.5 I_{yyA} + 0.5 I_{yyDF} - 0.5 I_{zzA} - 0.5 I_{zzDF} - 0.125 12^2 ma - 0.5 13^2 mc) \right. \\
&\quad \left. \sin[2\theta_{3c}[t]] \right) \theta_{1'}[t] \\
\mathbf{C32} &= \\
&11 (-0.5 12 ma - 0.5 13 mc) \cos[\theta_{2c}[t] - \theta_{3c}[t]] \theta_{2c}'[t] \\
\mathbf{C33} &= \\
&0 \\
\mathbf{G1} &= \\
&0 \\
\mathbf{G2} &= \\
&g \left( 11 ma \cos[\theta_{2c}[t]] + 0.5 11 mc \cos[\theta_{2c}[t]] + 15 me_b \cos[\theta_{2c}[t]] \right) \\
\mathbf{G3} &= \\
&g \left( \frac{1}{2} 12 ma \sin[\theta_{3c}[t]] + 13 mc \sin[\theta_{3c}[t]] - 16 md_f \sin[\theta_{3c}[t]] \right)
\end{aligned}$$

*Figure 0.5. Continued*

## B. LN of Haptic Interfaces

The linearity numbers corresponding to the three and six DOF configurations are presented in the following sections.

### B.1. LN of Three DOF Configuration

$$\begin{aligned}
& 0.75 I_{xx}^2 + 1.5 I_{xx2} I_{xx2a} + 0.75 I_{xx2a}^2 + 1.375 I_{xx}^3 + 2.75 I_{xx3} I_{xx3a} + 1.375 I_{xx3a}^2 + \\
& 0.75 I_{yy}^2 + 1.5 I_{yy2} I_{yy2a} + 0.75 I_{yy2a}^2 + 1.375 I_{zz}^2 + 2.75 I_{zz3} I_{zz3a} + \\
& 1.375 I_{zz3a}^2 + (-1.5 I_{xx2} I_{yy2} - 1.5 I_{xx2a} I_{yy2} - 1.5 I_{xx2} I_{yy2a} - 1.5 I_{xx2a} I_{yy2a} - \\
& \quad 2.75 I_{xx3} I_{zz3} - 2.75 I_{xx3a} I_{zz3} - 2.75 I_{xx3} I_{zz3a} - 2.75 I_{xx3a} I_{zz3a}) + \\
& 3. I_{xy}^2 + 6. I_{xy2} I_{xy2a} + 3. I_{xy2a}^2 + 5. I_{xy3}^2 + 10. I_{xy3} I_{xy3a} + 5. I_{xy3a}^2 + \\
& 1.5 I_{xz}^2 + 3. I_{xz2} I_{xz2a} + 1.5 I_{xz2a}^2 + 5.5 I_{xz3}^2 + 11. I_{xz3} I_{xz3a} + \\
& 5.5 I_{xz3a}^2 + 1.5 I_{yz}^2 + 3. I_{yz2} I_{yz2a} + 1.5 I_{yz2a}^2 + 5. I_{yz3}^2 + 10. I_{yz3} I_{yz3a} + \\
& 5. I_{yz3a}^2 + I_{xy2} (6. 12 m_2a r_{2ay} + (6. m_2a r_{2ax} r_{2ay} + 6. m_2 r_{2x} r_{2y})) + \\
& I_{xy2a} (6. 12 m_2a r_{2ay} + (6. m_2a r_{2ax} r_{2ay} + 6. m_2 r_{2x} r_{2y})) + \\
& I_{yz2} (3. m_2a r_{2ay} r_{2az} + 3. m_2 r_{2y} r_{2z}) + I_{yz2a} (3. m_2a r_{2ay} r_{2az} + 3. m_2 r_{2y} r_{2z}) + \\
& I_{xy3} (10. m_3a r_{3ax} r_{3ay} + 10. m_3 r_{3x} r_{3y}) + I_{xy3a} (10. m_3a r_{3ax} r_{3ay} + 10. m_3 r_{3x} r_{3y}) + \\
& I_{xz2} ((3. m_2a r_{2ax} r_{2az} + 3. m_2 r_{2x} r_{2z}) + 12 (3. m_2a r_{2az} - 3. m_3 r_{3y})) + \\
& I_{xz2a} ((3. m_2a r_{2ax} r_{2az} + 3. m_2 r_{2x} r_{2z}) + 12 (3. m_2a r_{2az} - 3. m_3 r_{3y})) + \\
& I_{xz3} (11. 13a m_3a r_{3ax} + (11. m_3a r_{3ax} r_{3az} + 11. m_3 r_{3x} r_{3z})) + \\
& I_{xz3a} (11. 13a m_3a r_{3ax} + (11. m_3a r_{3ax} r_{3az} + 11. m_3 r_{3x} r_{3z})) + \\
& I_{yz3} (13a (-10. m_2a r_{2az} + 10. m_3a r_{3ay}) + (10. m_3a r_{3ay} r_{3az} + 10. m_3 r_{3y} r_{3z})) + \\
& I_{yz3a} (13a (-10. m_2a r_{2az} + 10. m_3a r_{3ay}) + (10. m_3a r_{3ay} r_{3az} + 10. m_3 r_{3y} r_{3z})) + \\
& 12^2 m_2 (m_2a (1.5 r_{2x}^2 - 1.5 r_{2y}^2) + m_3 (1.5 r_{2x}^2 - 1.5 r_{2y}^2)) + \\
& 13a^2 m_3 (m_2a (-2.75 r_{3x}^2 + 2.75 r_{3z}^2) + m_3a (-2.75 r_{3x}^2 + 2.75 r_{3z}^2)) + \\
& 0.5 12^2 m_2a (-3. I_{xx2} + (-3. I_{xx2a} + (3. I_{yy2} + (3. I_{yy2a} + (12. 12^2 (1.5 m_2a + 1.5 m_3) + \\
& \quad (18. 12 m_2a r_{2ax} + 6. 12 (3. m_2a + 3. m_3) r_{2ax}) + 2. (21.5 13a^2 m_2a + \\
& \quad (2. m_2a (4.5 r_{2ax}^2 + 1.5 r_{2ay}^2 + 1.5 r_{2az}^2) + (1.5 m_3 r_{2ax}^2 - 1.5 m_3 r_{2ay}^2 + \\
& \quad 1.5 m_2 r_{2x}^2 - 1.5 m_2 r_{2y}^2 - 3. m_3 r_{2az} r_{3y})) + 21.5 13a m_3 r_{3z})))))) + \\
& 0.5 13a^2 m_3a (5.5 I_{xx3} + (5.5 I_{xx3a} + (-5.5 I_{zz3} + (-5.5 I_{zz3a} + (12. 13a^2 \\
& \quad (2.75 m_2a + 2.75 m_3a) + (33. 13a m_3a r_{3az} + 6. 13a (5.5 m_2a + 5.5 m_3a) r_{3az}) + \\
& \quad 2. (m_2a (-2.75 r_{3ax}^2 - 10. r_{2az} r_{3ay} + 2.75 r_{3az}^2) + (2.75 m_3a r_{3ax}^2 + \\
& \quad 5. m_3a r_{3ay}^2 + 8.25 m_3a r_{3az}^2 + m_3a (2.75 r_{3ax}^2 + 5. r_{3ay}^2 + 8.25 r_{3az}^2) - \\
& \quad 2.75 m_3 r_{3x}^2 + 2.75 m_3 r_{3z}^2)))))) + \\
& 0.5 13a^2 m_2a (5.5 I_{xx3} + (5.5 I_{xx3a} + (-5.5 I_{zz3} + (-5.5 I_{zz3a} + \\
& \quad (43. 12^2 m_2a + 86. 12 m_2a r_{2ax} + (12. 13a^2 (2.75 m_2a + 2.75 m_3a) + 33. 13a m_3a r_{3az} + \\
& \quad 2. (2. m_2a (10.75 r_{2ax}^2 + 10.75 r_{2ay}^2 + 5. r_{2az}^2) + (-2.75 m_3a r_{3ax}^2 - \\
& \quad 10. m_3a r_{2az} r_{3ay} + 2.75 m_3a r_{3az}^2 - 2.75 m_3 r_{3x}^2 + 2.75 m_3 r_{3z}^2)))))) + \\
& 0.5 12^2 m_3 (-3. I_{xx2} + (-3. I_{xx2a} + (3. I_{yy2} + (3. I_{yy2a} + (12. 12^2 (1.5 m_2a + 1.5 m_3) + \\
& \quad 18. 12 m_2a r_{2ax} + 2. (21.5 13a m_2a r_{3z} + (m_2a (1.5 r_{2ax}^2 - 1.5 r_{2ay}^2 - \\
& \quad 3. r_{2az} r_{3y}) + (1.5 m_2 r_{2x}^2 - 1.5 m_2 r_{2y}^2 + 10.75 m_3 r_{3x}^2 + 1.5 m_3 r_{3y}^2 + \\
& \quad 10.75 m_3 r_{3z}^2 + m_3 (10.75 r_{3x}^2 + 1.5 r_{3y}^2 + 10.75 r_{3z}^2)))))) + \\
& 12^4 (-8.25 m_2a^2 - 16.5 m_2a m_3 - 8.25 m_3^2) + 12^3 m_2a (-15. m_2a - 15. m_3) \\
& r_{2ax} + \\
& 12 (-3. I_{xx2} m_2a r_{2ax} - 3. I_{xx2a} m_2a r_{2ax} + 3. I_{yy2} m_2a r_{2ax} + \\
& \quad 3. I_{yy2a} m_2a r_{2ax} - 21.5 13a^2 m_2a^2 r_{2ax} + 3. m_2a^2 r_{2ax}^3 + \\
& \quad 3. m_2a^2 r_{2ax} r_{2ay}^2 + 3. m_2a^2 r_{2ax} r_{2az}^2 + 3. m_2 m_2a r_{2ax} r_{2x}^2 + \\
& \quad 6. m_2 m_2a r_{2ay} r_{2x} r_{2y} - 3. m_2 m_2a r_{2ax} r_{2y}^2 + 3. m_2 m_2a r_{2az} r_{2x} r_{2z} + \\
& \quad 7. 13a m_2a m_3 r_{2ay} r_{3x} - 3. m_2a m_3 r_{2ax} r_{2az} r_{3y} - \\
& \quad 3. m_2 m_3 r_{2x} r_{2z} r_{3y} + 21.5 13a m_2a m_3 r_{2ax} r_{3z}) + \\
& 12^2 (-32.25 13a^2 m_2a^2 - 21.5 13a m_2a m_3 r_{3z} + (m_2a^2 (-4.5 r_{2ax}^2 - 1.5 r_{2ay}^2 - 1.5 r_{2az}^2) + \\
& \quad m_2a (-1.5 m_3 r_{2ax}^2 + 1.5 m_3 r_{2ay}^2 - 1.5 m_2 r_{2x}^2 + 1.5 m_2 r_{2y}^2 + 3. m_3 r_{2az} r_{3y}) + \\
& \quad m_3 (-1.5 m_2 r_{2x}^2 + 1.5 m_2 r_{2y}^2 - 10.75 m_3 r_{3x}^2 - 1.5 m_3 r_{3y}^2 - 10.75 m_3 r_{3z}^2))) + \\
& (13a^4 (-15.125 m_2a^2 - 30.25 m_2a m_3a - 15.125 m_3a^2) + \\
& \quad 13a^3 (-27.5 m_2a - 27.5 m_3a) m_3a r_{3az} + \\
& \quad 13a (5.5 I_{xx3} m_3a r_{3az} + 5.5 I_{xx3a} m_3a r_{3az} - 5.5 I_{zz3} m_3a r_{3az} - 5.5 I_{zz3a} m_3a r_{3az} + \\
& \quad 5.5 m_3a^2 r_{3ax}^2 r_{3az} - 10. m_2a m_3a r_{2az} r_{3ay} r_{3az} + 10. m_3a^2 r_{3ay}^2 r_{3az} + \\
& \quad 5.5 m_3a^2 r_{3az}^3 - 5.5 m_3 m_3a r_{3az} r_{3x}^2 + 11. m_3 m_3a r_{3ax} r_{3x} r_{3z} - \\
& \quad 10. m_2a m_3 r_{2az} r_{3y} r_{3z} + 10. m_3 m_3a r_{3ay} r_{3y} r_{3z} + 5.5 m_3 m_3a r_{3az} r_{3z}^2) + \\
& \quad 13a^2 (m_2a (-10.75 r_{2ax}^2 - 10.75 r_{2ay}^2 - 5. r_{2az}^2) + \\
& \quad m_3a (-2.75 m_3a r_{3ax}^2 - 5. m_3a r_{3ay}^2 - 8.25 m_3a r_{3az}^2 + 2.75 m_3 r_{3x}^2 - 2.75 m_3 r_{3z}^2) +
\end{aligned}$$

Figure 0.6. LN of Three DOF Configuration

$$\begin{aligned}
& m2a (2.75 m3a r3ax^2 + 10. m3a r2az r3ay - 2.75 m3a r3az^2 + 2.75 m3 r3x^2 - 2.75 m3 r3z^2) + \\
& (Ixx2 (-1.5 m2a r2ax^2 + 1.5 m2a r2ay^2 - 1.5 m2 r2x^2 + 1.5 m2 r2y^2) + \\
& (-1.5 Ixx2a m2a r2ax^2 + 1.5 Iyy2 m2a r2ax^2 + 1.5 Iyy2a m2a r2ax^2 + 0.75 m2a^2 r2ax^4 + \\
& 1.5 Ixx2a m2a r2ay^2 - 1.5 Iyy2 m2a r2ay^2 - 1.5 Iyy2a m2a r2ay^2 + 1.5 m2a^2 r2ax^2 r2ay^2 + \\
& 0.75 m2a^2 r2ay^4 + 1.5 m2a^2 r2ax^2 r2az^2 + 1.5 m2a^2 r2ay^2 r2az^2 - 1.5 Ixx2a m2 r2x^2 + \\
& 1.5 Iyy2 m2 r2x^2 + 1.5 Iyy2a m2 r2x^2 + 1.5 m2 m2a r2ax^2 r2x^2 - 1.5 m2 m2a r2ay^2 r2x^2 + \\
& 0.75 m2^2 r2x^4 + 6. m2 m2a r2ax r2ay r2x r2y + 1.5 Ixx2a m2 r2y^2 - 1.5 Iyy2 m2 r2y^2 - \\
& 1.5 Iyy2a m2 r2y^2 - 1.5 m2 m2a r2ax^2 r2y^2 + 1.5 m2 m2a r2ay^2 r2y^2 + 1.5 m2^2 r2x^2 r2y^2 + \\
& 0.75 m2^2 r2y^4 + 3. m2 m2a r2ax r2az r2x r2z + 3. m2 m2a r2ay r2az r2y r2z + \\
& 1.5 m2^2 r2x^2 r2z^2 + 1.5 m2^2 r2y^2 r2z^2 - 2.75 Ixx3 m3a r3ax^2 - 2.75 Ixx3a m3a r3ax^2 + \\
& 2.75 Izz3 m3a r3ax^2 + 2.75 Izz3a m3a r3ax^2 + 1.375 m3a^2 r3ax^4 + 5. m3a^2 r3ax^2 r3ay^2 + \\
& 2.75 Ixx3 m3a r3az^2 + 2.75 Ixx3a m3a r3az^2 - 2.75 Izz3 m3a r3az^2 - 2.75 Izz3a m3a r3az^2 + \\
& 2.75 m3a^2 r3ax^2 r3az^2 + 5. m3a^2 r3ay^2 r3az^2 + 1.375 m3a^2 r3az^4 - 2.75 Ixx3 m3 r3x^2 - \\
& 2.75 Ixx3a m3 r3x^2 + 2.75 Izz3 m3 r3x^2 + 2.75 Izz3a m3 r3x^2 + 2.75 m3 m3a r3ax^2 r3x^2 - \\
& 2.75 m3 m3a r3az^2 r3x^2 + 1.375 m3^2 r3x^4 + 10. m3 m3a r3ax r3ay r3x r3y + 5. m3^2 r3x^2 r3y^2 + \\
& 11. m3 m3a r3ax r3az r3x r3z + 10. m3 m3a r3ay r3az r3y r3z + 2.75 Ixx3 m3 r3z^2 + \\
& 2.75 Ixx3a m3 r3z^2 - 2.75 Izz3 m3 r3z^2 - 2.75 Izz3a m3 r3z^2 - 2.75 m3 m3a r3ax^2 r3z^2 + \\
& 2.75 m3 m3a r3az^2 r3z^2 + 2.75 m3^2 r3x^2 r3z^2 + 5. m3^2 r3y^2 r3z^2 + 1.375 m3^2 r3z^4) + \\
& 0.5 g^2 (1. 12^2 m2a^2 + 2. 13a^2 m2a^2 + 2. 12^2 m2a m3 + 1. 12^2 m3^2 + 4. 13a^2 m2a m3a + \\
& 2. 13a^2 m3a^2 + 2. 12 m2a^2 r2ax + 2. 12 m2a m3 r2ax + \\
& 1. m2a^2 r2ax^2 + 1. m2a^2 r2ay^2 + 2. 12 m2 m2a r2x + \\
& 2. 12 m2 m3 r2x + 2. m2 m2a r2ax r2x + 1. m2^2 r2x^2 + \\
& 2. m2 m2a r2ay r2y + 1. m2^2 r2y^2 + 2. m3a^2 r3ax^2 + \\
& 4. 13a m2a m3a r3az + 4. 13a m3a^2 r3az + 2. m3a^2 r3az^2 + \\
& 4. m3 m3a r3ax r3x + 2. m3^2 r3x^2 + 4. 13a m2a m3 r3z + \\
& 4. 13a m3 m3a r3z + 4. m3 m3a r3az r3z + 2. m3^2 r3z^2)
\end{aligned}$$

Figure 0.6. Continued

## B.2. LN of Six DOF Configuration

$$\begin{aligned}
& 0.75 \text{Ixx}^2 + 1.5 \text{Ixx2 Ixx}2a + 0.75 \text{Ixx}2a^2 + 1.375 \text{Ixx}3^2 + 2.75 \text{Ixx3 Ixx}3a + 1.375 \text{Ixx}3a^2 + \\
& 1.375 \text{Ixx3 Ixx}4 + 1.375 \text{Ixx3a Ixx}4 + 6.15625 \text{Ixx}4^2 - 0.6875 \text{Ixx3 Ixx}5 - 0.6875 \text{Ixx3a Ixx}5 + \\
& 5.46875 \text{Ixx4 Ixx}5 + 11.6934 \text{Ixx}5^2 + 0.34375 \text{Ixx3 Ixx}6 + 0.34375 \text{Ixx3a Ixx}6 - \\
& 2.73437 \text{Ixx4 Ixx}6 + 8.61523 \text{Ixx5 Ixx}6 + 22.665 \text{Ixx}6^2 - 1.5 \text{Ixx2 Iyy}2 - 1.5 \text{Ixx2a Iyy}2 + \\
& 0.75 \text{Iyy}2^2 - 1.5 \text{Ixx2 Iyy}2a - 1.5 \text{Ixx2a Iyy}2a + 1.5 \text{Iyy}2 \text{Iyy}2a + 0.75 \text{Iyy}2a^2 + 5.375 \text{Iyy}4^2 - \\
& 1.375 \text{Iyy}4 \text{Iyy}5 + 13.9062 \text{Iyy}5^2 + 1.65625 \text{Iyy}4 \text{Iyy}6 + 10.8281 \text{Iyy}5 \text{Iyy}6 + 22.665 \text{Iyy}6^2 - \\
& 2.75 \text{Ixx3 Izz}3 - 2.75 \text{Ixx3a Izz}3 + 1.375 \text{Izz}3^2 - 2.75 \text{Ixx3 Izz}3a - 2.75 \text{Ixx3a Izz}3a + \\
& 2.75 \text{Izz}3 \text{Izz}3a + 1.375 \text{Izz}3a^2 - 1.375 \text{Izz}3 \text{Izz}4 - 1.375 \text{Izz}3a \text{Izz}4 + 6.15625 \text{Izz}4^2 + \\
& 0.6875 \text{Izz}3 \text{Izz}5 + 0.6875 \text{Izz}3a \text{Izz}5 - 6.15625 \text{Izz}4 \text{Izz}5 + 11.6934 \text{Izz}5^2 + 0.6875 \text{Izz}3 \text{Izz}6 + \\
& 0.6875 \text{Izz}3a \text{Izz}6 - 6.15625 \text{Izz}4 \text{Izz}6 + 23.3867 \text{Izz}5 \text{Izz}6 + 22.6934 \text{Izz}6^2 + 3. \text{Ixy}2^2 + \\
& 6. \text{Ixy}2 \text{Ixy}2a + 3. \text{Ixy}2a^2 + 5. \text{Ixy}3^2 + 10. \text{Ixy}3 \text{Ixy}3a + 5. \text{Ixy}3a^2 + 13.3125 \text{Ixy}4^2 + \\
& 32.3047 \text{Ixy}5^2 + 71.2168 \text{Ixy}6^2 + 1.5 \text{Ix}z2^2 + 3. \text{Ix}z2 \text{Ix}z2a + 1.5 \text{Ix}z2a^2 + 5.5 \text{Ix}z3^2 + \\
& 11. \text{Ix}z3 \text{Ix}z3a + 5.5 \text{Ix}z3a^2 + 23.25 \text{Ix}z4^2 + 36.6172 \text{Ix}z5^2 + 55.0322 \text{Ix}z6^2 + 1.5 \text{Iyz}2^2 + \\
& 3. \text{Iyz}2 \text{Iyz}2a + 1.5 \text{Iyz}2a^2 + 5. \text{Iyz}3^2 + 10. \text{Iyz}3 \text{Iyz}3a + 5. \text{Iyz}3a^2 + 13.3125 \text{Iyz}4^2 + \\
& 32.3047 \text{Iyz}5^2 + 55.0322 \text{Iyz}6^2 + \text{Ixy}2 (6.12 \text{m}2a \text{r}2ay + 6. \text{m}2a \text{r}2ax \text{r}2ay + 6. \text{m}2 \text{r}2x \text{r}2y) + \\
& \text{Ixy}2a (6.12 \text{m}2a \text{r}2ay + 6. \text{m}2a \text{r}2ax \text{r}2ay + 6. \text{m}2 \text{r}2x \text{r}2y) + \\
& \text{Iyz}2 (3. \text{m}2a \text{r}2ay \text{r}2az + 3. \text{m}2 \text{r}2y \text{r}2z) + \text{Iyz}2a (3. \text{m}2a \text{r}2ay \text{r}2az + 3. \text{m}2 \text{r}2y \text{r}2z) + \\
& \text{Ix}z2 (3.12 \text{m}2a \text{r}2az + 3. \text{m}2a \text{r}2ax \text{r}2az + 3. \text{m}2 \text{r}2x \text{r}2z - 3.12 \text{m}3 \text{r}3y) + \\
& \text{Ix}z2a (3.12 \text{m}2a \text{r}2az + 3. \text{m}2a \text{r}2ax \text{r}2az + 3. \text{m}2 \text{r}2x \text{r}2z - 3.12 \text{m}3 \text{r}3y) + \\
& \text{Ixy}3 (10. \text{m}3a \text{r}3ax \text{r}3ay + 10. \text{m}3 \text{r}3x \text{r}3y) + \text{Ixy}3a (10. \text{m}3a \text{r}3ax \text{r}3ay + 10. \text{m}3 \text{r}3x \text{r}3y) + \\
& \text{Ix}z3 (11.13a \text{m}3a \text{r}3ax + 11. \text{m}3a \text{r}3ax \text{r}3az + 11. \text{m}3 \text{r}3x \text{r}3z) + \\
& \text{Ix}z3a (11.13a \text{m}3a \text{r}3ax + 11. \text{m}3a \text{r}3ax \text{r}3az + 11. \text{m}3 \text{r}3x \text{r}3z) + \\
& \text{Iyz}3 (-10.13a \text{m}2a \text{r}2az + 10.13a \text{m}3a \text{r}3ay + 10. \text{m}3a \text{r}3ay \text{r}3az + 10. \text{m}3 \text{r}3y \text{r}3z) + \\
& \text{Iyz}3a (-10.13a \text{m}2a \text{r}2az + 10.13a \text{m}3a \text{r}3ay + 10. \text{m}3a \text{r}3ay \text{r}3az + 10. \text{m}3 \text{r}3y \text{r}3z) + \\
& 26.625 \text{Ixy}4 \text{m}4 \text{r}4x \text{r}4y + 46.5 \text{Ix}z4 \text{m}4 \text{r}4x \text{r}4z + 64.6094 \text{Ixy}5 \text{m}5 \text{r}5x \text{r}5y + \\
& \text{Iyz}4 (26.625 \text{m}4 \text{r}4y \text{r}4z - 26.625 \text{I}3 \text{m}5 \text{r}5y) + 73.2344 \text{Ix}z5 \text{m}5 \text{r}5x \text{r}5z + 64.6094 \text{Iyz}5 \text{m}5 \text{r}5y \text{r}5z + \\
& 142.434 \text{Ixy}6 \text{m}6 \text{r}6x \text{r}6y + 110.064 \text{Ix}z6 \text{m}6 \text{r}6x \text{r}6z + 110.064 \text{Iyz}6 \text{m}6 \text{r}6y \text{r}6z + 1.5 \text{Iyy}2 \text{I}2^2 \text{m}2a + \\
& 1.5 \text{Iyy}2a \text{I}2^2 \text{m}2a + 5.5 \text{Ixx}3 \text{I}3a^2 \text{m}2a + 5.5 \text{Ixx}3a \text{I}3a^2 \text{m}2a + 2.75 \text{Ixx}4 \text{I}3a^2 \text{m}2a - \\
& 1.375 \text{Ixx}5 \text{I}3a^2 \text{m}2a + 0.6875 \text{Ixx}6 \text{I}3a^2 \text{m}2a - 5.5 \text{Iyy}4 \text{I}3a^2 \text{m}2a + 2.75 \text{Iyy}5 \text{I}3a^2 \text{m}2a + \\
& 0.6875 \text{Iyy}6 \text{I}3a^2 \text{m}2a - 5.5 \text{Izz}3 \text{I}3a^2 \text{m}2a - 5.5 \text{Izz}3a \text{I}3a^2 \text{m}2a + 2.75 \text{Izz}4 \text{I}3a^2 \text{m}2a - \\
& 1.375 \text{Izz}5 \text{I}3a^2 \text{m}2a - 1.375 \text{Izz}6 \text{I}3a^2 \text{m}2a + 9.12^4 \text{m}2a^2 + 64.5 \text{I}2^2 \text{I}3a^2 \text{m}2a^2 + 33.13a^4 \text{m}2a^2 + \\
& 1.5 \text{Iyy}2 \text{I}2^2 \text{m}3 + 1.5 \text{Iyy}2a \text{I}2^2 \text{m}3 + 18.12^4 \text{m}2a \text{m}3 + 9.12^4 \text{m}3^2 + 5.5 \text{Ixx}3 \text{I}3a^2 \text{m}3a + \\
& 5.5 \text{Ixx}3a \text{I}3a^2 \text{m}3a + 2.75 \text{Ixx}4 \text{I}3a^2 \text{m}3a - 1.375 \text{Ixx}5 \text{I}3a^2 \text{m}3a + 0.6875 \text{Ixx}6 \text{I}3a^2 \text{m}3a - \\
& 5.5 \text{Iyy}4 \text{I}3a^2 \text{m}3a + 2.75 \text{Iyy}5 \text{I}3a^2 \text{m}3a + 0.6875 \text{Iyy}6 \text{I}3a^2 \text{m}3a - 5.5 \text{Izz}3 \text{I}3a^2 \text{m}3a - \\
& 5.5 \text{Izz}3a \text{I}3a^2 \text{m}3a + 2.75 \text{Izz}4 \text{I}3a^2 \text{m}3a - 1.375 \text{Izz}5 \text{I}3a^2 \text{m}3a - 1.375 \text{Izz}6 \text{I}3a^2 \text{m}3a + \\
& 66.13a^4 \text{m}2a \text{m}3a + 33.13a^4 \text{m}3a^2 + 1.5 \text{Iyy}2 \text{I}2^2 \text{m}4 + 1.5 \text{Iyy}2a \text{I}2^2 \text{m}4 + 18.12^4 \text{m}2a \text{m}4 + \\
& 18.12^4 \text{m}3 \text{m}4 + 9.12^4 \text{m}4^2 + 1.5 \text{Iyy}2 \text{I}2^2 \text{m}5 + 1.5 \text{Iyy}2a \text{I}2^2 \text{m}5 + 2.75 \text{Ixx}3 \text{I}3^2 \text{m}5 + \\
& 2.75 \text{Ixx}3a \text{I}3^2 \text{m}5 + 1.375 \text{Ixx}4 \text{I}3^2 \text{m}5 - 0.6875 \text{Ixx}5 \text{I}3^2 \text{m}5 + 0.34375 \text{Ixx}6 \text{I}3^2 \text{m}5 - \\
& 2.75 \text{Iyy}4 \text{I}3^2 \text{m}5 + 1.375 \text{Iyy}5 \text{I}3^2 \text{m}5 + 0.34375 \text{Iyy}6 \text{I}3^2 \text{m}5 - 2.75 \text{Izz}3 \text{I}3^2 \text{m}5 - \\
& 2.75 \text{Izz}3a \text{I}3^2 \text{m}5 + 1.375 \text{Izz}4 \text{I}3^2 \text{m}5 - 0.6875 \text{Izz}5 \text{I}3^2 \text{m}5 - 0.6875 \text{Izz}6 \text{I}3^2 \text{m}5 + 18.12^4 \text{m}2a \text{m}5 + \\
& 43.12^2 \text{I}3 \text{I}3a \text{m}2a \text{m}5 + 16.5 \text{I}3^2 \text{I}3a^2 \text{m}2a \text{m}5 + 18.12^4 \text{m}3 \text{m}5 + 16.5 \text{I}3^2 \text{I}3a^2 \text{m}3a \text{m}5 + 18.12^4 \text{m}4 \text{m}5 + \\
& 9.12^4 \text{m}5^2 + 43.12^2 \text{I}3^2 \text{m}5^2 + 16.5 \text{I}3^4 \text{m}5^2 + \text{Ix}x2 \text{I}2^2 (-1.5 \text{m}2a - 1.5 \text{m}3 - 1.5 \text{m}4 - 1.5 \text{m}5 - 1.5 \text{m}6) + \\
& \text{Ix}x2a \text{I}2^2 (-1.5 \text{m}2a - 1.5 \text{m}3 - 1.5 \text{m}4 - 1.5 \text{m}5 - 1.5 \text{m}6) + 1.5 \text{Iyy}2 \text{I}2^2 \text{m}6 + 1.5 \text{Iyy}2a \text{I}2^2 \text{m}6 + \\
& 2.75 \text{Ixx}3 \text{I}3^2 \text{m}6 + 2.75 \text{Ixx}3a \text{I}3^2 \text{m}6 + 1.375 \text{Ixx}4 \text{I}3^2 \text{m}6 - 0.6875 \text{Ixx}5 \text{I}3^2 \text{m}6 + \\
& 0.34375 \text{Ixx}6 \text{I}3^2 \text{m}6 - 2.75 \text{Iyy}4 \text{I}3^2 \text{m}6 + 1.375 \text{Iyy}5 \text{I}3^2 \text{m}6 + 0.34375 \text{Iyy}6 \text{I}3^2 \text{m}6 - \\
& 2.75 \text{Izz}3 \text{I}3^2 \text{m}6 - 2.75 \text{Izz}3a \text{I}3^2 \text{m}6 + 1.375 \text{Izz}4 \text{I}3^2 \text{m}6 - 0.6875 \text{Izz}5 \text{I}3^2 \text{m}6 - \\
& 0.6875 \text{Izz}6 \text{I}3^2 \text{m}6 + 18.12^4 \text{m}2a \text{m}6 + 43.12^2 \text{I}3 \text{I}3a \text{m}2a \text{m}6 + 16.5 \text{I}3^2 \text{I}3a^2 \text{m}2a \text{m}6 + 18.12^4 \text{m}3 \text{m}6 + \\
& 16.5 \text{I}3^2 \text{I}3a^2 \text{m}3a \text{m}6 + 18.12^4 \text{m}4 \text{m}6 + 18.12^4 \text{m}5 \text{m}6 + 86.12^2 \text{I}3^2 \text{m}5 \text{m}6 + 33.13^4 \text{m}5 \text{m}6 + \\
& 9.12^4 \text{m}6^2 + 43.12^2 \text{I}3^2 \text{m}6^2 + 16.5 \text{I}3^4 \text{m}6^2 + 18.12^3 \text{m}2a^2 \text{r}2ax + 86.12 \text{I}3a^2 \text{m}2a^2 \text{r}2ax + \\
& 18.12^3 \text{m}2a \text{m}3 \text{r}2ax + 18.12^3 \text{m}2a \text{m}4 \text{r}2ax + 18.12^3 \text{m}2a \text{m}5 \text{r}2ax + 18.12^3 \text{m}2a \text{m}6 \text{r}2ax + \\
& 9.12^2 \text{m}2a^2 \text{r}2ax^2 + 43.13a^2 \text{m}2a^2 \text{r}2ax^2 + 3.12^2 \text{m}2a \text{m}3 \text{r}2ax^2 + 3.12^2 \text{m}2a \text{m}4 \text{r}2ax^2 + \\
& 3.12^2 \text{m}2a \text{m}5 \text{r}2ax^2 + 3.12^2 \text{m}2a \text{m}6 \text{r}2ax^2 + 3.12^2 \text{m}2a^2 \text{r}2ay^2 + 43.13a^2 \text{m}2a^2 \text{r}2ay^2 - \\
& 3.12^2 \text{m}2a \text{m}3 \text{r}2ay^2 - 3.12^2 \text{m}2a \text{m}4 \text{r}2ay^2 - 3.12^2 \text{m}2a \text{m}5 \text{r}2ay^2 - 3.12^2 \text{m}2a \text{m}6 \text{r}2ay^2 + \\
& 3.12^2 \text{m}2a^2 \text{r}2az^2 + 20.13a^2 \text{m}2a^2 \text{r}2az^2 + 3.12^2 \text{m}2 \text{m}2a \text{r}2x^2 + 3.12^2 \text{m}2 \text{m}3 \text{r}2x^2 + 3.12^2 \text{m}2 \text{m}4 \text{r}2x^2 + \\
& 3.12^2 \text{m}2 \text{m}5 \text{r}2x^2 + 3.12^2 \text{m}2 \text{m}6 \text{r}2x^2 - 3.12^2 \text{m}2 \text{m}2a \text{r}2y^2 - 3.12^2 \text{m}2 \text{m}3 \text{r}2y^2 - 3.12^2 \text{m}2 \text{m}4 \text{r}2y^2 - \\
& 3.12^2 \text{m}2 \text{m}5 \text{r}2y^2 - 3.12^2 \text{m}2 \text{m}6 \text{r}2y^2 - 11.13a^2 \text{m}2a \text{m}3a \text{r}3ax^2 + 11.13a^2 \text{m}3a^2 \text{r}3ax^2 - \\
& 5.5 \text{I}3^2 \text{m}3a \text{m}5 \text{r}3ax^2 - 5.5 \text{I}3^2 \text{m}3a \text{m}6 \text{r}3ax^2 - 40.13a^2 \text{m}2a \text{m}3a \text{r}2az \text{r}3ay + 20.13a^2 \text{m}3a^2 \text{r}3ay^2 + \\
& 66.13a^3 \text{m}2a \text{m}3a \text{r}3az + 66.13a^3 \text{m}3a^2 \text{r}3az + 11.13^2 \text{I}3a \text{m}3a \text{m}5 \text{r}3az + 11.13^2 \text{I}3a \text{m}3a \text{m}6 \text{r}3az + \\
& 11.13a^2 \text{m}2a \text{m}3a \text{r}3az^2 + 33.13a^2 \text{m}3a^2 \text{r}3az^2 + 5.5 \text{I}3^2 \text{m}3a \text{m}5 \text{r}3az^2 + 5.5 \text{I}3^2 \text{m}3a \text{m}6 \text{r}3az^2 - \\
& 11.13a^2 \text{m}2a \text{m}3 \text{r}3x^2 + 21.5 \text{I}2^2 \text{m}3^2 \text{r}3x^2 - 11.13a^2 \text{m}3 \text{m}3a \text{r}3x^2 - 5.5 \text{I}3^2 \text{m}3 \text{m}5 \text{r}3x^2 - \\
& 5.5 \text{I}3^2 \text{m}3 \text{m}6 \text{r}3x^2 - 6.12^2 \text{m}2a \text{m}3 \text{r}2az \text{r}3y + 3.12^2 \text{m}3^2 \text{r}3y^2 + 43.12^2 \text{I}3a \text{m}2a \text{m}3 \text{r}3z + \\
& 43.12^2 \text{I}3 \text{m}3 \text{m}5 \text{r}3z + 43.12^2 \text{I}3 \text{m}3 \text{m}6 \text{r}3z + 11.13a^2 \text{m}2a \text{m}3 \text{r}3z^2 + 21.5 \text{I}2^2 \text{m}3^2 \text{r}3z^2 + \\
& 11.13a^2 \text{m}3 \text{m}3a \text{r}3z^2 + 5.5 \text{I}3^2 \text{m}3 \text{m}5 \text{r}3z^2 + 5.5 \text{I}3^2 \text{m}3 \text{m}6 \text{r}3z^2 - 5.5 \text{I}3a^2 \text{m}2a \text{m}4 \text{r}4x^2 - \\
& 5.5 \text{I}3a^2 \text{m}3a \text{m}4 \text{r}4x^2 + 25.12^2 \text{m}4^2 \text{r}4x^2 - 2.75 \text{I}3^2 \text{m}4 \text{m}5 \text{r}4x^2 - 2.75 \text{I}3^2 \text{m}4 \text{m}6 \text{r}4x^2 + \\
& 43.12^2 \text{I}3a \text{m}2a \text{m}4 \text{r}4y + 43.12^2 \text{I}3 \text{m}4 \text{m}5 \text{r}4y + 43.12^2 \text{I}3 \text{m}4 \text{m}6 \text{r}4y + 43.12^2 \text{m}3 \text{m}4 \text{r}3z \text{r}4y + \\
& 11.13a^2 \text{m}2a \text{m}4 \text{r}4y^2 + 11.13a^2 \text{m}3a \text{m}4 \text{r}4y^2 + 21.5 \text{I}2^2 \text{m}4^2 \text{r}4y^2 + 5.5 \text{I}3^2 \text{m}4 \text{m}5 \text{r}4y^2 +
\end{aligned}$$

Figure 0.7. LN of Six DOF Configuration

$5.5 13^2 m_4 m_6 r_4 y^2 - 5.5 13a^2 m_2 a m_4 r_4 z^2 - 5.5 13a^2 m_3 a m_4 r_4 z^2 + 25. 12^2 m_4^2 r_4 z^2 -$   
 $2.75 13^2 m_4 m_5 r_4 z^2 - 2.75 13^2 m_4 m_6 r_4 z^2 + 2.75 13a^2 m_2 a m_5 r_5 x^2 + 2.75 13a^2 m_3 a m_5 r_5 x^2 +$   
 $38.875 12^2 m_5^2 r_5 x^2 + 74.125 13^2 m_5^2 r_5 x^2 + 1.375 13^2 m_5 m_6 r_5 x^2 - 50. 12^2 m_4 m_5 r_4 z r_5 y -$   
 $5.5 13a^2 m_2 a m_5 r_5 y^2 - 5.5 13a^2 m_3 a m_5 r_5 y^2 + 25. 12^2 m_5^2 r_5 y^2 + 23.875 13^2 m_5^2 r_5 y^2 -$   
 $2.75 13^2 m_5 m_6 r_5 y^2 + 2.75 13a^2 m_2 a m_5 r_5 z^2 + 2.75 13a^2 m_3 a m_5 r_5 z^2 + 38.875 12^2 m_5^2 r_5 z^2 +$   
 $74.125 13^2 m_5^2 r_5 z^2 + 1.375 13^2 m_5 m_6 r_5 z^2 - 1.375 13a^2 m_2 a m_6 r_6 x^2 - 1.375 13a^2 m_3 a m_6 r_6 x^2 -$   
 $0.6875 13^2 m_5 m_6 r_6 x^2 + 50.125 12^2 m_6^2 r_6 x^2 + 83.0313 13^2 m_6^2 r_6 x^2 - 1.375 13a^2 m_2 a m_6 r_6 y^2 -$   
 $1.375 13a^2 m_3 a m_6 r_6 y^2 - 0.6875 13^2 m_5 m_6 r_6 y^2 + 50.125 12^2 m_6^2 r_6 y^2 + 83.0313 13^2 m_6^2 r_6 y^2 +$   
 $77.75 12^2 m_5 m_6 r_5 z r_6 z + 145.5 13^2 m_5 m_6 r_5 z r_6 z + 2.75 13a^2 m_2 a m_6 r_6 z^2 + 2.75 13a^2 m_3 a m_6 r_6 z^2 +$   
 $1.375 13^2 m_5 m_6 r_6 z^2 + 38.875 12^2 m_6^2 r_6 z^2 + 74.125 13^2 m_6^2 r_6 z^2 - 2.75 Ixx3 Iyy4 -$   
 $2.75 Ixx3a Iyy4 - 1.375 Ixx4 Iyy4 + 4.6875 Ixx5 Iyy4 + 1.65625 Ixx6 Iyy4 + 1.375 Ixx3 Iyy5 +$   
 $1.375 Ixx3a Iyy5 - 10.9375 Ixx4 Iyy5 - 6.15625 Ixx5 Iyy5 + 10.8281 Ixx6 Iyy5 +$   
 $0.34375 Ixx3 Iyy6 + 0.34375 Ixx3a Iyy6 - 2.73437 Ixx4 Iyy6 + 8.61523 Ixx5 Iyy6 -$   
 $25.8867 Ixx6 Iyy6 - 1.375 Ixx4 Izz3 + 0.6875 Ixx5 Izz3 - 0.34375 Ixx6 Izz3 + 2.75 Iyy4 Izz3 -$   
 $1.375 Iyy5 Izz3 - 0.34375 Iyy6 Izz3 - 1.375 Ixx4 Izz3a + 0.6875 Ixx5 Izz3a -$   
 $0.34375 Ixx6 Izz3a + 2.75 Iyy4 Izz3a - 1.375 Iyy5 Izz3a - 0.34375 Iyy6 Izz3a + 1.375 Ixx3 Izz4 +$   
 $1.375 Ixx3a Izz4 - 10.9375 Ixx4 Izz4 - 6.15625 Ixx5 Izz4 + 3.07813 Ixx6 Izz4 -$   
 $1.375 Iyy4 Izz4 + 12.3125 Iyy5 Izz4 + 3.07813 Iyy6 Izz4 - 0.6875 Ixx3 Izz5 -$   
 $0.6875 Ixx3a Izz5 + 5.46875 Ixx4 Izz5 - 13.2305 Ixx5 Izz5 - 9.69336 Ixx6 Izz5 +$   
 $4.6875 Iyy4 Izz5 - 6.15625 Iyy5 Izz5 - 9.69336 Iyy6 Izz5 - 0.6875 Ixx3 Izz6 -$   
 $0.6875 Ixx3a Izz6 + 5.46875 Ixx4 Izz6 - 13.2305 Ixx5 Izz6 - 9.69336 Ixx6 Izz6 +$   
 $4.6875 Iyy4 Izz6 - 6.15625 Iyy5 Izz6 - 9.69336 Iyy6 Izz6 - 2.75 Ixx3 13a^2 m_2 a -$   
 $2.75 Ixx3a 13a^2 m_2 a - 1.375 Ixx4 13a^2 m_2 a + 0.6875 Ixx5 13a^2 m_2 a - 0.34375 Ixx6 13a^2 m_2 a +$   
 $2.75 Iyy4 13a^2 m_2 a - 1.375 Iyy5 13a^2 m_2 a - 0.34375 Iyy6 13a^2 m_2 a + 2.75 Izz3 13a^2 m_2 a +$   
 $2.75 Izz3a 13a^2 m_2 a - 1.375 Izz4 13a^2 m_2 a + 0.6875 Izz5 13a^2 m_2 a + 0.6875 Izz6 13a^2 m_2 a -$   
 $8.25 12^4 m_2 a^2 - 53.75 13^2 12^2 13a^2 m_2 a^2 - 31.625 13a^4 m_2 a^2 - 16.5 12^4 m_2 a m_3 - 8.25 12^4 m_3^2 -$   
 $2.75 Ixx3 13a^2 m_3 a - 2.75 Ixx3a 13a^2 m_3 a - 1.375 Ixx4 13a^2 m_3 a + 0.6875 Ixx5 13a^2 m_3 a -$   
 $0.34375 Ixx6 13a^2 m_3 a + 2.75 Iyy4 13a^2 m_3 a - 1.375 Iyy5 13a^2 m_3 a - 0.34375 Iyy6 13a^2 m_3 a +$   
 $2.75 Izz3 13a^2 m_3 a + 2.75 Izz3a 13a^2 m_3 a - 1.375 Izz4 13a^2 m_3 a + 0.6875 Izz5 13a^2 m_3 a +$   
 $0.6875 Izz6 13a^2 m_3 a - 63.25 13a^4 m_2 a m_3 a - 31.625 13a^4 m_3 a^2 - 16.5 12^4 m_2 a m_4 -$   
 $16.5 12^4 m_3 m_4 - 8.25 12^4 m_4^2 - 16.5 12^4 m_2 a m_5 - 21.5 12^2 13 13a m_2 a m_5 - 13.75 13^2 13a^2 m_2 a m_5 -$   
 $16.5 12^4 m_3 m_5 - 13.75 13^2 13a^2 m_3 a m_5 - 16.5 12^4 m_4 m_5 - 8.25 12^4 m_5^2 - 32.25 12^2 13^2 m_5^2 -$   
 $15.125 13^4 m_5^2 - 16.5 12^4 m_2 a m_6 - 21.5 12^2 13 13a m_2 a m_6 - 13.75 13^2 13a^2 m_2 a m_6 -$   
 $16.5 12^4 m_3 m_6 - 13.75 13^2 13a^2 m_3 a m_6 - 16.5 12^4 m_4 m_6 - 16.5 12^4 m_5 m_6 - 64.5 12^2 13^2 m_5 m_6 -$   
 $30.25 13^4 m_5 m_6 - 8.25 12^4 m_6^2 - 32.25 12^2 13^2 m_6^2 - 15.125 13^4 m_6^2 + 3. Iyy2 12 m_2 a r_2 a x +$   
 $3. Iyy2a 12 m_2 a r_2 a x - 15. 13^2 m_2 a^2 r_2 a x - 64.5 12 13a^2 m_2 a^2 r_2 a x - 15. 13^2 m_2 a m_3 r_2 a x -$   
 $15. 12^2 m_2 a m_4 r_2 a x - 15. 13^2 m_2 a m_5 r_2 a x + 21.5 12 13 13a m_2 a m_5 r_2 a x - 15. 13^2 m_2 a m_6 r_2 a x +$   
 $21.5 12 13 13a m_2 a m_6 r_2 a x + 1.5 Iyy2 m_2 a r_2 a x^2 + 1.5 Iyy2a m_2 a r_2 a x^2 - 4.5 12^2 m_2 a^2 r_2 a x^2 -$   
 $32.25 13a^2 m_2 a^2 r_2 a x^2 - 1.5 12^2 m_2 a m_3 r_2 a x^2 - 1.5 12^2 m_2 a m_4 r_2 a x^2 - 1.5 12^2 m_2 a m_5 r_2 a x^2 -$   
 $1.5 12^2 m_2 a m_6 r_2 a x^2 + 3. 12 m_2 a^2 r_2 a x^3 + 0.75 m_2 a^2 r_2 a x^4 - 1.5 Iyy2 m_2 a r_2 a y^2 -$   
 $1.5 Iyy2a m_2 a r_2 a y^2 - 1.5 12^2 m_2 a^2 r_2 a y^2 - 32.25 13a^2 m_2 a^2 r_2 a y^2 + 1.5 12^2 m_2 a m_3 r_2 a y^2 +$   
 $1.5 12^2 m_2 a m_4 r_2 a y^2 + 1.5 12^2 m_2 a m_5 r_2 a y^2 + 1.5 12^2 m_2 a m_6 r_2 a y^2 + 3. 12 m_2 a^2 r_2 a x r_2 a y^2 +$   
 $1.5 m_2 a^2 r_2 a x^2 r_2 a y^2 + 0.75 m_2 a^2 r_2 a y^4 - 1.5 12^2 m_2 a^2 r_2 a z^2 - 15. 13a^2 m_2 a^2 r_2 a z^2 +$   
 $3. 12 m_2 a^2 r_2 a x r_2 a z^2 + 1.5 m_2 a^2 r_2 a x^2 r_2 a z^2 + 1.5 m_2 a^2 r_2 a y^2 r_2 a z^2 + 1.5 Iyy2 m_2 r_2 x^2 +$   
 $1.5 Iyy2a m_2 r_2 x^2 - 1.5 12^2 m_2 m_3 r_2 x^2 - 1.5 12^2 m_2 m_4 r_2 x^2 -$   
 $1.5 12^2 m_2 m_5 r_2 x^2 - 1.5 12^2 m_2 m_6 r_2 x^2 + 3. 12 m_2 m_2 a r_2 a x r_2 x^2 + 1.5 m_2 m_2 a r_2 a x^2 r_2 x^2 -$   
 $1.5 m_2 m_2 a r_2 a y^2 r_2 x^2 + 0.75 m_2^2 r_2 x^4 + 6. 12 m_2 m_2 a r_2 a y r_2 x r_2 y + 6. m_2 m_2 a r_2 a x r_2 a y r_2 x r_2 y -$   
 $1.5 Iyy2 m_2 r_2 y^2 - 1.5 Iyy2a m_2 r_2 y^2 + 1.5 12^2 m_2 m_2 a r_2 y^2 + 1.5 12^2 m_2 m_3 r_2 y^2 +$   
 $1.5 12^2 m_2 m_4 r_2 y^2 + 1.5 12^2 m_2 m_5 r_2 y^2 + 1.5 12^2 m_2 m_6 r_2 y^2 - 3. 12 m_2 m_2 a r_2 a x r_2 y^2 -$   
 $1.5 m_2 m_2 a r_2 a x^2 r_2 y^2 + 1.5 m_2 m_2 a r_2 a y^2 r_2 y^2 + 1.5 m_2^2 r_2 x^2 r_2 y^2 + 0.75 m_2^2 r_2 y^4 +$   
 $Ixx2 (-3. 12 m_2 a r_2 a x - 1.5 m_2 a r_2 a x^2 + 1.5 m_2 a r_2 a y^2 - 1.5 m_2 r_2 x^2 + 1.5 m_2 r_2 y^2) +$   
 $Ixx2a (-3. 12 m_2 a r_2 a x - 1.5 m_2 a r_2 a x^2 + 1.5 m_2 a r_2 a y^2 - 1.5 m_2 r_2 x^2 + 1.5 m_2 r_2 y^2) +$   
 $3. 12 m_2 m_2 a r_2 a z r_2 x r_2 z + 3. m_2 m_2 a r_2 a z r_2 x r_2 z + 3. m_2 m_2 a r_2 a y r_2 a z r_2 y r_2 z +$   
 $1.5 m_2^2 r_2 x^2 r_2 z^2 + 1.5 m_2^2 r_2 y^2 r_2 z^2 - 2.75 Ixx3 m_3 a r_3 a x^2 - 2.75 Ixx3a m_3 a r_3 a x^2 -$   
 $1.375 Ixx4 m_3 a r_3 a x^2 + 0.6875 Ixx5 m_3 a r_3 a x^2 - 0.34375 Ixx6 m_3 a r_3 a x^2 +$   
 $2.75 Iyy4 m_3 a r_3 a x^2 - 1.375 Iyy5 m_3 a r_3 a x^2 - 0.34375 Iyy6 m_3 a r_3 a x^2 + 2.75 Izz3 m_3 a r_3 a x^2 +$   
 $2.75 Izz3a m_3 a r_3 a x^2 - 1.375 Izz4 m_3 a r_3 a x^2 + 0.6875 Izz5 m_3 a r_3 a x^2 + 0.6875 Izz6 m_3 a r_3 a x^2 +$   
 $8.25 13a^2 m_2 a m_3 a r_3 a x^2 - 8.25 13a^2 m_3 a^2 r_3 a x^2 + 2.75 13^2 m_3 a m_5 r_3 a x^2 + 2.75 13^2 m_3 a m_6 r_3 a x^2 +$   
 $1.375 m_3 a^2 r_3 a x^4 + 30. 13a^2 m_2 a m_3 a r_2 a z r_3 a y - 15. 13a^2 m_3 a^2 r_3 a y^2 + 5. m_3 a^2 r_3 a x^2 r_3 a y^2 +$   
 $5.5 Ixx3 13a m_3 a r_3 a z + 5.5 Ixx3a 13a m_3 a r_3 a z + 2.75 Ixx4 13a m_3 a r_3 a z -$   
 $1.375 Ixx5 13a m_3 a r_3 a z + 0.6875 Ixx6 13a m_3 a r_3 a z - 5.5 Iyy4 13a m_3 a r_3 a z +$   
 $2.75 Iyy5 13a m_3 a r_3 a z + 0.6875 Iyy6 13a m_3 a r_3 a z - 5.5 Izz3 13a m_3 a r_3 a z -$   
 $5.5 Izz3a 13a m_3 a r_3 a z + 2.75 Izz4 13a m_3 a r_3 a z - 1.375 Izz5 13a m_3 a r_3 a z -$   
 $1.375 Izz6 13a m_3 a r_3 a z - 60.5 13a^3 m_2 a m_3 a r_3 a z - 60.5 13a^3 m_3 a^2 r_3 a z -$   
 $5.5 13^2 13a m_3 a m_5 r_3 a z - 5.5 13^2 13a m_3 a m_6 r_3 a z + 5.5 13a m_3 a^2 r_3 a x^2 r_3 a z -$   
 $10. 13a m_2 a m_3 a r_2 a z r_3 a y r_3 a z + 10. 13a m_3 a^2 r_3 a y^2 r_3 a z + 2.75 Ixx3 m_3 a r_3 a z^2 +$   
 $2.75 Ixx3a m_3 a r_3 a z^2 + 1.375 Ixx4 m_3 a r_3 a z^2 - 0.6875 Ixx5 m_3 a r_3 a z^2 + 0.34375 Ixx6 m_3 a r_3 a z^2 -$   
 $2.75 Iyy4 m_3 a r_3 a z^2 + 1.375 Iyy5 m_3 a r_3 a z^2 + 0.34375 Iyy6 m_3 a r_3 a z^2 - 2.75 Izz3 m_3 a r_3 a z^2 -$   
 $2.75 Izz3a m_3 a r_3 a z^2 + 1.375 Izz4 m_3 a r_3 a z^2 - 0.6875 Izz5 m_3 a r_3 a z^2 - 0.6875 Izz6 m_3 a r_3 a z^2 -$   
 $8.25 13a^2 m_2 a m_3 a r_3 a z^2 - 24.75 13a^2 m_3 a^2 r_3 a z^2 - 2.75 13^2 m_3 a m_5 r_3 a z^2 - 2.75 13^2 m_3 a m_6 r_3 a z^2 +$   
 $2.75 m_3 a^2 r_3 a x^2 r_3 a z^2 + 5. m_3 a^2 r_3 a y^2 r_3 a z^2 + 5.5 13a m_3 a^2 r_3 a z^3 + 1.375 m_3 a^2 r_3 a z^4 +$

Figure 0.7. Continued

7.  $12\ 13a\ m_2\ m_3\ r_2\ a\ y\ r_3\ x - 2.75\ Ixx_3\ m_3\ r_3\ x^2 - 2.75\ Ixx_3\ a\ m_3\ r_3\ x^2 - 1.375\ Ixx_4\ m_3\ r_3\ x^2 +$   
 $0.6875\ Ixx_5\ m_3\ r_3\ x^2 - 0.34375\ Ixx_6\ m_3\ r_3\ x^2 + 2.75\ Iyy_4\ m_3\ r_3\ x^2 - 1.375\ Iyy_5\ m_3\ r_3\ x^2 -$   
 $0.34375\ Iyy_6\ m_3\ r_3\ x^2 + 2.75\ Izz_3\ m_3\ r_3\ x^2 + 2.75\ Izz_3\ a\ m_3\ r_3\ x^2 - 1.375\ Izz_4\ m_3\ r_3\ x^2 +$   
 $0.6875\ Izz_5\ m_3\ r_3\ x^2 + 0.6875\ Izz_6\ m_3\ r_3\ x^2 + 8.25\ 13a^2\ m_2\ a\ m_3\ r_3\ x^2 - 10.75\ 12^2\ m_3^2\ r_3\ x^2 +$   
 $8.25\ 13a^2\ m_3\ m_3\ a\ r_3\ x^2 + 2.75\ 13^2\ m_3\ m_5\ r_3\ x^2 + 2.75\ 13^2\ m_3\ m_6\ r_3\ x^2 + 2.75\ m_3\ m_3\ a\ r_3\ a\ x^2\ r_3\ x^2 -$   
 $5.5\ 13a\ m_3\ m_3\ a\ r_3\ a\ z\ r_3\ x^2 - 2.75\ m_3\ m_3\ a\ r_3\ a\ z^2\ r_3\ x^2 + 1.375\ m_3^2\ r_3\ x^4 + 3.12^2\ m_2\ a\ m_3\ r_2\ a\ z\ r_3\ y -$   
 $3.12\ m_2\ a\ m_3\ r_2\ a\ z\ r_2\ a\ z\ r_3\ y - 3.12\ m_2\ m_3\ r_2\ x\ r_2\ z\ r_3\ y + 10. m_3\ m_3\ a\ r_3\ a\ x\ r_3\ a\ y\ r_3\ x\ r_3\ y -$   
 $1.5\ 12^2\ m_3^2\ r_3\ y^2 + 5. m_3^2\ r_3\ x^2\ r_3\ y^2 - 21.5\ 12^2\ 13a\ m_2\ a\ m_3\ r_3\ z - 21.5\ 12^2\ 13\ m_3\ m_5\ r_3\ z -$   
 $21.5\ 12^2\ 13\ m_3\ m_6\ r_3\ z + 21.5\ 12\ 13a\ m_2\ a\ m_3\ r_2\ a\ x\ r_3\ z + 11. 13a\ m_3\ m_3\ a\ r_3\ a\ x\ r_3\ x\ r_3\ z +$   
 $11. m_3\ m_3\ a\ r_3\ a\ x\ r_3\ a\ z\ r_3\ x\ r_3\ z - 10. 13a\ m_2\ a\ m_3\ r_2\ a\ z\ r_3\ y\ r_3\ z + 10. 13a\ m_3\ m_3\ a\ r_3\ a\ y\ r_3\ y\ r_3\ z +$   
 $10. m_3\ m_3\ a\ r_3\ a\ y\ r_3\ a\ z\ r_3\ y\ r_3\ z + 2.75\ Ixx_3\ m_3\ r_3\ z^2 + 2.75\ Ixx_3\ a\ m_3\ r_3\ z^2 + 1.375\ Ixx_4\ m_3\ r_3\ z^2 -$   
 $0.6875\ Ixx_5\ m_3\ r_3\ z^2 + 0.34375\ Ixx_6\ m_3\ r_3\ z^2 - 2.75\ Iyy_4\ m_3\ r_3\ z^2 + 1.375\ Iyy_5\ m_3\ r_3\ z^2 +$   
 $0.34375\ Iyy_6\ m_3\ r_3\ z^2 - 2.75\ Izz_3\ m_3\ r_3\ z^2 - 2.75\ Izz_3\ a\ m_3\ r_3\ z^2 + 1.375\ Izz_4\ m_3\ r_3\ z^2 -$   
 $0.6875\ Izz_5\ m_3\ r_3\ z^2 - 0.6875\ Izz_6\ m_3\ r_3\ z^2 - 8.25\ 13a^2\ m_2\ a\ m_3\ r_3\ z^2 - 10.75\ 12^2\ m_3^2\ r_3\ z^2 -$   
 $8.25\ 13a^2\ m_3\ m_3\ a\ r_3\ z^2 - 2.75\ 13^2\ m_3\ m_5\ r_3\ z^2 - 2.75\ 13^2\ m_3\ m_6\ r_3\ z^2 - 2.75\ m_3\ m_3\ a\ r_3\ a\ x^2\ r_3\ z^2 +$   
 $5.5\ 13a\ m_3\ m_3\ a\ r_3\ a\ z\ r_3\ z^2 + 2.75\ m_3\ m_3\ a\ r_3\ a\ z^2\ r_3\ z^2 + 2.75\ m_3^2\ r_3\ x^2\ r_3\ z^2 + 5. m_3^2\ r_3\ y^2\ r_3\ z^2 +$   
 $1.375\ m_3^2\ r_3\ z^4 - 1.375\ Ixx_3\ m_4\ r_4\ x^2 - 1.375\ Ixx_3\ a\ m_4\ r_4\ x^2 - 12.3125\ Ixx_4\ m_4\ r_4\ x^2 -$   
 $1.46875\ Ixx_5\ m_4\ r_4\ x^2 + 4.73437\ Ixx_6\ m_4\ r_4\ x^2 + 9.375\ Iyy_4\ m_4\ r_4\ x^2 + 10.9375\ Iyy_5\ m_4\ r_4\ x^2 +$   
 $4.73437\ Iyy_6\ m_4\ r_4\ x^2 + 1.375\ Izz_3\ m_4\ r_4\ x^2 + 1.375\ Izz_3\ a\ m_4\ r_4\ x^2 + 10.9375\ Izz_4\ m_4\ r_4\ x^2 -$   
 $1.46875\ Izz_5\ m_4\ r_4\ x^2 - 1.46875\ Izz_6\ m_4\ r_4\ x^2 + 4.125\ 13a^2\ m_2\ a\ m_4\ r_4\ x^2 + 4.125\ 13a^2\ m_3\ a\ m_4\ r_4\ x^2 -$   
 $12.5\ 12^2\ m_4^2\ r_4\ x^2 + 1.375\ 13^2\ m_4\ m_5\ r_4\ x^2 + 1.375\ 13^2\ m_4\ m_6\ r_4\ x^2 + 1.375\ m_3\ a\ m_4\ r_3\ a\ x^2\ r_4\ x^2 -$   
 $2.75\ 13a\ m_3\ a\ m_4\ r_3\ a\ z\ r_4\ x^2 - 1.375\ m_3\ a\ m_4\ r_3\ a\ z^2\ r_4\ x^2 + 1.375\ m_3\ m_4\ r_3\ x^2\ r_4\ x^2 -$   
 $1.375\ m_3\ m_4\ r_3\ z^2\ r_4\ x^2 + 10.1563\ m_4^2\ r_4\ x^4 - 21.5\ 12^2\ 13a\ m_2\ a\ m_4\ r_4\ y - 21.5\ 12^2\ 13\ m_4\ m_5\ r_4\ y -$   
 $21.5\ 12^2\ 13\ m_4\ m_6\ r_4\ y + 21.5\ 12\ 13a\ m_2\ a\ m_4\ r_2\ a\ x\ r_4\ y - 21.5\ 12^2\ m_3\ m_4\ r_3\ z\ r_4\ y + 2.75\ Ixx_3\ m_4\ r_4\ y^2 +$   
 $2.75\ Ixx_3\ a\ m_4\ r_4\ y^2 + 1.375\ Ixx_4\ m_4\ r_4\ y^2 - 0.6875\ Ixx_5\ m_4\ r_4\ y^2 + 0.34375\ Ixx_6\ m_4\ r_4\ y^2 -$   
 $2.75\ Iyy_4\ m_4\ r_4\ y^2 + 1.375\ Iyy_5\ m_4\ r_4\ y^2 + 0.34375\ Iyy_6\ m_4\ r_4\ y^2 - 2.75\ Izz_3\ m_4\ r_4\ y^2 -$   
 $2.75\ Izz_3\ a\ m_4\ r_4\ y^2 + 1.375\ Izz_4\ m_4\ r_4\ y^2 - 0.6875\ Izz_5\ m_4\ r_4\ y^2 - 0.6875\ Izz_6\ m_4\ r_4\ y^2 -$   
 $8.25\ 13a^2\ m_2\ a\ m_4\ r_4\ y^2 - 8.25\ 13a^2\ m_3\ a\ m_4\ r_4\ y^2 - 10.75\ 12^2\ m_4^2\ r_4\ y^2 - 2.75\ 13^2\ m_4\ m_5\ r_4\ y^2 -$   
 $2.75\ 13^2\ m_4\ m_6\ r_4\ y^2 - 2.75\ m_3\ a\ m_4\ r_3\ a\ x^2\ r_4\ y^2 + 5.5\ 13a\ m_3\ a\ m_4\ r_3\ a\ z\ r_4\ y^2 + 2.75\ m_3\ a\ m_4\ r_3\ a\ z^2\ r_4\ y^2 -$   
 $2.75\ m_3\ m_4\ r_3\ x^2\ r_4\ y^2 + 2.75\ m_3\ m_4\ r_3\ z^2\ r_4\ y^2 + 11.9375\ m_4^2\ r_4\ x^2\ r_4\ y^2 + 1.375\ m_4^2\ r_4\ y^4 -$   
 $1.375\ Ixx_3\ m_4\ r_4\ z^2 - 1.375\ Ixx_3\ a\ m_4\ r_4\ z^2 + 10.9375\ Ixx_4\ m_4\ r_4\ z^2 + 10.1563\ Ixx_5\ m_4\ r_4\ z^2 -$   
 $1.07813\ Ixx_6\ m_4\ r_4\ z^2 + 9.375\ Iyy_4\ m_4\ r_4\ z^2 - 12.3125\ Iyy_5\ m_4\ r_4\ z^2 - 1.07813\ Iyy_6\ m_4\ r_4\ z^2 +$   
 $1.375\ Izz_3\ m_4\ r_4\ z^2 + 1.375\ Izz_3\ a\ m_4\ r_4\ z^2 - 12.3125\ Izz_4\ m_4\ r_4\ z^2 + 10.1563\ Izz_5\ m_4\ r_4\ z^2 +$   
 $10.1563\ Izz_6\ m_4\ r_4\ z^2 + 4.125\ 13a^2\ m_2\ a\ m_4\ r_4\ z^2 + 4.125\ 13a^2\ m_3\ a\ m_4\ r_4\ z^2 - 12.5\ 12^2\ m_4^2\ r_4\ z^2 +$   
 $1.375\ 13^2\ m_4\ m_5\ r_4\ z^2 + 1.375\ 13^2\ m_4\ m_6\ r_4\ z^2 + 1.375\ m_3\ a\ m_4\ r_3\ a\ x^2\ r_4\ z^2 - 2.75\ 13a\ m_3\ a\ m_4\ r_3\ a\ z\ r_4\ z^2 -$   
 $1.375\ m_3\ a\ m_4\ r_3\ a\ z^2\ r_4\ z^2 + 1.375\ m_3\ m_4\ r_3\ x^2\ r_4\ z^2 - 1.375\ m_3\ m_4\ r_3\ z^2\ r_4\ z^2 + 20.3125\ m_4^2\ r_4\ x^2\ r_4\ z^2 +$   
 $11.9375\ m_4^2\ r_4\ y^2\ r_4\ z^2 + 10.1563\ m_4^2\ r_4\ z^4 + 0.6875\ Ixx_3\ m_5\ r_5\ x^2 + 0.6875\ Ixx_3\ a\ m_5\ r_5\ x^2 -$   
 $5.46875\ Ixx_4\ m_5\ r_5\ x^2 - 19.3867\ Ixx_5\ m_5\ r_5\ x^2 + 1.13477\ Ixx_6\ m_5\ r_5\ x^2 + 3.3125\ Iyy_4\ m_5\ r_5\ x^2 +$   
 $21.6563\ Iyy_5\ m_5\ r_5\ x^2 + 1.13477\ Iyy_6\ m_5\ r_5\ x^2 - 0.6875\ Izz_3\ m_5\ r_5\ x^2 - 0.6875\ Izz_3\ a\ m_5\ r_5\ x^2 +$   
 $6.15625\ Izz_4\ m_5\ r_5\ x^2 + 17.2305\ Izz_5\ m_5\ r_5\ x^2 + 17.2305\ Izz_6\ m_5\ r_5\ x^2 - 2.0625\ 13a^2\ m_2\ a\ m_5\ r_5\ x^2 -$   
 $2.0625\ 13a^2\ m_3\ a\ m_5\ r_5\ x^2 - 19.4375\ 12^2\ m_5^2\ r_5\ x^2 - 37.0625\ 13^2\ m_5^2\ r_5\ x^2 - 0.6875\ 13^2\ m_5\ m_6\ r_5\ x^2 -$   
 $0.6875\ m_3\ a\ m_5\ r_3\ a\ x^2\ r_5\ x^2 + 1.375\ 13a\ m_3\ a\ m_5\ r_3\ a\ z\ r_5\ x^2 + 0.6875\ m_3\ a\ m_5\ r_3\ a\ z^2\ r_5\ x^2 -$   
 $0.6875\ m_3\ m_5\ r_3\ x^2\ r_5\ x^2 + 0.6875\ m_3\ m_5\ r_3\ z^2\ r_5\ x^2 + 9.46875\ m_4\ m_5\ r_4\ x^2\ r_5\ x^2 +$   
 $0.6875\ m_4\ m_5\ r_4\ y^2\ r_5\ x^2 - 2.15625\ m_4\ m_5\ r_4\ z^2\ r_5\ x^2 + 19.4434\ m_5^2\ r_5\ x^4 + 25.12^2\ m_4\ m_5\ r_4\ z\ r_5\ y -$   
 $26.625\ 13\ m_4\ m_5\ r_4\ y\ r_4\ z\ r_5\ y - 1.375\ Ixx_3\ m_5\ r_5\ y^2 - 1.375\ Ixx_3\ a\ m_5\ r_5\ y^2 + 10.9375\ Ixx_4\ m_5\ r_5\ y^2 +$   
 $10.1563\ Ixx_5\ m_5\ r_5\ y^2 - 1.07813\ Ixx_6\ m_5\ r_5\ y^2 + 9.375\ Iyy_4\ m_5\ r_5\ y^2 - 12.3125\ Iyy_5\ m_5\ r_5\ y^2 -$   
 $1.07813\ Iyy_6\ m_5\ r_5\ y^2 + 1.375\ Izz_3\ m_5\ r_5\ y^2 + 1.375\ Izz_3\ a\ m_5\ r_5\ y^2 - 12.3125\ Izz_4\ m_5\ r_5\ y^2 +$   
 $10.1563\ Izz_5\ m_5\ r_5\ y^2 - 10.1563\ Izz_6\ m_5\ r_5\ y^2 + 4.125\ 13a^2\ m_2\ a\ m_5\ r_5\ y^2 + 4.125\ 13a^2\ m_3\ a\ m_5\ r_5\ y^2 -$   
 $12.5\ 12^2\ m_5^2\ r_5\ y^2 - 11.9375\ 13^2\ m_5^2\ r_5\ y^2 + 1.375\ 13^2\ m_5\ m_6\ r_5\ y^2 + 1.375\ m_3\ a\ m_5\ r_3\ a\ x^2\ r_5\ y^2 -$   
 $2.75\ 13a\ m_3\ a\ m_5\ r_3\ a\ z\ r_5\ y^2 - 1.375\ m_3\ a\ m_5\ r_3\ a\ z^2\ r_5\ y^2 + 1.375\ m_3\ m_5\ r_3\ x^2\ r_5\ y^2 -$   
 $1.375\ m_3\ m_5\ r_3\ z^2\ r_5\ y^2 - 2.9375\ m_4\ m_5\ r_4\ x^2\ r_5\ y^2 - 1.375\ m_4\ m_5\ r_4\ y^2\ r_5\ y^2 + 20.3125\ m_4\ m_5\ r_4\ z^2\ r_5\ y^2 +$   
 $30.1484\ m_5^2\ r_5\ x^2\ r_5\ y^2 + 10.1563\ m_5^2\ r_5\ y^4 + 0.6875\ Ixx_3\ m_5\ r_5\ z^2 + 0.6875\ Ixx_3\ a\ m_5\ r_5\ z^2 -$   
 $5.46875\ Ixx_4\ m_5\ r_5\ z^2 + 17.2305\ Ixx_5\ m_5\ r_5\ z^2 + 19.4434\ Ixx_6\ m_5\ r_5\ z^2 + 3.3125\ Iyy_4\ m_5\ r_5\ z^2 +$   
 $21.6563\ Iyy_5\ m_5\ r_5\ z^2 + 19.4434\ Iyy_6\ m_5\ r_5\ z^2 - 0.6875\ Izz_3\ m_5\ r_5\ z^2 - 0.6875\ Izz_3\ a\ m_5\ r_5\ z^2 +$   
 $6.15625\ Izz_4\ m_5\ r_5\ z^2 - 19.3867\ Izz_5\ m_5\ r_5\ z^2 - 19.3867\ Izz_6\ m_5\ r_5\ z^2 - 2.0625\ 13a^2\ m_2\ a\ m_5\ r_5\ z^2 -$   
 $2.0625\ 13a^2\ m_3\ a\ m_5\ r_5\ z^2 - 19.4375\ 12^2\ m_5^2\ r_5\ z^2 - 37.0625\ 13^2\ m_5^2\ r_5\ z^2 - 0.6875\ 13^2\ m_5\ m_6\ r_5\ z^2 -$   
 $0.6875\ m_3\ a\ m_5\ r_3\ a\ x^2\ r_5\ z^2 + 1.375\ 13a\ m_3\ a\ m_5\ r_3\ a\ z\ r_5\ z^2 + 0.6875\ m_3\ a\ m_5\ r_3\ a\ z^2\ r_5\ z^2 -$   
 $0.6875\ m_3\ m_5\ r_3\ x^2\ r_5\ z^2 + 0.6875\ m_3\ m_5\ r_3\ z^2\ r_5\ z^2 + 9.46875\ m_4\ m_5\ r_4\ x^2\ r_5\ z^2 + 0.6875\ m_4\ m_5\ r_4\ y^2\ r_5\ z^2 -$   
 $2.15625\ m_4\ m_5\ r_4\ z^2\ r_5\ z^2 + 38.8867\ m_5^2\ r_5\ x^2\ r_5\ z^2 + 30.1484\ m_5^2\ r_5\ y^2\ r_5\ z^2 + 19.4434\ m_5^2\ r_5\ z^4 -$   
 $0.34375\ Ixx_3\ m_6\ r_6\ x^2 - 0.34375\ Ixx_3\ a\ m_6\ r_6\ x^2 + 2.73437\ Ixx_4\ m_6\ r_6\ x^2 - 4.61523\ Ixx_5\ m_6\ r_6\ x^2 -$   
 $35.5801\ Ixx_6\ m_6\ r_6\ x^2 + 6.34375\ Iyy_4\ m_6\ r_6\ x^2 + 4.67187\ Iyy_5\ m_6\ r_6\ x^2 + 35.6367\ Iyy_6\ m_6\ r_6\ x^2 +$   
 $0.34375\ Izz_3\ m_6\ r_6\ x^2 + 0.34375\ Izz_3\ a\ m_6\ r_6\ x^2 - 3.07813\ Izz_4\ m_6\ r_6\ x^2 + 13.6934\ Izz_5\ m_6\ r_6\ x^2 +$   
 $35.6934\ Izz_6\ m_6\ r_6\ x^2 + 1.03125\ 13a^2\ m_2\ a\ m_6\ r_6\ x^2 + 1.03125\ 13a^2\ m_3\ a\ m_6\ r_6\ x^2 +$   
 $0.34375\ 13^2\ m_5\ m_6\ r_6\ x^2 - 25.0625\ 12^2\ m_6^2\ r_6\ x^2 - 41.5156\ 13^2\ m_6^2\ r_6\ x^2 + 0.34375\ m_3\ a\ m_6\ r_3\ a\ x^2\ r_6\ x^2 -$   
 $0.6875\ 13a\ m_3\ a\ m_6\ r_3\ a\ z\ r_6\ x^2 - 0.34375\ m_3\ a\ m_6\ r_3\ a\ z^2\ r_6\ x^2 + 0.34375\ m_3\ m_6\ r_3\ x^2\ r_6\ x^2 -$   
 $0.34375\ m_3\ m_6\ r_3\ z^2\ r_6\ x^2 + 3.26563\ m_4\ m_6\ r_4\ x^2\ r_6\ x^2 - 0.34375\ m_4\ m_6\ r_4\ y^2\ r_6\ x^2 +$   
 $9.07813\ m_4\ m_6\ r_4\ z^2\ r_6\ x^2 + 18.3652\ m_5\ m_6\ r_5\ x^2\ r_6\ x^2 + 9.07813\ m_5\ m_6\ r_5\ y^2\ r_6\ x^2 +$   
 $0.0566406\ m_5\ m_6\ r_5\ z^2\ r_6\ x^2 + 35.665\ m_6^2\ r_6\ x^4 - 0.34375\ Ixx_3\ m_6\ r_6\ y^2 - 0.34375\ Ixx_3\ a\ m_6\ r_6\ y^2 +$   
 $2.73437\ Ixx_4\ m_6\ r_6\ y^2 - 4.61523\ Ixx_5\ m_6\ r_6\ y^2 + 35.6367\ Ixx_6\ m_6\ r_6\ y^2 + 6.34375\ Iyy_4\ m_6\ r_6\ y^2 +$   
 $4.67187\ Iyy_5\ m_6\ r_6\ y^2 - 35.5801\ Iyy_6\ m_6\ r_6\ y^2 + 0.34375\ Izz_3\ m_6\ r_6\ y^2 + 0.34375\ Izz_3\ a\ m_6\ r_6\ y^2 -$   
 $3.07813\ Izz_4\ m_6\ r_6\ y^2 + 13.6934\ Izz_5\ m_6\ r_6\ y^2 + 35.6934\ Izz_6\ m_6\ r_6\ y^2 + 1.03125\ 13a^2\ m_2\ a\ m_6\ r_6\ y^2 +$   
 $1.03125\ 13a^2\ m_3\ a\ m_6\ r_6\ y^2 + 0.34375\ 13^2\ m_5\ m_6\ r_6\ y^2 - 25.0625\ 12^2\ m_6^2\ r_6\ y^2 - 41.5156\ 13^2\ m_6^2\ r_6\ y^2 +$

Figure 0.7. Continued

$$\begin{aligned}
& 0.34375 m_3 a m_6 r_3 a x^2 r_6 y^2 - 0.6875 l_3 a m_3 a m_6 r_3 a z r_6 y^2 - 0.34375 m_3 a m_6 r_3 a z^2 r_6 y^2 + \\
& 0.34375 m_3 m_6 r_3 x^2 r_6 y^2 - 0.34375 m_3 m_6 r_3 z^2 r_6 y^2 + 3.26563 m_4 m_6 r_4 x^2 r_6 y^2 - \\
& 0.34375 m_4 m_6 r_4 y^2 r_6 y^2 + 9.07813 m_4 m_6 r_4 z^2 r_6 y^2 + 18.3652 m_5 m_6 r_5 x^2 r_6 y^2 + \\
& 9.07813 m_5 m_6 r_5 y^2 r_6 y^2 + 0.0566406 m_5 m_6 r_5 z^2 r_6 y^2 + 71.3301 m_6^2 r_6 x^2 r_6 y^2 + 35.665 m_6^2 r_6 y^4 - \\
& 38.875 l_2^2 m_5 m_6 r_5 z r_6 z - 72.75 l_3^2 m_5 m_6 r_5 z r_6 z + 0.6875 I_{xx3} m_6 r_6 z^2 + 0.6875 I_{xx3a} m_6 r_6 z^2 - \\
& 5.46875 I_{xx4} m_6 r_6 z^2 + 17.2305 I_{xx5} m_6 r_6 z^2 + 19.4434 I_{xx6} m_6 r_6 z^2 + 3.3125 I_{yy4} m_6 r_6 z^2 + \\
& 21.6563 I_{yy5} m_6 r_6 z^2 + 19.4434 I_{yy6} m_6 r_6 z^2 - 0.6875 I_{zz3} m_6 r_6 z^2 - 0.6875 I_{zz3a} m_6 r_6 z^2 + \\
& 6.15625 I_{zz4} m_6 r_6 z^2 - 19.3867 I_{zz5} m_6 r_6 z^2 - 19.3867 I_{zz6} m_6 r_6 z^2 - 2.0625 l_3 a^2 m_2 a m_6 r_6 z^2 - \\
& 2.0625 l_3 a^2 m_3 a m_6 r_6 z^2 - 0.6875 l_3^2 m_5 m_6 r_6 z^2 - 19.4375 l_2^2 m_6^2 r_6 z^2 - 37.0625 l_3^2 m_6^2 r_6 z^2 - \\
& 0.6875 m_3 a m_6 r_3 a x^2 r_6 z^2 + 1.375 l_3 a m_3 a m_6 r_3 a z r_6 z^2 + 0.6875 m_3 a m_6 r_3 a z^2 r_6 z^2 - \\
& 0.6875 m_3 m_6 r_3 x^2 r_6 z^2 + 0.6875 m_3 m_6 r_3 z^2 r_6 z^2 + 9.46875 m_4 m_6 r_4 x^2 r_6 z^2 + 0.6875 m_4 m_6 r_4 y^2 r_6 z^2 - \\
& 2.15625 m_4 m_6 r_4 z^2 r_6 z^2 + 2.26953 m_5 m_6 r_5 x^2 r_6 z^2 - 2.15625 m_5 m_6 r_5 y^2 r_6 z^2 + \\
& 38.8867 m_5 m_6 r_5 z^2 r_6 z^2 + 55.0889 m_6^2 r_6 x^2 r_6 z^2 + 55.0889 m_6^2 r_6 y^2 r_6 z^2 + 19.4434 m_6^2 r_6 z^4 + \\
& 0.5 g^2 (13 a^2 (2. m_2 a^2 + 4. m_2 a m_3 a + 2. m_3 a^2) + 2. l_3^2 m_5^2 + 4. l_3^2 m_5 m_6 + 2. l_3^2 m_6^2 + \\
& 12^2 (1. m_2 a^2 + 1. m_3^2 + 1. m_4^2 + 2. m_4 m_5 + 1. m_5^2 + 2. m_4 m_6 + 2. m_5 m_6 + 1. m_6^2 + m_3 (2. m_4 + \\
& 2. m_5 + 2. m_6) + m_2 a (2. m_3 + 2. m_4 + 2. m_5 + 2. m_6)) + 1. m_2 a^2 r_2 a x^2 + 1. m_2 a^2 r_2 a y^2 + \\
& 2. m_2 m_2 a r_2 a x r_2 x + 1. m_2^2 r_2 x^2 + 12 (2. m_2 a^2 r_2 a x + m_2 (2. m_3 + 2. m_4 + 2. m_5 + 2. m_6) r_2 x + \\
& m_2 a (2. m_3 r_2 a x + 2. m_4 r_2 a x + 2. m_5 r_2 a x + 2. m_6 r_2 a x + 2. m_2 r_2 x)) + 2. m_2 m_2 a r_2 a y r_2 y + \\
& 1. m_2^2 r_2 y^2 + 2. m_3 a^2 r_3 a x^2 + 4. l_3 m_3 a m_5 r_3 a z + 4. l_3 m_3 a m_6 r_3 a z + 2. m_3 a^2 r_3 a z^2 + \\
& 4. m_3 m_3 a r_3 a x r_3 x + 2. m_3^2 r_3 x^2 + 4. l_3 m_3 m_5 r_3 z + 4. l_3 m_3 m_6 r_3 z + 4. m_3 m_3 a r_3 a z r_3 z + \\
& 2. m_3^2 r_3 z^2 + 1.5 m_4^2 r_4 x^2 + 4. l_3 m_4 m_5 r_4 y + 4. l_3 m_4 m_6 r_4 y + 4. m_3 a m_4 r_3 a z r_4 y + 4. m_3 m_4 \\
& r_3 z r_4 y + 2. m_4^2 r_4 y^2 + 13 a (l_3 (4. m_2 a m_5 + 4. m_3 a m_5 + 4. m_2 a m_6 + 4. m_3 a m_6) + (m_2 a + m_3 a) \\
& (4. m_3 a r_3 a z + 4. m_3 r_3 z + 4. m_4 r_4 y)) + 1.5 m_4^2 r_4 z^2 + 2.5 m_5^2 r_5 x^2 - 3. m_4 m_5 r_4 z r_5 y + \\
& 1.5 m_5^2 r_5 y^2 + 2.5 m_5^2 r_5 z^2 + 2.625 m_6^2 r_6 x^2 + 2.625 m_6^2 r_6 y^2 + 5. m_5 m_6 r_5 z r_6 z + 2.5 m_6^2 r_6 z^2)
\end{aligned}$$

Figure 0.7. Continued

### C. Optimization of Three Degrees of Freedom Configuration

Numerical optimization of LN of the three DOF haptic manipulator is realized. Among the hundred manipulators constructed for the each LN, the design variables of five manipulators are given as below.

#### C.1. LN = 0

{5.4226029181339245049  $\times 10^{-18}$ , {Ixx2  $\rightarrow$  0.0011733514387590658588,  
 Ixx2a  $\rightarrow$  0.0093066025454951792104, Ixx3  $\rightarrow$  0.00040021188715578078558,  
 Ixx3a  $\rightarrow$  0.0054548641411743240707, Iyy2  $\rightarrow$  0.00067559686505411680334,  
 Iyy2a  $\rightarrow$  0.0081896792270521317772, Iyy3  $\rightarrow$  0.0041443644432972245743,  
 Iyy3a  $\rightarrow$  0.000010843134082099519896, Izz2  $\rightarrow$  0.0000100000000000000000,  
 Izz2a  $\rightarrow$  0.000010000000000000000000, Izz3  $\rightarrow$  0.0027749020086155339559,  
 Izz3a  $\rightarrow$  0.0031040552724836931852, m2  $\rightarrow$  0.20766121830149764430,  
 m2a  $\rightarrow$  0.020000483437983116500, m3  $\rightarrow$  0.027637816439597598037,  
 m3a  $\rightarrow$  0.15143138782990673626, r2ax  $\rightarrow$  -0.14998793142145893514,  
 r2ay  $\rightarrow$  4.8643398722623338339  $\times 10^{-7}$ , r2az  $\rightarrow$  -0.064508934857405935503,  
 r2x  $\rightarrow$  -0.034876051484402890728, r2y  $\rightarrow$  -4.6884978531490106914  $\times 10^{-8}$ ,  
 r2z  $\rightarrow$  -0.092109948673362878252, r3ax  $\rightarrow$  -3.4395971301284333382  $\times 10^{-9}$ ,  
 r3ay  $\rightarrow$  0.049927938952440119002, r3az  $\rightarrow$  -0.035494518773529816711,  
 r3x  $\rightarrow$  1.8569245789328180432  $\times 10^{-8}$ , r3y  $\rightarrow$  0.098149653083862637166,  
 r3z  $\rightarrow$  -0.0071116900617382270465}}, {1.2843014176798917626  $\times 10^{-17}$ ,  
 {Ixx2  $\rightarrow$  0.0084024393518595198531, Ixx2a  $\rightarrow$  0.0062415692683401319610,  
 Ixx3  $\rightarrow$  0.0068617040633007764801, Ixx3a  $\rightarrow$  0.0030598877920020840665,  
 Iyy2  $\rightarrow$  0.0061990361883599992127, Iyy2a  $\rightarrow$  0.0063764933106619528769,  
 Iyy3  $\rightarrow$  0.0044412681049358221807, Iyy3a  $\rightarrow$  0.0099999988664789950238,  
 Izz2  $\rightarrow$  0.00082773618238889664485, Izz2a  $\rightarrow$  0.0099999988663013130483,  
 Izz3  $\rightarrow$  0.0097129380204654885532, Izz3a  $\rightarrow$  0.00023467906421802286793,  
 m2  $\rightarrow$  0.18873977484187758274, m2a  $\rightarrow$  0.020032813992214232974,  
 m3  $\rightarrow$  0.029841237593635840959, m3a  $\rightarrow$  0.15111699375847877273,  
 r2ax  $\rightarrow$  -0.096739606829275609351, r2ay  $\rightarrow$  3.7731933757418166993  $\times 10^{-7}$ ,  
 r2az  $\rightarrow$  0.057629430124204160642, r2x  $\rightarrow$  -0.046545327043396450240,  
 r2y  $\rightarrow$  -4.0072768899786585264  $\times 10^{-8}$ , r2z  $\rightarrow$  0.042550897106894096778,  
 r3ax  $\rightarrow$  -7.4628696025683276577  $\times 10^{-9}$ , r3ay  $\rightarrow$  -0.082872009900786521378,  
 r3az  $\rightarrow$  -0.034438560336342578079, r3x  $\rightarrow$  3.7543552939615248354  $\times 10^{-8}$ ,  
 r3y  $\rightarrow$  -0.036982915176104793064, r3z  $\rightarrow$  -0.012000743814411403785}},  
 {6.3692301197203531136  $\times 10^{-19}$ , {Ixx2  $\rightarrow$  0.000076682878120916731688,  
 Ixx2a  $\rightarrow$  0.0034933188295028718299, Ixx3  $\rightarrow$  0.0029177056422457555175,  
 Ixx3a  $\rightarrow$  0.0049571193546914207934, Iyy2  $\rightarrow$  0.00056946463048604265439,  
 Iyy2a  $\rightarrow$  0.0015636844349186711803, Iyy3  $\rightarrow$  0.000010000005861860890756,  
 Iyy3a  $\rightarrow$  0.0099999991538031837172, Izz2  $\rightarrow$  0.00001000000000001435164,

Figure 0.8. Example Manipulator Designs for LN = 0

$Izz2a \rightarrow 0.000010000000000000000000$ ,  $Izz3 \rightarrow 0.0016435840587676564096$ ,  
 $Izz3a \rightarrow 0.0062574885216510602628$ ,  $m2 \rightarrow 0.17144944447444476517$ ,  
 $m2a \rightarrow 0.020001698508086250992$ ,  $m3 \rightarrow 0.021252383645552573014$ ,  
 $m3a \rightarrow 0.15427467497880390757$ ,  $r2ax \rightarrow -0.11450883124823080102$ ,  
 $r2ay \rightarrow 6.7278940637766970848 \times 10^{-8}$ ,  $r2az \rightarrow 0.0071529612935470580776$ ,  
 $r2x \rightarrow -0.038374324115640171560$ ,  $r2y \rightarrow -7.8594786880806727501 \times 10^{-9}$ ,  
 $r2z \rightarrow 0.061251692749790529213$ ,  $r3ax \rightarrow -3.7434244016902763140 \times 10^{-9}$ ,  
 $r3ay \rightarrow 0.061208431494707346611$ ,  $r3az \rightarrow -0.034744168891077011919$ ,  
 $r3x \rightarrow 2.6870176091020003614 \times 10^{-8}$ ,  $r3y \rightarrow -0.085049417259170112964$ ,  
 $r3z \rightarrow -0.014296597798076690906$ }, {6.4925458809830727390  $\times 10^{-17}$ ,  
{Ixx2  $\rightarrow 0.0077047966013165180707$ , Ixx2a  $\rightarrow 0.0015312080666332143794$ ,  
Ixx3  $\rightarrow 0.0026061506413807176827$ , Ixx3a  $\rightarrow 0.0024353254460997432962$ ,  
Iyy2  $\rightarrow 0.0077575831941205448156$ , Iyy2a  $\rightarrow 0.00028457768213672426805$ ,  
Iyy3  $\rightarrow 0.0027412663222114833859$ , Iyy3a  $\rightarrow 0.000010001401321078064389$ ,  
Izz2  $\rightarrow 0.0099999996819541986498$ , Izz2a  $\rightarrow 0.00999999934358821682300$ ,  
Izz3  $\rightarrow 0.0033512587686773727659$ , Izz3a  $\rightarrow 0.0017146378410586778815$ ,  
m2  $\rightarrow 0.17341138077429719690$ , m2a  $\rightarrow 0.020000618828924091942$ ,  
m3  $\rightarrow 0.020014362519606490454$ , m3a  $\rightarrow 0.15444595410603320183$ ,  
r2ax  $\rightarrow -0.14919867814208333400$ , r2ay  $\rightarrow 5.1361661842902110298 \times 10^{-7}$ ,  
r2az  $\rightarrow -0.047670996978443180776$ , r2x  $\rightarrow -0.032403612051677291350$ ,  
r2y  $\rightarrow -5.9268678452319221053 \times 10^{-8}$ , r2z  $\rightarrow -0.0046871452668306021705$ ,  
r3ax  $\rightarrow -3.2078099534639072547 \times 10^{-9}$ , r3ay  $\rightarrow 0.072418514759623430416$ ,  
r3az  $\rightarrow -0.035420638353343369617$ , r3x  $\rightarrow 2.4371566419741525604 \times 10^{-8}$ ,  
r3y  $\rightarrow -0.0084593653595182222914$ , r3z  $\rightarrow -0.0099398296499399968652$ }},  
{4.8420914383088959244  $\times 10^{-18}$ , {Ixx2  $\rightarrow 0.00060395410020686993518$ ,  
Ixx2a  $\rightarrow 0.0091171309801175849846$ , Ixx3  $\rightarrow 0.0060353440101345142288$ ,  
Ixx3a  $\rightarrow 0.0041242214848171491198$ , Iyy2  $\rightarrow 0.00087398879235813501010$ ,  
Iyy2a  $\rightarrow 0.0070037009973421378701$ , Iyy3  $\rightarrow 0.0018475900225291407993$ ,  
Iyy3a  $\rightarrow 0.00040170481748964259574$ , Izz2  $\rightarrow 0.0035816698579277822953$ ,  
Izz2a  $\rightarrow 0.000010000000000000000000$ , Izz3  $\rightarrow 0.0091618485720170744854$ ,  
Izz3a  $\rightarrow 0.0010243307749655930408$ , m2  $\rightarrow 0.15149378302979994616$ ,  
m2a  $\rightarrow 0.02000000333907215762$ , m3  $\rightarrow 0.025146376550785789384$ ,  
m3a  $\rightarrow 0.22782176389453331343$ , r2ax  $\rightarrow -0.096356158085866634927$ ,  
r2ay  $\rightarrow 1.3816707404185400649 \times 10^{-7}$ , r2az  $\rightarrow 0.089967326046603917870$ ,  
r2x  $\rightarrow -0.051350937890876796867$ , r2y  $\rightarrow -1.8284088277564109052 \times 10^{-8}$ ,  
r2z  $\rightarrow 0.075709079851651078677$ , r3ax  $\rightarrow -9.2259996225458940410 \times 10^{-9}$ ,  
r3ay  $\rightarrow -0.11522890431539743338$ , r3az  $\rightarrow -0.033778679775432343469$ ,  
r3x  $\rightarrow 8.3120105840804517492 \times 10^{-8}$ , r3y  $\rightarrow -0.069451194747196721584$ ,  
r3z  $\rightarrow -0.014264040556215840890$ }}}}}}

Figure 0.8. Continued

C.2. LN = 0.001

```

{0.0010000000000141695457, {Ixx2 → 0.0041164045180219092543,
Ixx2a → 0.00048729486500180036665, Ixx3 → 0.0099906357783209743444,
Ixx3a → 0.0077523561924868830646, Iyy2 → 0.0058555392625869395486,
Iyy2a → 0.0058722052438868202430, Iyy3 → 0.0093651162855769335820,
Iyy3a → 0.0099999995490232555712, Izz2 → 0.0000100004293947445989329,
Izz2a → 0.0080843113033992097082, Izz3 → 0.0064564637618375110897,
Izz3a → 0.0016059900140548937428, m2 → 0.16288474738894190841,
m2a → 0.020002736923469334985, m3 → 0.020905924050628504296,
m3a → 0.15356126677622873681, r2ax → -0.14427772681665618945,
r2ay → 0.000012836921382623531349, r2az → -0.017863334583093006533,
r2x → -0.063042422251846466302, r2y → -1.7949580282383734700 × 10-6,
r2z → 0.0084232625894467359452, r3ax → -0.00076589977301122031781,
r3ay → 0.036398841405771681810, r3az → -0.040366592737371786204,
r3x → -0.00010260552994748071052, r3y → -0.017513683466258261705,
r3z → -0.011914559995709080010}}, {0.0010000000004430763964,
{Ixx2 → 0.0059268074858144712136, Ixx2a → 0.0097182860221517395056,
Ixx3 → 0.0065622996025606428649, Ixx3a → 0.0093304000181709958285,
Iyy2 → 0.0012399319898912495066, Iyy2a → 0.0084625664050239893805,
Iyy3 → 0.0080061604532866840996, Iyy3a → 0.0000100000000000000000,
Izz2 → 0.0099999993569590745690, Izz2a → 0.0099999993569590745690,
Izz3 → 0.0094043777666366197849, Izz3a → 0.0079901318403495413192,
m2 → 0.18077672305469963314, m2a → 0.020000000734035824357,
m3 → 0.054727615716845909932, m3a → 0.16071149221022238334,
r2ax → 0.065068813274832857396, r2ay → 0.00024985013054561205818,
r2az → 0.079892680067810666513, r2x → -0.12127655080882330310,
r2y → 0.00045890323782364518316, r2z → 0.047800972710920713668,
r3ax → -0.000067180463227048364072, r3ay → 0.11187485777418429395,
r3az → -0.031653132616181826983, r3x → -0.00029714101826490854473,
r3y → -0.034699891997502147889, r3z → -0.013254370894006890876}},
{0.001000000035741576201, {Ixx2 → 0.0095461980406010605342,
Ixx2a → 0.0012146495959772457406, Ixx3 → 0.0045518666825344724041,
Ixx3a → 0.0066539056150485925150, Iyy2 → 0.0027868002932812311472,
Iyy2a → 0.0051859450386311981399, Iyy3 → 0.0078937431483036295620,
Iyy3a → 0.00093913140646544095559, Izz2 → 0.0095795874907968060308,
Izz2a → 0.0028053281261389204314, Izz3 → 0.0087889527389372198604,
Izz3a → 0.0053704038217232597594, m2 → 0.21180895605553335287,
m2a → 0.021088158850174920803, m3 → 0.020000003450622627556,
m3a → 0.15690158824840083377, r2ax → -0.14722664413768775357,
r2ay → 2.6183369327358698848 × 10-7, r2az → 0.089619267631728847407,
r2x → -0.048395284978061680788, r2y → 2.2541979319255978535 × 10-7,
r2z → 0.030558319275737633292, r3ax → -0.0022640594062608690419,
r3ay → -0.12582021167466100042, r3az → -0.036699117685676428159,
r3x → -0.00032088100294356935237, r3y → -0.013975922500151978956,
r3z → -0.0093288016891847216830}}, {0.001000000001275252279,
{Ixx2 → 0.00025751433693921950060, Ixx2a → 0.0000345824217772727210337,
Ixx3 → 0.000039435692537163566250, Ixx3a → 0.0099797382034503984182,
Iyy2 → 0.000051484576110198622093, Iyy2a → 0.0099881089468066897626,
Iyy3 → 0.0099331931109132076633, Iyy3a → 0.00081233340443938581427,
Izz2 → 0.0099991726234395442287, Izz2a → 0.0099999997548455570364,
Izz3 → 0.000030036344844336830209, Izz3a → 0.000023531100917957093169,
m2 → 0.29987953019569371075, m2a → 0.020674067230408857869,
m3 → 0.034857466815454691453, m3a → 0.15001765793590743026,
r2ax → -0.010212267164719421987, r2ay → 0.028106883915971657306,
r2az → -0.14999890993137259083, r2x → -0.028193044459371114388,
r2y → 0.0030170488086351103914, r2z → 0.0035223727380271271528,
r3ax → -0.0032878434464436988062, r3ay → -0.14250371949618487685,
r3az → -0.028133599835099714391, r3x → 0.023969644797852618892,
r3y → 0.12759711121479423582, r3z → -0.091187834207524036650}},

```

Figure 0.9. Example Manipulator Designs for LN = 0.001

```

{0.0010000000018424631674, {Ixx2 → 0.0099898717463614154613,
  Ixx2a → 0.0099834735644258354775, Ixx3 → 0.000016903215456056106042,
  Ixx3a → 0.000014764993307000489477, Iyy2 → 0.000025898541415027277574,
  Iyy2a → 0.000030000537520291326922, Iyy3 → 0.00062137173821982802446,
  Iyy3a → 0.0047904492044358020766, Izz2 → 0.000010003493118705973236,
  Izz2a → 0.0099999998421419120393, Izz3 → 0.0040114676715144620553,
  Izz3a → 0.0037383879555157293920, m2 → 0.16647682246024824730,
  m2a → 0.020068521261426235367, m3 → 0.031191418013035183545,
  m3a → 0.21222194978666838760, r2ax → -0.14024807342401861866,
  r2ay → 0.00020777899944302865655, r2az → -0.011836361549316546726,
  r2x → -0.037681689154630943249, r2y → 0.0022117361033520333871,
  r2z → 0.0015590490903162596820, r3ax → -0.0088426838857794087222,
  r3ay → -0.0092615924832538475540, r3az → -0.044599561857608828930,
  r3x → 0.0065705582809977435968, r3y → 0.0086905950873614121350,
  r3z → -0.011378287121725161256}}}}

```

*Figure 0.9. Continued*

### C.3. LN = 0.01

```

{0.010000000001303506917, {Ixx2 → 0.00099875012833529795415,
  Ixx2a → 0.000014791826882632183058, Ixx3 → 0.0028235286241286231035,
  Ixx3a → 0.0098976052254858666992, Iyy2 → 0.0011708533166501263668,
  Iyy2a → 0.00018311034258121287360, Iyy3 → 0.000031058640324645908079,
  Iyy3a → 0.00074081682110289916358, Izz2 → 0.0039504033557966695805,
  Izz2a → 0.0034497470654254879268, Izz3 → 0.00015236761821806401361,
  Izz3a → 0.00015236761821806286035, m2 → 0.17708605735819723732,
  m2a → 0.097496687185264379627, m3 → 0.027507455444395585276,
  m3a → 0.15060863824573259631, r2ax → -0.041501285323880988904,
  r2ay → -0.0027491170016684324407, r2az → -0.14988924536624001517,
  r2x → -0.069201546997749553386, r2y → -0.050889369757466375060,
  r2z → 0.069321002779168615566, r3ax → -0.01606726588200518491,
  r3ay → -0.14882475050612620986, r3az → -0.047653729892749876618,
  r3x → 0.081192403806129968463, r3y → -0.075345120665148639446,
  r3z → 0.045138194131468843406}}, {0.010000000000345136564,
  {Ixx2 → 0.00063203853146516848307, Ixx2a → 0.0038544518185915354969,
  Ixx3 → 0.0092849694747554280483, Ixx3a → 0.0094280762470837375267,
  Iyy2 → 0.0090213496010588691835, Iyy2a → 0.00040886924036126919159,
  Iyy3 → 0.0000100000000000000000, Iyy3a → 0.0099735435590974778060,
  Izz2 → 0.0099735435590974778060, Izz2a → 0.0099735435590974778060,
  Izz3 → 0.0055628723819015305953, Izz3a → 0.0059491242818402696566,
  m2 → 0.15277514988838311412, m2a → 0.027471212590164264472,
  m3 → 0.023615512905909898820, m3a → 0.17740269276067750121,
  r2ax → -0.14556024931086115761, r2ay → -0.0011015719944289051348,
  r2az → -0.071578950264563731116, r2x → -0.077053736236724380246,
  r2y → 0.033065195814037032806, r2z → -0.047597384301644392470,
  r3ax → 0.035475020374746673768, r3ay → 0.019881137892454253251,
  r3az → -0.056163009248161641877, r3x → 0.046416168554530058346,
  r3y → 0.00082838199908527776880, r3z → -0.072208911680859101415}},
{0.010000000001887531679, {Ixx2 → 0.00011642829019063450558,
  Ixx2a → 0.0061752187985100771795, Ixx3 → 0.0099808571215622041835,
  Ixx3a → 0.0088195213499203944468, Iyy2 → 0.000017660217305270746754,
  Iyy2a → 0.00037615620130578874910, Iyy3 → 0.0049828192259792965417,
  Iyy3a → 0.0050288716443696716761, Izz2 → 0.0000100000000000000000,
  Izz2a → 0.0016252070439879457348, Izz3 → 0.0027416111332353921609,
  Izz3a → 0.000032074052923227216824, m2 → 0.29973121893366751283,
  m2a → 0.020912384926410563815, m3 → 0.023895234400856742949,
  m3a → 0.15295019988865364064, r2ax → -0.14588878270830925479,
  r2ay → -0.14949767867212124023, r2az → -0.14946461107253120241,
  r2x → 0.0089177187944077330007, r2y → 0.046850990835571501875,
  r2z → -0.14804959800885509086, r3ax → -0.011343397012486227374,
  r3ay → -0.14945578517084265575, r3az → -0.049044448259846116276,
  r3x → 0.041640246329854003118, r3y → 0.14944702506468806412,
  r3z → 0.10634087578150438890}}, {0.010000000000241469170,
  {Ixx2 → 0.0016544553166566380671, Ixx2a → 0.0027812857322699223712,
  Ixx3 → 0.0034987334508389515229, Ixx3a → 0.0099095321348405428354,
  Iyy2 → 0.0098829275731262032122, Iyy2a → 0.0094609221993067020448,
  Iyy3 → 0.0020525057330666353279, Iyy3a → 0.0051319372019633961904,
  Izz2 → 0.0099999998798311968472, Izz2a → 0.0099999998798311968472,
  Izz3 → 0.0016372406942692625797, Izz3a → 0.00010387117431424236669,
  m2 → 0.18898261207803764655, m2a → 0.050119669952896143842,
  m3 → 0.021126819403208559294, m3a → 0.15509687225262218464,
  r2ax → -0.11534518455380475787, r2ay → -0.035072962108123004507,
  r2az → -0.14999488989453740294, r2x → -0.075892728626297975648,
  r2y → 0.033276828824564267937, r2z → -0.14979610903294759743,
  r3ax → 0.053430081404894154314, r3ay → 0.0071211465159705473993,
  r3az → -0.027526832048553328312, r3x → 0.0061773959638731835086,
  r3y → 0.14140684287466327377, r3z → 0.041053977474285752992}}},

```

Figure 0.10. Example Manipulator Designs for LN = 0.01

```

{0.010000000000070666623, {Ixx2 → 0.00033590680330008463852,
  Ixx2a → 0.0099552274599504035904, Ixx3 → 0.0015751545290523886097,
  Ixx3a → 0.0015984727203106238924, Iyy2 → 0.000032452175512404412100,
  Iyy2a → 0.0032948785535380345970, Iyy3 → 0.00028035635356649558703,
  Iyy3a → 0.0000100000000000000000,
  Izz2 → 0.0048426758119747651204, Izz2a → 0.0000100000000000000000,
  Izz3 → 0.0088515617138840726141, Izz3a → 0.0037574601326288179407,
  m2 → 0.16394786993065292405, m2a → 0.10272126181925356558,
  m3 → 0.020383025146975664052, m3a → 0.15303436815649423042,
  r2ax → -0.14961080880786374416, r2ay → 0.0012993145545695982053,
  r2az → 0.0070557496222167937139, r2x → -0.086730419605430060640,
  r2y → 0.028733491039491898744, r2z → -0.14851598597780174480,
  r3ax → 0.050415610042477443042, r3ay → -0.031940953607960154519,
  r3az → -0.015812943022817224095, r3x → -0.14902338884720308161,
  r3y → 0.14925733467076124731, r3z → 0.10706756975363705343}}}}

```

*Figure 0.10. Continued*

C.4. LN = 0.1

```

{0.10000000000003582272, {Ixx2 → 0.0099656836253746734781,
  Ixx2a → 0.0024447986606577502209, Ixx3 → 0.00033445400735988179892,
  Ixx3a → 0.0099999998756823337023, Iyy2 → 0.0031511324045590768085,
  Iyy2a → 0.000044421672524531134553, Iyy3 → 0.0081490642354439802600,
  Iyy3a → 0.0099999998998456285585, Izz2 → 0.0039210656612325772666,
  Izz2a → 0.0033058751682660069025, Izz3 → 0.000010000000048817386957,
  Izz3a → 0.00034106507982008261478, m2 → 0.26741803731972520737,
  m2a → 0.079603165878447048532, m3 → 0.050353919558688575022,
  m3a → 0.24353590334643107285, r2ax → 0.041611143791819564307,
  r2ay → 0.071112223097486258814, r2az → -0.14998820592505942060,
  r2x → -0.078128159604775016193, r2y → 0.0038053414760671986135,
  r2z → -0.089072074823875610119, r3ax → 0.14999999952474662095,
  r3ay → 0.14999999987771497565, r3az → -0.025884877273668115829,
  r3x → -0.11166493041336128032, r3y → -0.149999999999208470,
  r3z → -0.13532040110878762413}}, {0.10000000000473801776,
  {Ixx2 → 0.0099999648662823656560, Ixx2a → 0.0057096875212611785611,
  Ixx3 → 0.0099999998999817048148, Ixx3a → 0.000082914478391281921891,
  Iyy2 → 0.0082712278521169792692, Iyy2a → 0.0058272121148159237990,
  Iyy3 → 0.0035965615492350467552, Iyy3a → 0.0099999999011186921315,
  Izz2 → 0.0021456537972656347879, Izz2a → 0.00065593776764772988648,
  Izz3 → 0.00075317475619341178621, Izz3a → 0.0046700769165165462782,
  m2 → 0.17543579346291875669, m2a → 0.021359343356984657787,
  m3 → 0.033361491233685288674, m3a → 0.17527172722712916872,
  r2ax → -0.14999999997572554671, r2ay → 0.14615397609270170703,
  r2az → 0.14999999990116425344, r2x → -0.14999999983297031830,
  r2y → -0.14393669815571050210, r2z → -0.14999544327597856938,
  r3ax → 0.13128521373624746823, r3ay → 0.095117125498774983091,
  r3az → -0.077041803197721568804, r3x → 0.063078087212442820521,
  r3y → -0.14995525735435877832, r3z → 0.14535040633360765627}},
{0.10000008296118196636, {Ixx2 → 0.0016659302455100473359,
  Ixx2a → 0.0016595706076595526240, Ixx3 → 0.0041711092177854538399,
  Ixx3a → 0.0000100000000000000000, Iyy2 → 0.0000100000000000000000,
  Iyy2a → 0.0000100000000000000000, Iyy3 → 0.0047521067046738520553,
  Iyy3a → 0.0050125357539488983289, Izz2 → 0.0020806493870690342525,
  Izz2a → 0.01000000000000000000, Izz3 → 0.01000000000000000000,
  Izz3a → 0.0000100000000000000000, m2 → 0.150000000000000000,
  m2a → 0.02000000000000000000, m3 → 0.02000000000000000000,
  m3a → 0.15000000000000000000, r2ax → 0.15000000000000000000,
  r2ay → 0.14999895436568258265, r2az → 0.15000000000000000000,
  r2x → -0.028004369228038555560, r2y → 0.15000000000000000000,
  r2z → -0.15000000000000000000, r3ax → 0.070170847547341890936,
  r3ay → -0.014324002229707167471, r3az → 0.15000000000000000000,
  r3x → -0.13849994503630908490, r3y → -0.077337258715579310508,
  r3z → -0.14998841640305301768}}, {0.10000041953730985171,
  {Ixx2 → 0.0098982679088352807518, Ixx2a → 0.0061705584258086782427,
  Ixx3 → 0.0087133115252115754099, Ixx3a → 0.0099999736193467724994,
  Iyy2 → 0.01000000000000000000, Iyy2a → 0.0000100000000000000000,
  Iyy3 → 0.0000100000000000000000, Iyy3a → 0.0031564993455095521361,
  Izz2 → 0.0000100000000000000000, Izz2a → 0.01000000000000000000,
  Izz3 → 0.0000100000000000000000, Izz3a → 0.0064242394958656124355,
  m2 → 0.15000000000000000000, m2a → 0.11335318869838674705,
  m3 → 0.02000000000000000000, m3a → 0.15000000000000000000,
  r2ax → 0.15000000000000000000, r2ay → -0.080614466865613775299,
  r2az → 0.060666258462794333702, r2x → -0.15000000000000000000,
  r2y → 0.15000000000000000000, r2z → 0.065977486629552874879,
  r3ax → 0.15000000000000000000, r3ay → 0.15000000000000000000,
  r3az → -0.15000000000000000000, r3x → 0.058668825911686703880,
  r3y → -0.15000000000000000000, r3z → 0.15000000000000000000}},

```

Figure 0.11. Example Manipulator Designs for LN = 0.1

```

{0.1000000000023441508, {Ixx2 → 0.0049355527618869038075,
  Ixx2a → 0.0000100000000000000000, Ixx3 → 0.0035860065618290900706,
  Ixx3a → 0.0034508832390156635200, Iyy2 → 0.000074001126250267498655,
  Iyy2a → 0.000074012349105440516070, Iyy3 → 0.0034193715738671907743,
  Iyy3a → 0.0045050349437860615804, Izz2 → 0.0000100000000000000000,
  Izz2a → 0.0000100000000000000000,
  Izz3 → 0.0000100000000000000000, Izz3a → 0.0014811008630882580343,
  m2 → 0.16873137540901311315, m2a → 0.097077613195067932543,
  m3 → 0.14999999847624997617, m3a → 0.15630431063205554544,
  r2ax → -0.12913636912962844097, r2ay → 0.14615570418502630118,
  r2az → -0.093440468479721421063, r2x → -0.069307098289372626386,
  r2y → -0.076888084231862034439, r2z → -0.027704680260962742231,
  r3ax → 0.043726097611588927564, r3ay → 0.14998077330940384516,
  r3az → -0.0388025015188605903280, r3x → -0.031240942077226696888,
  r3y → 0.1499999989843706685, r3z → 0.1499999929287099484}}}}

```

Figure 0.11. Continued

C.5. LN = 1

```

{1.0000000000182602839, {Ixx2 → 0.0098097205405216920135,
Ixx2a → 0.0063644018216445058192, Ixx3 → 0.0097114545368474317535,
Ixx3a → 0.000045732152674647811337,
Iyy2 → 0.0021580271413095603886, Iyy2a → 0.0099995438259614045007,
Iyy3 → 0.0099999992254723929908, Iyy3a → 0.0030507242544491352288,
Izz2 → 0.0099999992254723929908, Izz2a → 0.0028094570502632870934,
Izz3 → 0.0036344179497201431611, Izz3a → 0.0048179228019575237364,
m2 → 0.18706753378127707912, m2a → 0.090811464533238644316,
m3 → 0.1499999846000451398, m3a → 0.25496699566436973548,
r2ax → 0.062356064481896441902, r2ay → 0.14999749955469274268,
r2az → -0.0019111460487982771129, r2x → 0.14999999959086745341,
r2y → -0.054103210160225837108, r2z → -0.10775821839797406403,
r3ax → -0.14999939249921285926, r3ay → -0.1499997341063322519,
r3az → 0.14998578439030898189, r3x → -0.0071825534903738848995,
r3y → 0.047415188337478072630, r3z → 0.14996969373142938478}},
{1.0000000000136469808, {Ixx2 → 0.000010208955738140678757,
Ixx2a → 0.0094820600129795581137, Ixx3 → 0.0088212426753776882248,
Ixx3a → 0.000014560480849739948918, Iyy2 → 0.000011666443898229061181,
Iyy2a → 0.0030635135023778244044, Iyy3 → 0.0055600835872065499997,
Iyy3a → 0.0027774002242509280792, Izz2 → 0.0040151862528611809503,
Izz2a → 0.0099999999098841675437, Izz3 → 0.00001000000026349555190,
Izz3a → 0.00001000000026349555190, m2 → 0.29858391067781535786,
m2a → 0.14986635407263669600, m3 → 0.1499999993797352371,
m3a → 0.29984800662305458826, r2ax → 0.015871810263393227683,
r2ay → -0.14989890633865413682, r2az → -0.14999916834431192842,
r2x → 0.14986879403407354266, r2y → -0.14990962295053698220,
r2z → 0.14999994770392849007, r3ax → 0.14993088990061705127,
r3ay → -0.087438927505655906515, r3az → 0.14987521537084583561,
r3x → -0.14908308768469330160, r3y → -0.149999999999744822,
r3z → -0.14849109087379971613}}, {1.000000000016341439,
{Ixx2 → 0.000010001527420466796024, Ixx2a → 0.0099753877643392535991,
Ixx3 → 0.0061848922340977735107, Ixx3a → 0.0099999992124331058064,
Iyy2 → 0.009999983723962911793, Iyy2a → 0.0087770338634980697561,
Iyy3 → 0.009999998493370846751, Iyy3a → 0.009999998493370846751,
Izz2 → 0.0058875078257434855093, Izz2a → 0.0000100000000000000000,
Izz3 → 0.0027244751153510498971, Izz3a → 0.0013316240103631600649,
m2 → 0.25083986977849629900, m2a → 0.14567443656324760563,
m3 → 0.11149629792693383621, m3a → 0.23531878967593542713,
r2ax → 0.067623132474170653983, r2ay → -0.11217643779148452338,
r2az → 0.1499998400221021695, r2x → 0.10587082173577637334,
r2y → -0.10523039211729401055, r2z → -0.14999977341997673545,
r3ax → -0.14997312888989029418, r3ay → -0.068869219157366927308,
r3az → 0.095450535563185422676, r3x → -0.14995589120714484456,
r3y → -0.1499995592745349260, r3z → 0.14163224085489333149}},
{1.0000000000308344251, {Ixx2 → 0.0099946772096190613947,
Ixx2a → 0.0000100000000000000000, Ixx3 → 0.000010466694408433910168,
Ixx3a → 0.009999999220705650817, Iyy2 → 0.009999999311420610756,
Iyy2a → 0.0023298411060168069049, Iyy3 → 0.0030744998471110091642,
Iyy3a → 0.0011587902270332820199, Izz2 → 0.0000100000000000000000,
Izz2a → 0.0000100000000000000000, Izz3 → 0.0027546935347942652588,
Izz3a → 0.0000100000000000000000, m2 → 0.29998911345269099049,
m2a → 0.1499999991306168191, m3 → 0.13166280652803982397,
m3a → 0.29995855164667782389, r2ax → 0.050814645191940442444,
r2ay → -0.052155813060535906288, r2az → 0.14999999720004601633,
r2x → 0.10459474790000581050, r2y → 0.053340422144459360947,
r2z → 0.14999999405112213843, r3ax → -0.14998619947844189290,
r3ay → 0.14999995782658232561, r3az → -0.13619973500575718053,
r3x → -0.14995869409049031807, r3y → 0.049964214036277632172,
r3z → -0.064642511896702153165}}, {1.0000111188584007048,

```

Figure 0.12. Example Manipulator Designs for LN = 1

```

{Ixx2 → 0.0067568301436973133629, Ixx2a → 0.0023177452941258972504,
Ixx3 → 0.01000000000000000000, Ixx3a → 0.000010058300675237861853,
Iyy2 → 0.0025089789277803676361, Iyy2a → 0.0099999640674349151133,
Iyy3 → 0.0074188658255775309611, Iyy3a → 0.0000100000000000000000,
Izz2 → 0.01000000000000000000, Izz2a → 0.0000100000000000000000,
Izz3 → 0.0016496836448206199350, Izz3a → 0.0044242196753430955366,
m2 → 0.30000000000000000000, m2a → 0.13132950835984008474,
m3 → 0.098796225971471389268, m3a → 0.30000000000000000000,
r2ax → 0.088061977414242250947, r2ay → 0.030318717762777394745,
r2az → 0.021202167840756010037, r2x → 0.15000000000000000000,
r2y → -0.15000000000000000000, r2z → -0.026518920586925471456,
r3ax → -0.15000000000000000000, r3ay → 0.043873289079275535201,
r3az → 0.078563147634299006156, r3x → -0.025512338363746190765,
r3y → 0.15000000000000000000, r3z → 0.032934986062286728336}}}}

```

*Figure 0.12. Continued*

C.6. LN = 2

```

{2.00000000000000002747, {Ixx2 → 0.000015737892593268931912,
Ixx2a → 0.0099835887074950822751, Ixx3 → 0.0075309778049606680733,
Ixx3a → 0.0039541207971309898166, Iyy2 → 0.0099999741093700660806,
Iyy2a → 0.0043118991709447501290, Iyy3 → 0.0043113798800057362471,
Iyy3a → 0.009999962308044321453, Izz2 → 0.0057974305723139574237,
Izz2a → 0.0070095028651107773359, Izz3 → 0.0019410003381839061228,
Izz3a → 0.0061839175389112877634, m2 → 0.27937928909270988435,
m2a → 0.14999999714268638996, m3 → 0.14418876414850404492,
m3a → 0.29477040050146079362, r2ax → 0.14999423161900912358,
r2ay → 0.14999872182562961487, r2az → -0.0019323052767661761109,
r2x → 0.14995610751234670533, r2y → 0.14237390110377502931,
r2z → 0.079650882710890419259, r3ax → 0.14999279797195502683,
r3ay → 0.1499995826379168128, r3az → 0.14745269797715926786,
r3x → 0.14970632862811397455, r3y → 0.14999996701071210139,
r3z → 0.14998898465754485326}}, {2.0000000000353462144,
{Ixx2 → 0.0099947317616408942964, Ixx2a → 0.0098253490846339502845,
Ixx3 → 0.00001360513157718682653, Ixx3a → 0.0099999713576088109099,
Iyy2 → 0.009999863707180293307, Iyy2a → 0.000015265560781446874034,
Iyy3 → 0.0000100000000000000000, Iyy3a → 0.0000100000000000000000,
Izz2 → 0.0014264658969574431977, Izz2a → 0.0099769268111198208476,
Izz3 → 0.0020321364975868916318, Izz3a → 0.0080386477324959976148,
m2 → 0.29998759480933778541, m2a → 0.14511693863866426870,
m3 → 0.14999999846644123841, m3a → 0.29998528418317455874,
r2ax → 0.12754053751938106349, r2ay → -0.14999769742058131191,
r2az → 0.052887847500297509227, r2x → 0.12948752760565897830,
r2y → -0.14999999262215295472, r2z → 0.011732163289193696675,
r3ax → 0.14999805246092869280, r3ay → -0.081231962711898965569,
r3az → 0.14979105070570922848, r3x → 0.14862525537418832041,
r3y → 0.14999992059505314474, r3z → 0.14998906615184145588}},
{2.0000003705358918478, {Ixx2 → 0.00017025792916699234425,
Ixx2a → 0.0047592376801114604411, Ixx3 → 0.01000000000000000000,
Ixx3a → 0.0099987382030238462259, Iyy2 → 0.01000000000000000000,
Iyy2a → 0.0000100000000000000000,
Iyy3 → 0.0000100000000000000000, Iyy3a → 0.000010007787112638864069,
Izz2 → 0.01000000000000000000, Izz2a → 0.0092980789126347017475,
Izz3 → 0.0036371943681080104459, Izz3a → 0.009999364814437316207,
m2 → 0.30000000000000000000, m2a → 0.15000000000000000000,
m3 → 0.14828224121665363209, m3a → 0.29664827007867963509,
r2ax → 0.13609100520481193321, r2ay → 0.094277984637905549103,
r2az → 0.085650756795525983964, r2x → 0.14999986511125504413,
r2y → 0.14206392630924352522, r2z → 0.15000000000000000000,
r3ax → 0.15000000000000000000, r3ay → -0.11921215904823444723,
r3az → 0.14960264657551752072, r3x → 0.15000000000000000000,
r3y → -0.15000000000000000000, r3z → 0.13751112696133275729}},
{2.0000197749352445797, {Ixx2 → 0.0052458161790760139315,
Ixx2a → 0.0073811274084030537744, Ixx3 → 0.000010052234103330577657,
Ixx3a → 0.0000100000000000000000, Iyy2 → 0.0000100000000000000000,
Iyy2a → 0.009999317386461307342, Iyy3 → 0.0087087915680435063272,
Iyy3a → 0.0000100000000000000000, Izz2 → 0.0016946729367474083682,
Izz2a → 0.0000100000000000000000, Izz3 → 0.01000000000000000000,
Izz3a → 0.0000100000000000000000, m2 → 0.29687408913874583844,
m2a → 0.14998999844981535754, m3 → 0.14999602332494695129,
m3a → 0.29999664118462933176, r2ax → 0.14476994346394536311,
r2ay → 0.14993207781600943298, r2az → 0.15000000000000000000,
r2x → 0.14999759450498620403, r2y → 0.14791775150187885831,
r2z → -0.14999639444054605534, r3ax → 0.15000000000000000000,
r3ay → 0.14764008313627110290, r3az → 0.13564351540798283813,
r3x → 0.14974971630189090865, r3y → -0.071943080114810346219,
r3z → 0.12352078559030437982}}, {2.000026089978358506,

```

Figure 0.13. Example Manipulator Designs for LN = 2

```

(Ixx2 → 0.009999043645920327309, Ixx2a → 0.0094230281365404298997,
Ixx3 → 0.0068405273348887244486, Ixx3a → 0.0000100000000000000000,
Iyy2 → 0.0067921439250126162911, Iyy2a → 0.0000100000000000000000,
Iyy3 → 0.009999760687792238390, Iyy3a → 0.009999924196580412403,
Izz2 → 0.0044851165191999760747, Izz2a → 0.0019537680506487033797,
Izz3 → 0.0049794374012472877646, Izz3a → 0.0099999441400893046929,
m2 → 0.29889219508182239339, m2a → 0.150000000000000000,
m3 → 0.14941069251957374950, m3a → 0.29771022663329563690,
r2ax → 0.091083271015714703361, r2ay → 0.14989990259033491664,
r2az → 0.150000000000000000, r2x → 0.150000000000000000,
r2y → 0.14781439339846459096, r2z → -0.150000000000000000,
r3ax → 0.14999774862707410241, r3ay → 0.10497483885776695273,
r3az → 0.14689569042954082868, r3x → 0.14901404489228945885,
r3y → -0.14568484110339948818, r3z → 0.14999978481133810302}}}}

```

*Figure 0.13.* Continued

## D. Optimization of Six Degrees of Freedom Configuration

The empty solution set is obtained via the following MATHEMATICA codes as below.

```

solution6dof = FindInstance[D[LN, Ixx4] == 0 && D[LN, Ixy4] == 0 &&
D[LN, Ixz4] == 0 && D[LN, Iyy4] == 0 && D[LN, Iyz4] == 0 && D[LN, Izz4] == 0 &&
D[LN, Ixx5] == 0 && D[LN, Ixy5] == 0 && D[LN, Ixz5] == 0 &&
D[LN, Iyy5] == 0 && D[LN, Iyz5] == 0 && D[LN, Izz5] == 0 &&
D[LN, Ixx6] == 0 && D[LN, Ixy6] == 0 && D[LN, Ixz6] == 0 &&
D[LN, Iyy6] == 0 && D[LN, Iyz6] == 0 && D[LN, Izz6] == 0 &&
Ixx1 Iyy1 - Ixy1^2 > 0 &&
Ixx1 Iyy1 Izz1 - Ixx1 Iyz1^2 - Ixy1^2 Izz1 - 2 Ixy1 Ixz1 Iyz1 - Ixz1^2 Iyy1 > 0 &&
Ixx2 Iyy2 - Ixy2^2 > 0 &&
Ixx2 Iyy2 Izz2 - Ixx2 Iyz2^2 - Ixy2^2 Izz2 - 2 Ixy2 Ixz2 Iyz2 - Ixz2^2 Iyy2 > 0 &&
Ixx3 Iyy3 - Ixy3^2 > 0 &&
Ixx3 Iyy3 Izz3 - Ixx3 Iyz3^2 - Ixy3^2 Izz3 - 2 Ixy3 Ixz3 Iyz3 - Ixz3^2 Iyy3 > 0 &&
Ixx2a Iyy2a - Ixy2a^2 > 0 &&
Ixx2a Iyy2a Izz2a - Ixx2a Iyz2a^2 -
  Ixy2a^2 Izz2a - 2 Ixy2a Ixz2a Iyz2a - Ixz2a^2 Iyy2a > 0 &&
Ixx3a Iyy3a - Ixy3a^2 > 0 &&
Ixx3a Iyy3a Izz3a - Ixx3a Iyz3a^2 -
  Ixy3a^2 Izz3a - 2 Ixy3a Ixz3a Iyz3a - Ixz3a^2 Iyy3a > 0 &&
Ixx4 Iyy4 - Ixy4^2 > 0 &&
Ixx4 Iyy4 Izz4 - Ixx4 Iyz4^2 - Ixy4^2 Izz4 - 2 Ixy4 Ixz4 Iyz4 - Ixz4^2 Iyy4 > 0 &&
Ixx5 Iyy5 - Ixy5^2 > 0 &&
Ixx5 Iyy5 Izz5 - Ixx5 Iyz5^2 - Ixy5^2 Izz5 - 2 Ixy5 Ixz5 Iyz5 - Ixz5^2 Iyy5 > 0 &&
Ixx6 Iyy6 - Ixy6^2 > 0 &&
Ixx6 Iyy6 Izz6 - Ixx6 Iyz6^2 - Ixy6^2 Izz6 - 2 Ixy6 Ixz6 Iyz6 - Ixz6^2 Iyy6 > 0 &&
mub > m1 > mlb && mub > m2 > mlb && mub > m2a > mlb && mub > m3 > mlb &&
mub > m3a > mlb && mub > m4 > mlb && mub > m5 > mlb && mub > m6 > mlb &&
iub > Ixx1 > ilb && iub > Iyy1 > ilb && iub > Izz1 > ilb &&
iub > Ixx2 > ilb && iub > Iyy2 > ilb && iub > Izz2 > ilb &&
iub > Ixx2a > ilb && iub > Iyy2a > ilb && iub > Izz2a > ilb &&
iub > Ixx3 > ilb && iub > Iyy3 > ilb && iub > Izz3 > ilb &&
iub > Ixx3a > ilb && iub > Iyy3a > ilb && iub > Izz3a > ilb &&
iub > Ixx4 > ilb && iub > Iyy4 > ilb && iub > Izz4 > ilb &&
iub > Ixx5 > ilb && iub > Iyy5 > ilb && iub > Izz5 > ilb &&
iub > Ixx6 > ilb && iub > Iyy6 > ilb && iub > Izz6 > ilb &&
rub > r1x > r1b && rub > r1y > r1b && rub > r1z > r1b &&
rub > r2x > r1b && rub > r2y > r1b && rub > r2z > r1b &&
rub > r2ax > r1b && rub > r2ay > r1b && rub > r2az > r1b &&
rub > r3x > r1b && rub > r3y > r1b && rub > r3z > r1b &&
rub > r3ax > r1b && rub > r3ay > r1b && rub > r3az > r1b &&
rub > r4x > r1b && rub > r4y > r1b && rub > r4z > r1b &&
rub > r5x > r1b && rub > r5y > r1b && rub > r5z > r1b &&
rub > r6x > r1b && rub > r6y > r1b && rub > r6z > r1b,
{Ixx1, Ixx2, Ixx2a, Ixx3, Ixx3a, Ixx4, Ixx5, Ixx6, Ixy1, Ixy2, Ixy2a, Ixy3, Ixy3a,
Ixy4, Ixy5, Ixy6, Ixya2, Ixz1, Ixz2, Ixz2a, Ixz3, Ixz3a, Ixz4, Ixz5, Ixz6, Iyy1,
Iyy2, Iyy2a, Iyy3, Iyy3a, Iyy4, Iyy5, Iyy6, Iyz1, Iyz2, Iyz2a, Iyz3, Iyz3a,
Iyz4, Iyz5, Iyz6, Izz1, Izz2, Izz2a, Izz3, Izz3a, Izz4, Izz5, Izz6, m1, m2,
m2a, m3, m3a, m4, m5, m6, r1x, r1y, r1z, r2ax, r2ay, r2az, r2x, r2y, r2z, r3ax,
r3ay, r3az, r3x, r3y, r3z, r4x, r4y, r4z, r5x, r5y, r5z, r6x, r6y, r6z}, Reals]
()

```

Figure 0.14. LN Optimization of Six DOF